To the Graduate Council:

I am submitting herewith a dissertation written by Donald Philip Armstrong entitled "The Multiphoton Ionization of Uranium Hexafluoride." I have examined the final copy of this dissertation for form and content and recommend that it be accepted in partial fulfillment of the requirements for the degree of Doctor of Philosophy, with a major in Chemistry.

Robert N. Compton, Major Professor

We have read this dissertation

and recommend its acceptance:

Accepted for the Council:

Associate Vice Chancellor

and Dean of the Graduate School

The Multiphoton Ionization Of Uranium Hexafluoride

A Dissertation

Presented for the

Doctor of Philosophy

Degree

The University of Tennessee, Knoxville

Donald Philip Armstrong

May 1992

ACKNOWLEDGMENTS

The journey has been long. There have been many people along the way who have provided help, inspiration, motivation, and (many) other stimuli. I would be remiss in not mentioning the ones who were the most important. It is fitting to begin at the beginning. Dean Tate, of Paducah, Ky., was responsible for my being in Tennessee in the first place. Had it not been for his simple act of kindness and loyalty, I would not be here today and I fear my life might have been drastically different. I know that I can never repay that kindness. As my work and school have always run a parallel course, I have many to thank. Let me begin with my coworkers, past and present. Over 15 years ago I resumed my undergraduate program and the man who, more than anyone else, made that possible was John E. Shoemaker. I'm still not sure what made him take a chance on me. My good friend Richard Faulkner made it possible for me to complete my B.S. degree, and for that I am deeply indebted. Bill McCulla, my first mentor as an apprenticing laserjock, left for the greener pastures of Los Alamos Scientific Laboratory. John Stockdale likewise left, but his destination was Lawrence Livermore National Laboratory. Bill Bostick and Bob Reiner, excellent scientists in their own right, have always taken the time to help out. Without a doubt the most important person for the last many years has been my supervisor, Lee Trowbridge. He has always been encouraging, helpful, protective, and delightfully cynical. Many thanks are due to Dajun Ding for his expertise in utilizing the photoelectron spectrometer at ORNL and to Cathy Dulling for her expertise and assistance in the preparation of this manuscript. Doug Billings, of Quanta-Ray, always went the extra mile for me. He is a credit to his organization. My life in academia has also given me the opportunity to become acquainted with many special people. Bill Fletcher was one of my first chemistry professors over 10 years ago and has consulted with this laser laboratory for many years now,

dating back to the days of Bill McCulla. He has often had to serve as an unofficial advisor, sounding board, coauthor, and friend. Ironically, I had not even considered graduate school until receiving the letter of invitation from George Schweitzer, who later was to be my advisor. This simple act transformed my life for the better. There were four very special people in the class of '82 (of which I am the last to exit). Don Bierer, Ric Booth, Mike Capacci, Tony Balchunas and myself were to later become known as the "A-team", along with honorary members Chuck Kettler and Bruce Tromberg. Special friends such as these made graduate school more like fun than hard work. A very special thank you to my best friend, Tony Balchunas, and to his wonderful wife, Kathy. A man could not possibly ask for better friends. A very special thank you is reserved for my former classmate and current coworker, David Harkins. He is an impressive and skilled chemist (provided no tools are used), as well as a rather amazing magician with computers. He has been invaluable. A very special thank you for Jeannine, she too is invaluable. I am sincerely grateful to Robert Compton, whose enthusiasm for a good piece of science is seemingly boundless. He has been a tremendous inspiration and truly makes one aspire to greatness.

This dissertation is dedicated to my family. I thank my mother, Lola, and my father, Philip, who has passed away, for equiping me with a strong sense of determination, dedication, and integrity which has sustained me through some dark times. My father was never quite sure why I am so driven, but I'm sure if he were here he would be proud. Last, but certainly not least, this is dedicated to Bret. There are no words that can express my love for my son. If one day he should decide that a career in science is the proper choice for him, then perhaps this will serve as an inspiration. However, if he should choose otherwise then perhaps this will stand as a testament to the beliefs that patience and perseverance are rewarded. You're never too old to try.

ABSTRACT

Multiphoton ionization (MPI) time-of-flight mass spectroscopy and photoelectron spectroscopy studies of UF_6 have been conducted using focused light from the Nd:YAG laser fundamental (λ=1064 nm) and its harmonics (λ=532, 355, or 266 nm), as well as other wavelengths provided by a tunable dye laser. The MPI mass spectra are dominated by the singly and multiply charged uranium ions rather than by the UF_x^+ fragment ions even at the lowest laser power densities at which signal could be detected. The laser power dependence of U^{n+} ion signals indicates that saturation can occur for many of the steps required for their ionization. In general, the doubly-charged uranium ion (U^{2+}) intensity is much greater than that of the singly-charged uranium ion (U^+). For the case of the tunable dye laser experiments, the U^{n+} (n = 1-4) wavelength dependence is relatively unstructured and does not show observable resonance enhancement at known atomic uranium excitation wavelengths. The dominance of the U^{2+} ion and the absence or very small intensities of UF_x^+ fragments, along with the unstructured wavelength dependence, indicate that mechanisms may exist other than ionization of bare U atoms after the stepwise photodissociation of F atoms from the parent molecule. The data also argue against step-wise photodissociation of UF_x^+ (x=5,6) ions. Neither of the traditional photoinduced mechanisms, the "neutral ladder" or the "ion ladder", are believed to adequately describe the ionization phenomena observed. These results suggest an alternate mechanism which better explains the multiphoton excitation and dissociative ionization of UF_6. It is likely that the multiphoton excitation of UF_6 under these experimental conditions results in a superexcited molecule, UF_6^{**}, which primarily dissociates into U^{n+} (through multiple channels), fluorine atoms, and "slow" electrons. The excitation of such superexcited molecules may be facilitated by the existence of a previously reported "giant resonance" at 12-14 eV.

TABLE OF CONTENTS

CHAPTER PAGE

I. INTRODUCTION 1

A. Historical Perspective 1

B. Interactions Of Light With UF_6 2

C. Fundamental Aspects Of Multiphoton Ionization 5

D. Previous MPI Studies Of UF_6 11

II. EXPERIMENTAL APPARATUS AND METHODS 14

A. Overview 14

B. Laser System 14

C. Time-Of-Flight Mass Spectrometer 16

D. Data Acquisition System 22

E. Photoelectron Spectrometer 27

III. RESULTS 32

A. Overview 32

B. MPI Results Using The Nd:YAG Laser 32

C. MPI Results Using The Dye Laser 55

D. MPI and Photoelectron Results Using The PES System 68

IV. DISCUSSION 76

V. CONCLUSIONS 94

LIST OF REFERENCES 97

APPENDIX 103

VITA 106

LIST OF FIGURES

FIGURE PAGE

1. Possible MPI ladder climbing schemes 7
2. Ideal ionic ladder climbing 9
3. The "superexcited" molecular system 10
4. Beam attenuation using quartz plates 17
5. Time-of-flight mass spectrometer details 19
6. Time-of-flight mass spectrometer calibration 21
7. MCP detector responsivity 23
8. Trigger sequence 25
9. Dye laser calibration using xenon resonance 26
10. MPI-TOFMS experimental apparatus 28
11. MPI-PES experimental apparatus 31
12. MPI mass spectrum using λ=1064 nm 33
13. MPI mass spectrum using λ=532 nm 35
14. MPI mass spectrum using λ=355 nm 37
15. MPI mass spectra using λ=266 nm (7.5-cm lens) 38
16. Slope of signal vs. intensity for U^{n+} (7.5-cm lens) 40
17. Slope of signal vs. intensity for UF_x^+ (7.5-cm lens) 41
18. MPI mass spectra using λ=266 nm (35-cm lens) 43
19. Slope of signal vs. intensity for U^{n+} (35-cm lens) 44
20. Reversal of the dominant ion intensities 45
21. Slope of signal vs. intensity for UF_x^+ (35-cm lens) 46
22. MPI mass spectra using λ=266 nm (50-cm lens) 48

FIGURE PAGE

23. Slope of signal vs. intensity for U^{n+} (50-cm lens) 49

24. Slope of signal vs. intensity for UF_x^+ (50-cm lens) 50

25. Combined slope data for U^+ 51

26. Combined slope data for U^{2+} 52

27. Combined slope data for U^{3+} 53

28. MPI mass spectra using λ=266 nm, single "slice" 54

29. Magnification of TOF region: 5 - 15 μsec (from Fig. 28) 56

30. Magnification of TOF region: 27.4 - 31.4 μsec (from Fig. 28) 57

31. Magnification of TOF region: 15.9 - 19.9 μsec (from Fig. 28) 58

32. Wavelength scan of the "blue" xenon resonance 59

33. MPI mass spectra using λ=591 nm, low power 61

34. MPI mass spectra using λ=591 nm, high power 63

35. Magnification of Figure 34 by 20X 64

36. Magnification of TOF region: 27 - 32 μsec (from Fig. 35) 65

37. Magnification of TOF region: 19.3 - 21.3 μsec (from Fig. 35) 66

38. Magnification of TOF region: 7.5 - 16.5 μsec (from Fig. 35) 67

39. MPI mass spectrum using MPI-PES apparatus 69

40. Photoelectron spectrum of UF_6 using λ=266 nm 70

41. Photoelectron spectrum of UF_6 using λ=355 nm 71

42. Photoelectron spectrum of UF_6 using λ=532 nm 72

43. Photoelectron spectrum of UF_6 and xenon using λ=440.88 nm 73

44. Ion signal ratios for circular and linear polarizations 75

45. UV absorption spectrum for UF_6 81

FIGURE PAGE

46. "Giant Resonance" in UF_6 83

47. "Superexcited" UF_6 energy diagram 85

CHAPTER I

INTRODUCTION

A. Historical Perspective

Uranium was first discovered in 1789 in the mineral pitchblende by Klaproth, the first professor of chemistry at the University of Berlin, and was named after the planet Uranus. The French chemist Peligot, who was a professor of analytical chemistry, glassmaker, and director of assays at the Paris mint, showed that Klaproth's "semi-metallic" element was actually the dioxide, and succeeded in preparing elemental uranium in 1841. In 1896, Becquerel discovered that uranium underwent radioactive decay. Some years later, the Curies were able to isolate radium from uranium ore. For over a century uranium had languished in relative elemental obscurity and was chiefly obtained as an unwanted by-product of radium processing. Its only other practical application was as a coloring agent for glass and ceramics. By 1934 Fermi had produced trace amounts of new radioactive elements by bombarding uranium with neutrons; however, the discovery in 1939, by Hahn and Strassman, of nuclear fission in uranium vaulted the element from obscurity to a position of major industrial importance. The soon-to-be discovered role of uranium in the nuclear power industry as well as the defense industry brought about a need to acquire large amounts of the fissionable isotope, ^{235}U (0.711% natural abundance), and required separating it from the nonfissionable isotope, ^{238}U (99.275% natural abundance), on an industrial scale. For a given sample, increasing the percentage of ^{235}U which is present is known as enrichment, and all practical enrichment processes require the uranium to be in the form of a gas, specifically uranium hexafluoride (UF_6).[1] The two predominant commercial processes for enrichment are gaseous diffusion and gas centrifuge, both of which were devised to take advantage of the monoisotopicity of fluorine and the fact that UF_6 readily sublimes. The monoisotopic nature

of fluorine yields the advantage that the separation process depends solely on the isotopes of uranium. In the United States, the enrichment of UF_6 was initiated on a large scale during the Manhattan Project of the early 1940's. During and since that time the chemistry and spectroscopy of uranium and uranium compounds has been studied in great detail. It is neither practical nor desirable to attempt to catalog all of the published works which deal with uranium and its compounds; rather, the author has attempted to highlight those studies which were most pertinent to the topic considered here.

B. Interactions Of Light With UF_6

If one begins with a basic approach to spectroscopy, then the 1948 study where Bigeleisen *et al.* reported the Raman spectrum of liquid UF_6 and of UF_6 dissolved in C_7F_{16} is one of the earliest attempts at using spectroscopy to understand the properties of UF_6.[2] These authors specifically established the O_h symmetry of UF_6. In 1952, Burke *et al.* provided the infrared spectra of UF_6 vapor as additional evidence for the O_h symmetry.[3] Efforts continued which resulted in more infrared spectral data of UF_6 vapor by Gaunt[4] in 1953 and Raman spectral data of UF_6 vapor by Claassen *et al.*[5] in 1956. By 1965, Weinstock and Goodman had published their review article on the vibrational properties of hexafluoride molecules, including UF_6, in which they considered all the data which had been reported up to that date.[6] Subsequent to this time, laboratory lasers became available which ignited another series of Raman studies. In 1970, Claassen *et al.* reported the Raman spectrum of UF_6 vapor in one of the earliest studies which used the light from a laser (i.e., an Ar^+ laser).[7] Many laser Raman studies have been completed since that time with one of the most recent being by this author and coworkers in 1989.[8]

The photodissociation of UF_6 to produce UF_5 and F is a well known reaction. One of

the earliest demonstrations of this phenomenon was by Kompa and Pimentel in 1967.[9] In this experiment they devised an HF chemical laser by photolyzing a mixture of UF_6 and H_2 in a laser cavity, having recognized that UF_6 is an excellent F atom source which can readily produce HF under these conditions. The photodissociation of UF_6 is a very efficient reaction for the production of UF_5. Different fluorine scavengers have been described in the literature, with H_2 and CO being the best performers. The photolysis of UF_6 and CO mixtures, as described by Asprey and Paine[10], is an excellent method for the production of β-UF_5 and has been used in this laboratory many times. Much literature dealing with the photodissociation of UF_6 to produce UF_5 has been written over the years, but ultimately, the origins of the laser photodissociation of UF_6 into UF_5 takes its roots from the early works involving SF_6. As is often the case with an infant technology, in the early days of laser photochemistry a principal difficulty was finding an interesting sample which could interact with the available lasers. Such was the case with SF_6, which was an ideal candidate for studies with infrared CO_2 lasers (in the 10.6μ spectral region). Pioneering efforts in this field were reported by Lyman *et al.*[11,12] and by Ambartzumian *et al.*[13,14]

The laser chemistry of UF_6 begins with the multiphoton excitation (MPE) and multiphoton dissociation (MPD) processes which were demonstrated in SF_6, the basic features of which have been described in the review article by Ronn.[15] The concepts of MPE involve the absorption of infrared (IR) photons whose energy matches that of the rovibrational levels of the molecule's ground state. This is the most basic "ladder-climbing" model and it infers that after each photon absorption the energy of the next photon will match another discrete transition to a yet higher rovibrational level. The end result is a molecule which has been excited by (the absorption of) multiple photons. Anharmonicity dictates that as the ladder is climbed, there is a decreased probability that each successive level will have an available

transition with an energy identical to the first one. However, in the case of many-atom molecules there will exist, at levels of high vibrational excitation, a "quasi-continuum" of states. A quasi-continuum of states describes that energy region which is very dense with available energy states, so dense that the constraints on the energy matching of successive incoming photons are considerably reduced. The end result of MPE which produces dissociation is referred to as multiphoton dissociation (MPD); therefore, MPE simply describes how the "ladder" is climbed to result in MPD. In the case of the MPD of SF_6, the importance of the quasi-continuum is revealed in that the number of IR photons (λ=10.61μ for $^{32}SF_6$) to dissociate one fluorine atom is 35, but only the first three or four need be resonant in the rovibrational ladder. Spurred onward by the early, widely held hope that lasers could provide bond-selective excitation, enrichment of sulfur isotopes was first demonstrated using an IR MPE/MPD scheme. Indeed, the IR MPD of UF_6 was demonstrated and described as "trivial" by Tiee and Wittig[16] and was also demonstrated by Rabinowitz *et al.*[17], both in 1978. The relative ease with which sulfur isotopes were enriched using laser light from ordinary CO_2 lasers touched off intensive and widespread programs to investigate the possibilities of enriching the isotopes of uranium using lasers, due to the perceived economic benefits of using advanced laser technologies. The relative economics and merits of laser technology for uranium enrichment have been presented elsewhere and are not addressed here. The reader is referred to an early review by Jensen *et al.* for more details.[18] Typically, MPE/MPD mechanisms will not terminate from an excited electronic state using only IR photons. In most systems, reaching the excited electronic state requires the use of either visible or ultraviolet (UV) photons to achieve the rovibronic transition. Dissociation from this excited electronic state is possible. MPE/MPD schemes which use both IR and UV photons are possible as well. The laser method of choice resulting from these enrichment studies was a

combination of IR and UV photons, whereby isotope selectivity in nozzle-cooled UF_6 was accomplished with IR excitation and the dissociative step was via a UV photon to give a product of enriched $^{235}UF_5$. The use of a UV photon as the dissociative step preserves the isotopic selectivity of the IR excitation since the ground state quasi-continuum is not utilized. The topic of laser separation of isotopes, including uranium, using MPE/MPD schemes has been reviewed by Zare.[19] A sampling of the literature dealing with the photolysis of UF_6 is described in References 20-26. Curiously enough, the intense interest in this particular topic of the photochemistry of UF_6 resulted in the literature being virtually barren of any other photochemical investigations of UF_6. An exception to this is investigations in the area of laser-induced emissions and fluorescence from UF_6, such as the one by Allison.[27] An interesting consequence of his study was that when intense pulses from a nitrogen laser (λ=337.1 nm) were used to induce electrical breakdown in the UF_6 sample, the resulting emission lines were identified as arising from excited U atoms and from U^+ ions. One must note, however, that the UF_6 sample pressures as well as the laser power densities were much higher than those employed in this study. In 1980, De Silvestri *et al.* reviewed the laser induced fluorescence properties of UF_6.[28]

C. Fundamental Aspects Of Multiphoton Ionization

As is the case with uranium and its compounds, the amount of literature available on the general topic of the interactions of matter with laser light is enormous. The relatively common availability of the laboratory laser for the last two decades has caused the fields of laser chemistry and physics to mushroom at a remarkable rate. Consequently, though one may be skilled in the art, it is still essential to lay a foundation from which to begin to understand the rather complicated phenomena associated with the multiphoton ionization

(MPI) of many-atom molecules and of atoms. There are few references which adequately describe all types of multiphoton processes; however, there are many which individually describe very well the different types of processes. An understanding of the fundamentals of MPI can begin from these.

The topic of multiphoton ionization is a very complicated one even when reduced to its most basic components. Unfortunately, organic molecules are the ones most often studied and the results are not necessarily always directly transferrable to inorganic molecules, especially a heavy atom molecule like UF_6. In addition, one must eventually address the topic of multiphoton ionization of atoms and this encompasses yet another set of complexities. For the purpose of this writing, the author has borrowed the concepts and results described by Robin[29,30], Bernstein[31], El-Sayed *et al.*[32], Letokhov[33], Chin and Lambropoulos[34], and Mainfray and Manus[35] to compose a representative picture of the MPI of UF_6. MPE leading to MPI is generally depicted as either "neutral" ladder climbing or "ionic" ladder climbing and these two pathways are represented for UF_6 in Figure 1. Note that Figure 1 is drawn to scale using the U-F bond energies for the successive fragments as the levels of the neutral ladder and using the ionization potentials for the levels of the ionic ladder. The ionization potentials for UF_6, UF_5, and UF_4 are known values. The values for UF_3, UF_2, and UF are not known, but are represented by an $\approx$ 2 electron volt (eV) range where they should occur. These values can be estimated from ion appearance potentials obtained by electron impact ionization of UF_6 using known UF_x bond dissociation energies. There are some noteworthy differences in the characteristic observations associated with neutral ladder climbing and ionic ladder climbing. The parent ion, in the strictest definition, is UF_6^+; however, this ion is rarely seen even in electron impact mass spectrometry. Consequently, for the purposes of this discussion, the parent ion is UF_5^+. This is an acceptable assumption given that the difference between

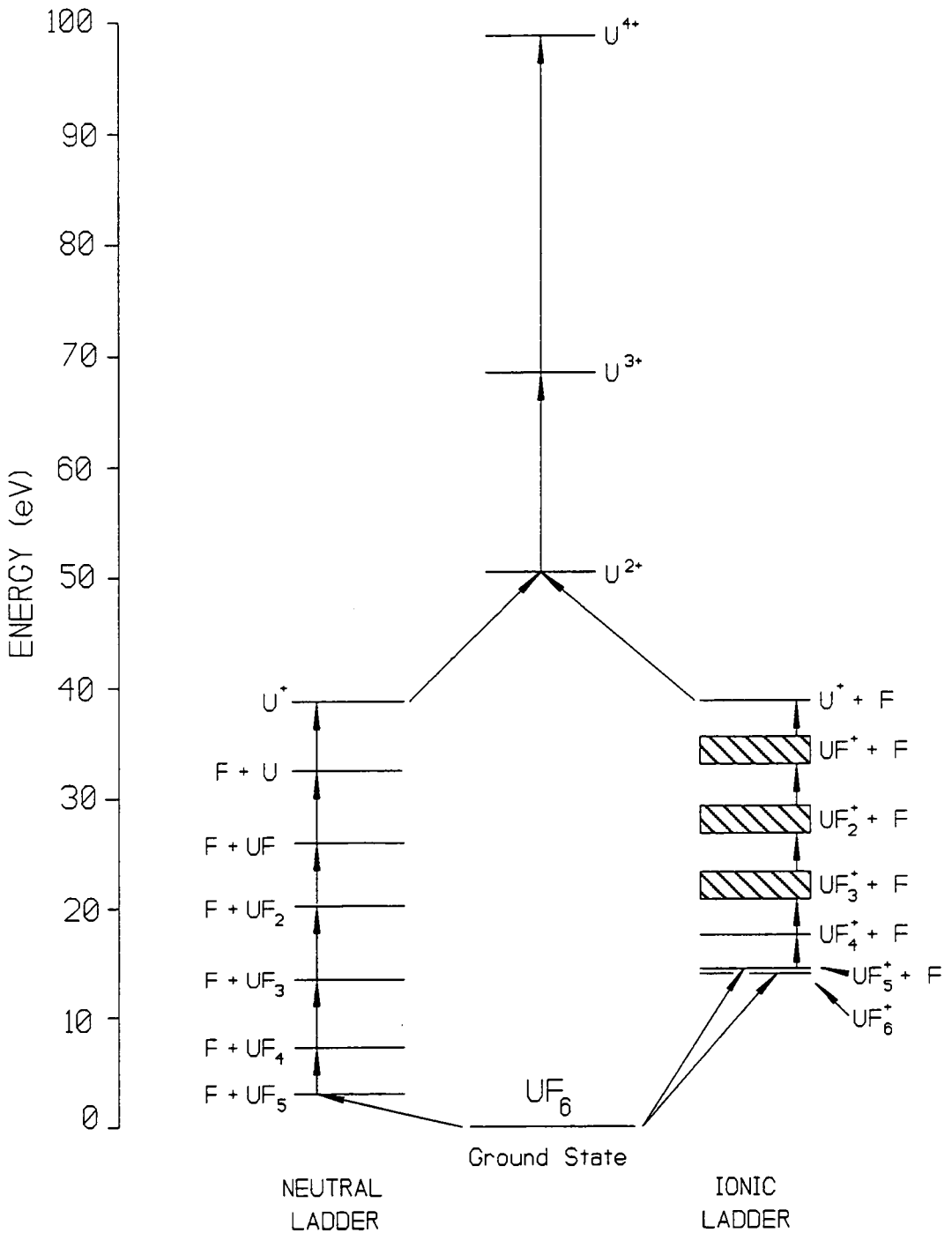


Figure 1. Possible MPI ladder climbing schemes.

the ionization potentials of UF_6 and UF_5 is only 0.25 eV. For the neutral ladder, the system is first atomized (by successive bond dissociation of F) and then ionized in the final step, producing only U^+. The MPI will show atomic resonances independent of the sample molecule and they may arise from ground or excited states of U. At high laser powers the molecular fragments can ladder-switch to the ionic ladder. For the ionic ladder, the system is ionized and then atomized (by loss of fluorines). At low powers the parent ion will dominate the mass spectrum with lesser populations of UF_x^+ (where $x \leq 4$). As the laser power is increased, U^+ dominates the mass spectrum with lesser contributions from the UF_x^+ fragments. The differences between climbing the ionic ladder at low laser powers and at high laser powers is demonstrated in Figure 2 by using a "stick" diagram. Ladder-switching to the neutral ladder at higher laser powers does not occur. There is a third method of ladder climbing which involves a "superexcited" molecular state, UF_6^{**}. In Figure 3 the features of the superexcited molecular system are superimposed on the neutral and ionic ladders (of Figure 1) for comparison. The noteworthy characteristics of the superexcited ladder are that the molecular system is atomized and ionized simultaneously, that it produces constant ratios of the various ions at all powers, and that it shows no resonances. In Figure 3, virtual states are shown to emphasize that they must be considered and a resonant state is shown because most systems will have at least one, often more; however, these states are included for illustration only and are not to scale. Likewise, the illustration of the "superexcited" is represented with an arbitrarily chosen energy. The importance of a resonance state is its longer lifetime ($\approx 10^{-9}$s) versus the "instantaneous" lifetime ($\approx 10^{-15}$s) for a virtual state. Transition probabilities are increased when resonant states are employed for the optical transitions. Multiphoton ionization which is enhanced by one or more of these states is termed a resonantly-enhanced multiphoton ionization (REMPI) process. The transition

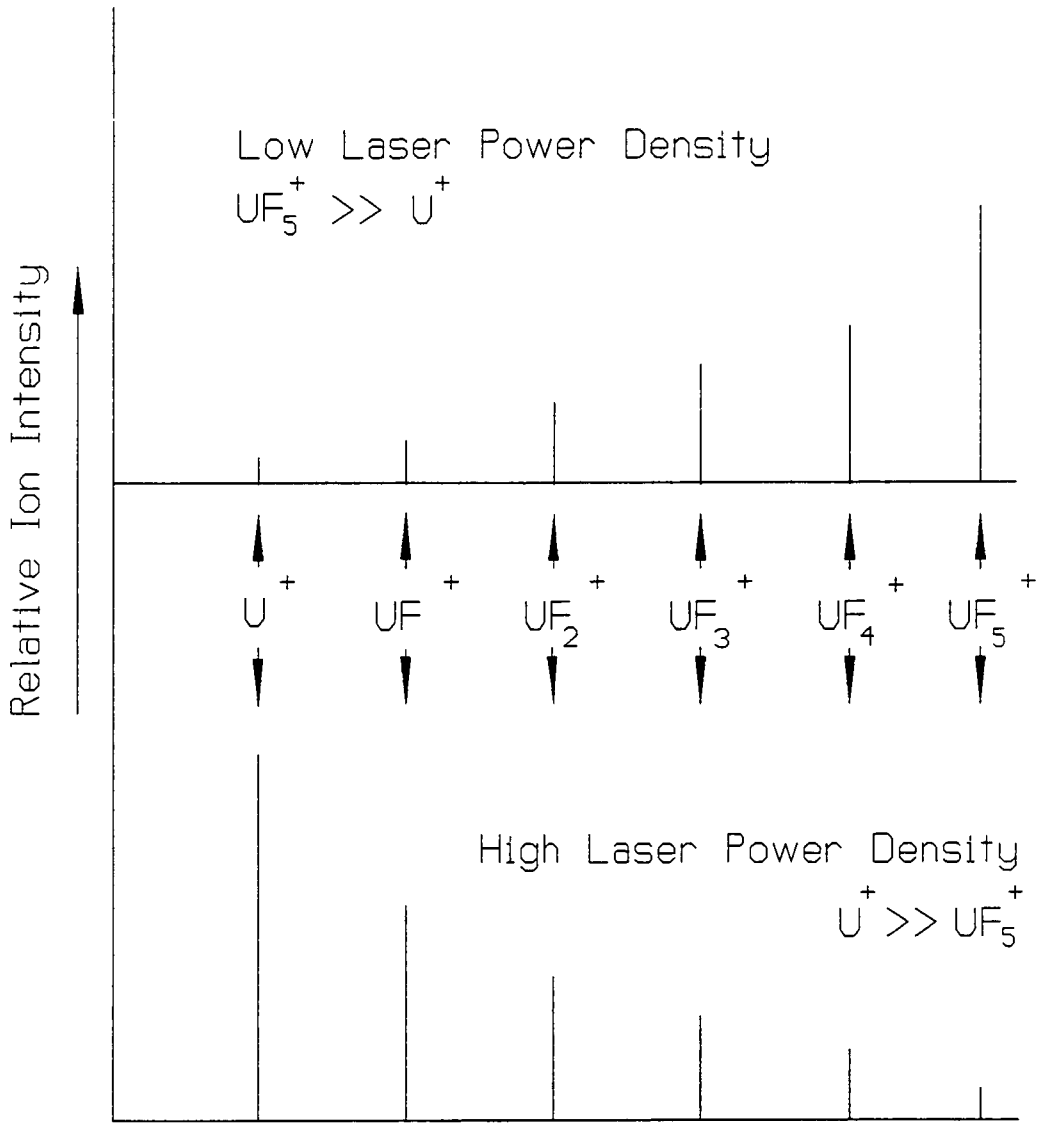


Figure 2. Ideal ionic ladder climbing.

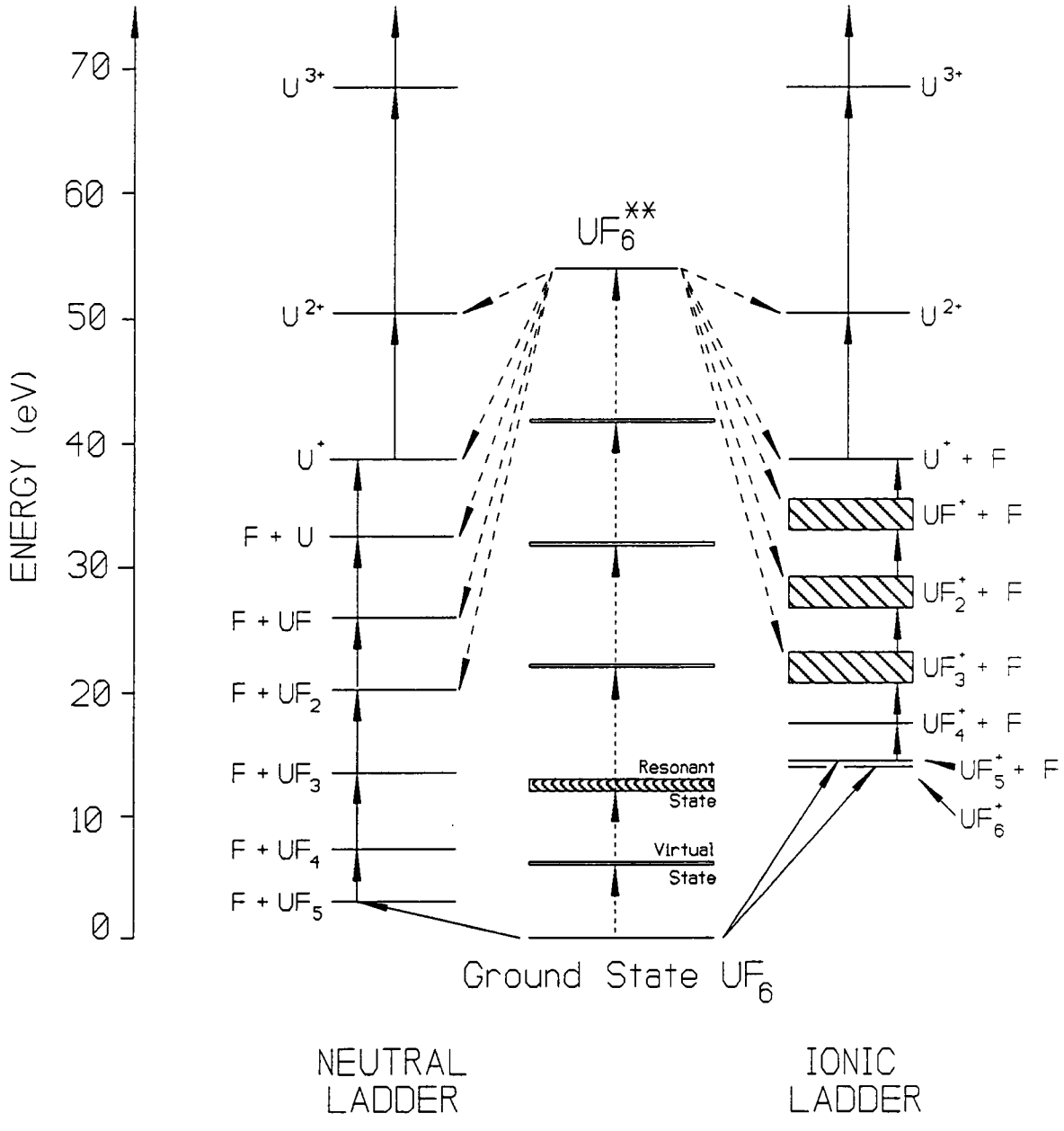


Figure 3. The "superexcited" molecular system.

probabilities for many photon processes which involve only virtual states are much smaller. For the production of highly charged uranium ions, U^{n+} (where $n \geq 2$), the MPI process can potentially be initiated from U atoms, ground state or excited, from U^+ ions, or from U^{2+} ions as well. The three mechanisms, as shown, represent the simplest summary of MPI processes. As other de-excitation mechanisms are introduced, along with potential ladder-switching and MPI of the MPI-generated fragments, the picture becomes very complicated indeed. The basic concepts, though, are very straightforward. Discussions of the data interpretation are based on the fundamentals of these mechanisms.

D. Previous MPI Studies Of UF_6

Since the development of the pulsed laser and the pulsed, tunable dye laser, there have been many experimental investigations of low laser field (e.g., $< 10^{10}$ W/cm^2) multiphoton ionization of light atoms and small molecules.[36] There is increasing interest in multiphoton ionization studies of small molecules at high (e.g., $> 10^{15}$ W/cm^2) laser fields.[37-42] The intense laser irradiation gives rise to energetic fragment ions arising from coulombic explosion of multiply charged parent molecular ions. Multiply charged atomic fragments are also observed. Laser multiphoton ionization of more complex molecules containing at least one heavy atom (M) often results in a positive ion mass spectrum containing the bare heavy ion (M^+) as the dominant ion. Interestingly enough, high laser power densities were not required to produce M^+ from highly coordinated (5-6 ligands) metal atoms. Power densities as low as the range of 10^5 - 10^8 W/cm^2 can be used. The most striking example was the production of Fe^+, Cr^+, and Mo^+ from their respective metal carbonyls by Duncan *et al.*[43] Karny *et al.*[44] and Engelking[45] have also observed this result in similar molecules where the central metal atom is surrounded by a closed shell of ligands. If the atomic number of the heavy atom is

sufficiently large such that the neutral atom posesses a large density of low-lying excited states and a correspondingly low ionization potential, the ion yield is often found to be approximately independent of the wavelength of the laser.

For the specific case of uranium hexafluoride, the author is aware of only six journal reports which address the MPI of UF_6. In 1979, Wampler *et al.* reported using a KrF laser (λ=248.4 nm) to produce photoionization in UF_6 at relatively high (0.2 Torr) sample pressures.[46] As the positive ion mass spectrum was not obtained in these experiments, the ion current arising from the MPI was attributed to UF_6. Most remarkable among these studies, and the place from which the current experiments began, is that of Stuke and Wittig who have reported multiply charged atomic and molecular ions from the MPI of uranium hexafluoride in 1981.[47] Also in 1981, Stuke, Reisler, and Wittig reported similar results for uranium pentafluoride[48]. The studies of UF_5 reported the use of one laser beam (λ=266 nm) to produce UF_5 from the photodissociation of UF_6 and a second laser (λ=532 nm) to multiphoton ionize the UF_5 photolysis product of UF_6. In both experiments, the laser power density was similar to those density ranges employed in the current experiments. Despite the low power densities employed in these studies, copious amounts of multiply charged uranium ions (U^{2+} and U^{3+}) were observed. One can estimate that U^{3+} from UF_6 requires over 30 photons at λ=532 nm. The experiments were described as "collision-free" though an effusive UF_6 vapor source was used to produce pressures of $\approx 10^{-5}$ Torr (typical). The MPI fragments were detected using a quadrupole mass spectrometer. The MPI positive ion mass spectra reported for these two experiments, one set arising from the MPI of UF_6 and one set arising from the MPI of UF_5, were nearly identical. In 1982, Wittig *et al.* published a paper which complimented the previous two, with the added features of using a TOFMS and a dye laser whose output was in the blue spectral region.[49] Rhodes *et al.* have studied multiphoton

ionization of UF_6 using a picosecond ArF excimer laser (λ=193 nm) at much higher power densities than those employed here.[50] These experiments implicitly assumed that uranium atoms were first produced by multiphoton dissociation of UF_6 followed by MPI of U atoms. Multiply charged uranium ions up to U^{10+} were observed which corresponds to the absorption of > 100 photons. The mechanisms responsible for the production of multiply charged ions in high laser field MPI is a matter of great interest and some controversy.[51] In 1985, Dore *et al.* reported on the photodissociation of UF_6 and subsequent MPI of UF_5, although the positive ions responsible for the ionization signal were not identified.[52] Instead, the presence of photoionization signal is assumed to arise from UF_5^+. These experimenters also report that the MPI signal is observed throughout the wavelength range, λ=440 - 532 nm, although the intensity falls off at longer wavelengths.

CHAPTER II

EXPERIMENTAL APPARATUS AND METHODS

A. Overview

Laser pulses were focused into a pulsed nozzle beam of UF_6, typically in a carrier gas, and the positive ions resulting from the multiphoton ionization process were mass analyzed by a linear time-of-flight mass spectrometer (TOFMS) operating under the Wiley-McLaren[53] space focusing condition. This experimental apparatus was comprised of three general parts: the laser system, the TOF mass spectrometer, and the data acquisition and manipulation system. This experimental apparatus was part of a larger laser laboratory located at the Oak Ridge K-25 Site as part of the Uranium Enrichment Organization and managed by the author. For the most part, each of the components were commercially available although each component was not necessarily new at the time the system was assembled for this work. The apparatus is described below in some detail.

B. Laser System

A pulsed, Q-switched Nd:YAG laser (Quanta-Ray DCR-2A-10) is used to produce nanosecond laser pulses of the fundamental wavelength, 1064nm. The harmonic wavelengths, 532 nm, 355 nm, and 266 nm, are produced using the harmonic generator (SHG) and the prism harmonic separator (PHS-1). The PHS unit permits the experimenter to use the beams individually or in combinations. The PHS also permits the user to select whether horizontally or vertically polarized light pulses were emitted, by appropriate changes to the internal waveplates. The DCR-2A Nd:YAG laser employed an unstable resonator design with conventional "dot" optics which produced the familiar donut-shaped spatial mode pattern.

The laser was not injection seeded; therefore, the emitted pulses were multimode not single mode.[54] The emitted beam from the laser can also be used to optically pump a pulsed dye laser to provide additional wavelengths. Two Quanta-Ray pulsed dye lasers (PDL-1's) are arranged on the optical table such that they may both be used simultaneously, one used in conjunction with a harmonic beam, or used alone as a single color excitation source. For these studies, yellow wavelengths (e.g., λ=591 nm) were produced using Kiton Red (Exciton, Inc.) laser dye in an "end pumped" configuration and blue wavelengths (e.g., λ=440 nm) were obtained using Coumarin 440 (Exciton, Inc.) laser dye in a "side pumped" configuration. Both dyes were mixed, using methanol as the solvent, in accordance with the recommended molar concentrations found in the Quanta-Ray PDL-1 dye laser owner's manual. Hardware and instrumentation limitations prevented actual measurements of the percentage of the dye laser pulse power which could be attributed to amplified spontaneous emission (ASE), but it was believed to have been minimized.[55] The dye lasers are fitted with stepper motor controls, constructed in-house, such that the wavelength may be scanned in a controlled fashion, though they are not computer controlled nor synchronized to the laser pulse. The optical pathways between the dye lasers and the vacuum chamber counter-propagate and are nearly identical, their pathlength differing by about 12 nanoseconds, as measured by a Scientech model 301-020 high speed photodiode detector. Low laser power measurements were made using a Scientech disc calorimeter model 372 power/energy meter with a 36-0001 surface absorbing head. Higher laser power measurements were made using a Coherent model 210 power meter. Power densities at the sample focal volume were varied using the appropriate combination of oscillator (or amplifier) lamp energy adjustment, Q-switch delay, quartz plate stacks, and lens focal length. The quartz plate stack could be varied to contain from 0 to 26 plates, which permitted stepwise variations in the beam transmission ranging from 100% to

24% of the incident beam (presuming uniform surface losses per plate). When the plate stack was used for attenuation, power densities were obtained by measuring the initial power and calculating the resultant power reduction as quartz plates were added into the beam path. This proved to be a valid approximation, as indicated by the comparison of calculated vs. measured beam power as shown in Figure 4. Three UV-grade fused silica lenses were individually employed to vary the focal volume. A 7.5-cm focal length lens was "permanently" mounted inside the vacuum chamber along optical path "A" via an externally adjustable positioner. The 35-cm focal length lens or the 50- cm focal length lens was positioned outside of the chamber along the second optical path, "B". Uncoated UV-grade fused silica right angle prisms were used to direct the laser beams into the sample interaction region. A number of iris diaphragms appropriately placed in the beam path serve to assist in rapid coarse alignment when changing beams and to reduce spurious beam reflections. Power density calculations were corrected for any turning prisms, lenses, or chamber windows through which the beam travelled.

C. Time-Of-Flight Mass Spectrometer

The time-of-flight mass spectrometer (R. M. Jordan Co.) consisted of a flight tube assembly which was 138.9 cm long from the centerline of the photoionization region to the face of the first microchannel plate (MCP) of the detector. The drift region (137 cm long) was fitted with a pair of X and Y steering plates to provide for two-dimensional steering of the ions to correct for the initial perpendicular direction of the nozzle jet's pulse. The detector was comprised of a pair of Varian VUW-8900ES microchannel plates in a Chevron arrangement.[56] The accompanying power supply was capable of applying variable voltages ranging from 0 to +4500 V to the repeller plate (VA1) and to the extractor plate (VA2),

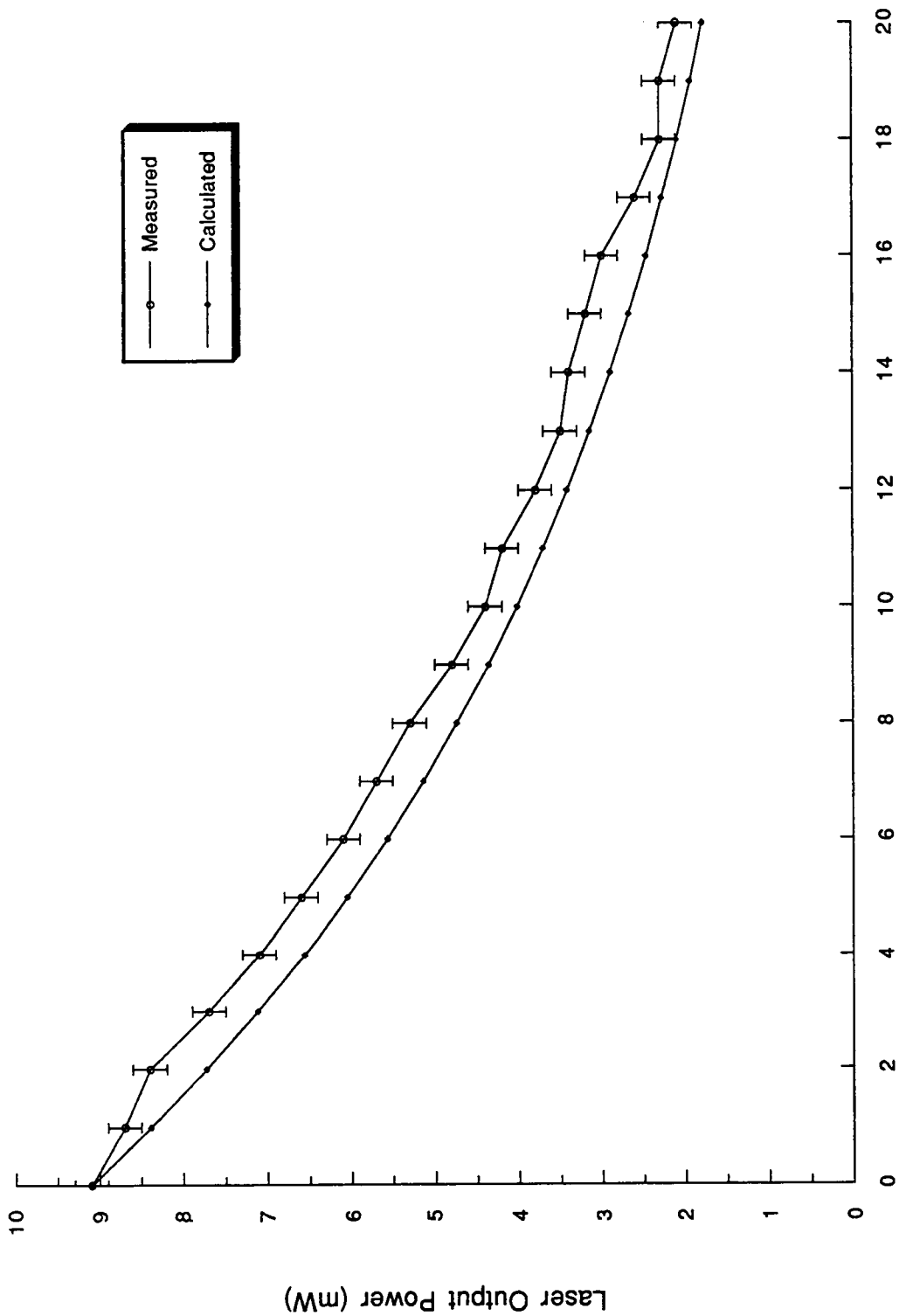


Figure 4. Beam attenuation using quartz plates.

from 0 to +/-250 V to the steering plates, and from 0 to -2200 V to the first detector plate (VD1). By design, the second microchannel plate voltage (VD2) was regulated by the power supply to 54.5% of that of VD1 and the third plate (VD3) was regulated to 9.1% of VD1. Details of the TOFMS are depicted in Figure 5. Signals from the microchannel plate detector were routed through an EG&G Ortec model 9301 fast preamplifier attached directly at the exit connection of the flight tube in order to minimize "ringing" in the TOF mass spectra. The flight tube assembly was mounted onto one 10-inch diameter flange of a 6-way Conflat™ cross such that the centerline of the TOF photoionization region was at the center of the vacuum chamber. The correct experimental geometry required that the laser pulse, gas pulse, and the flight tube be orthogonal; therefore, the orientation of the components was such that the flight tube is mounted vertically along the z-axis which allows the counter-propagating laser beam paths to travel along the y-axis. The pulsed molecular beam valve was a Lasertechnics model LPV with a model 203B valve driver. The LPV was located approximately 42 mm from the center of the ion drawout region of the TOF flight tube assembly and had a 0.1 mm orifice. The nozzle jet was directed along the x-axis of the vacuum chamber towards the turbomolecular pump. The gas pulse was synchronized to the laser pulse in order to overlap the laser pulse at the center of the TOF ion drawout region to provide maximum MPI signal. Vacuum service was provided to the chamber by a Leybold-Heraeus vertical pumping system comprised of a TMP220CF turbomolecular pump, NT220 frequency converter, D4A rotary vane pump, and their associated hardware. The unrestricted pumping speed was rated at 220 liters sec^{-1}. The pumping system was connected to the vacuum chamber with a 6-inch Conflat™ "tee" (connected along the x-axis) and could be isolated from the main chamber using a 6-inch gate valve. Typical background chamber pressure was 8 x (10^{-9}) Torr as measured by a Granville-Philips model 274003 ionization

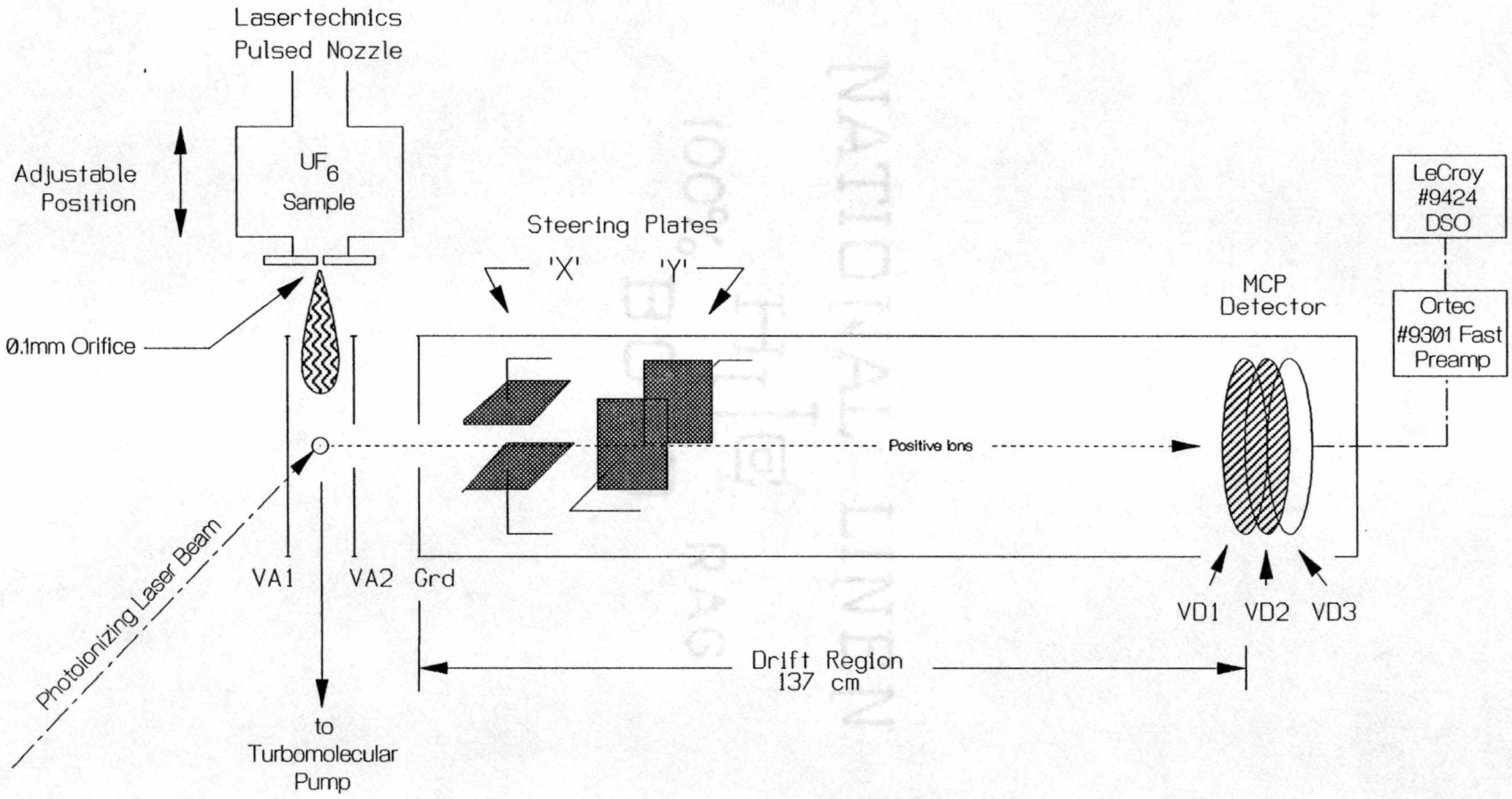


Figure 5. Time-of-flight mass spectrometer details.

gauge. Typical average background pressures during operation of the pulsed valve were 2 - 6 x (10^{-6}) Torr. Although neat UF_6 could be used, samples were typically prepared by mixing a small percentage of UF_6 with an excess of carrier gas (Xe, Ar, SF_6, or CO, all by Matheson Products). Xenon was chosen as a carrier gas so that it could serve the dual purpose as a mass calibrant for the TOFMS and for wavelength calibration of the dye laser as well. The xenon/UF_6 mixture routinely employed was 7.3% UF_6. The UF_6 sample was from laboratory stock with an assay of 99.86% $^{238}UF_6$. Samples were introduced to the reservoir of the LPV by a separate gas handling vacuum manifold to achieve a typical backing pressure of 20 - 45 Torr. Passivation of the backing systems and LPV was carried out using low pressures of fluorine gas at room temperature for brief periods. Use of a pulsed valve and low backing pressures allowed only a small gas loading of the system and helped to extend the operating life for those components whose performance might have been degraded by exposure to corrosive gases. In fact, after over two years of service the MCP detector has yet to require service and the pulsed valve poppet required servicing only after 18 months of regular use. A representative calibration of the TOFMS using the positive ions, H^+, C^+, N^+, NH^+, NH_2^+, NH_3^+, U^{3+}, U^{2+}, Xe^+ (7 isotopes), U^+, UF^+, UF_2^+, and UF_3^+ is shown in Figure 6. Ammonia was added to provide the source for H^+ and NH_x^+ ions. The source of the mass peak belonging to C^+ was the very low concentrations of pump oil which were present initially. By installing a foreline trap, signals arising from the low concentration, residual pump oil were eliminated. The presence of multiply charged ions required that the responsivity of the MCP detector be examined carefully to preclude the possibility that the U^{2+} ion signals were dominant simply because they were twice as energetic as the U^+ ions. A pulse height comparison was made by statistically analyzing the detector response for a collection of single laser shots. Low power laser pulses were used to avoid producing multiple

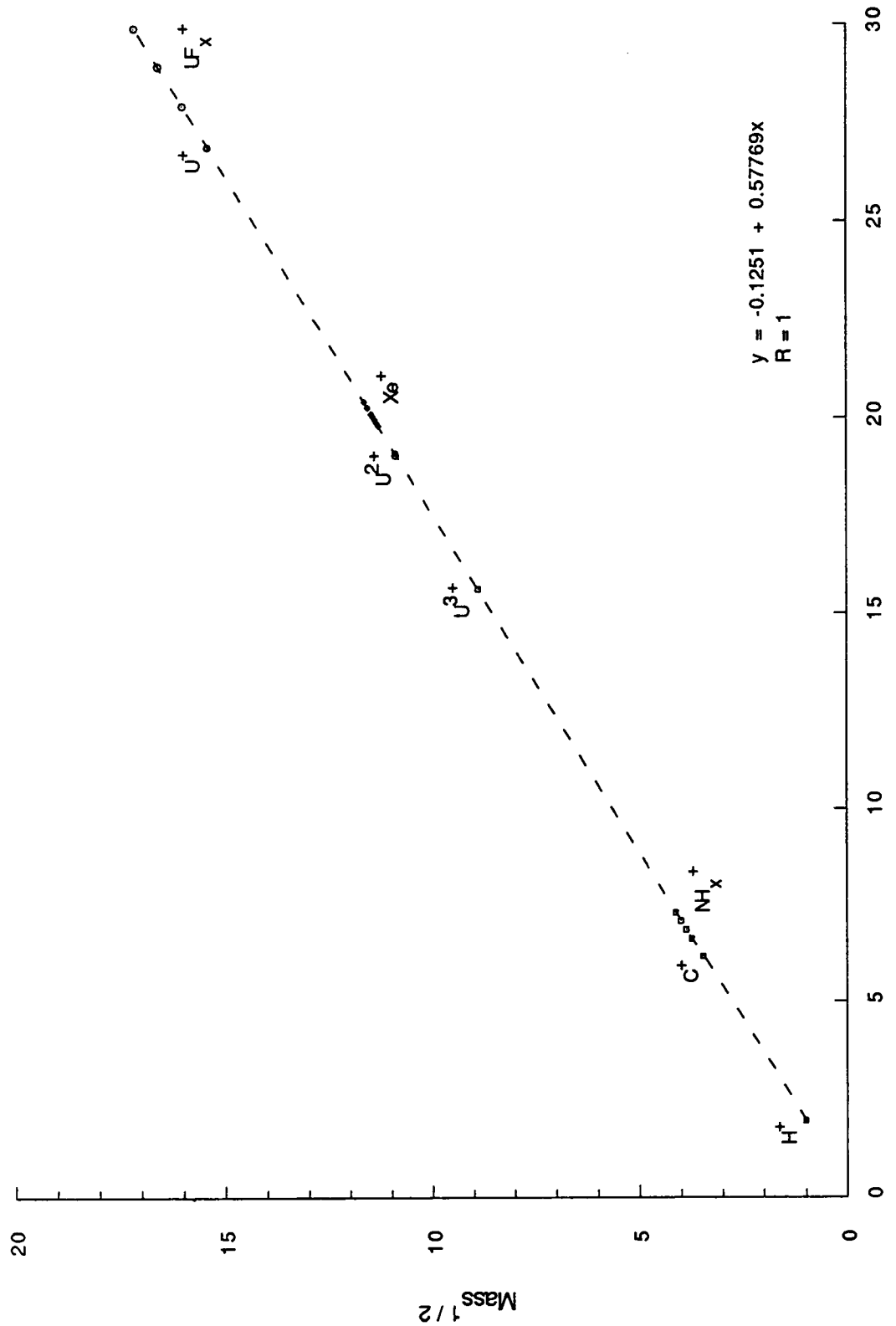


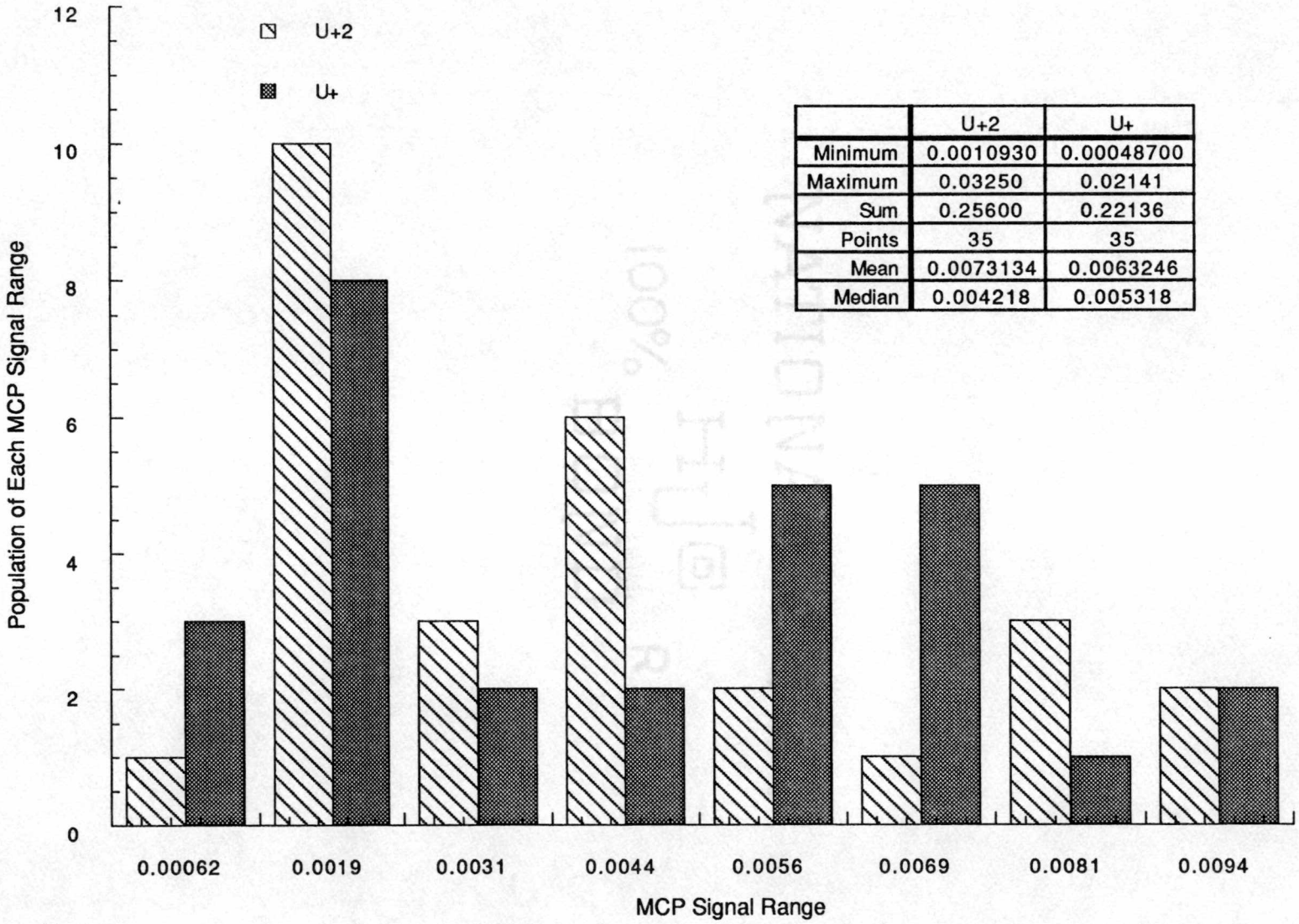
Figure 6. Time-of-flight mass spectrometer calibration.

ions having the same mass/charge ratio. The pulse height analysis for n=35 laser shots is shown in Figure 7. For each MCP signal range (i.e., voltage produced from the impinging ions), the ion populations for U^{2+} and U^{+} were tabulated for comparison. It was not possible to say with certainty that each shot only produces a single ion of each type; however, one might certainly suppose that the probability of single ion events was more plausible at the lowest MCP signals. With this in mind, the fact that the lowest signal ranges were approximately equally populated confirmed that the detector response was not biased toward the multiply charged species. Additional assurance could be found in the fact that the mean and median values for U^{2+} and U^{+} were essentially equivalent.

The requirements for mass resolution for this experiment were not stringent. Since the xenon isotopes are separated by at least 1 amu, the required mass resolution, using the $m/\Delta m$ relationship, needed only to be $\approx$ 130. However, when the actual resolution was measured the performance was much better. Consider, for a typical U^{+} mass peak at 27.919 μsec flight time with a FWHM value of 36 nsec, then the $t/\Delta t$ relationship gives a value of 775. Since $t/2\Delta t = m/\Delta m$, then the measured mass resolution is $\approx$ 387. Under the conditions of these experiments, the Xe^{+} isotopes and ions resulting from $^{235}U^{n+}$ and $^{238}U^{n+}$ were completely resolved.

D. Data Acquisition System

Data acquisition and manipulation were carried out by routing the output of the MCPs (via the fast preamplifier) to a LeCroy 9424 digital storage oscilloscope (DSO), or "transient digitizer". The resident waveform processing software of the LeCroy 9424 provided the experimenter with extensive capabilities for data accumulation and representation. Typically, one mass spectrum, i.e. signal intensity (in volts) vs. ion flight time (in microseconds), was an



	U+2	U+
Minimum	0.0010930	0.00048700
Maximum	0.03250	0.02141
Sum	0.25600	0.22136
Points	35	35
Mean	0.0073134	0.0063246
Median	0.004218	0.005318

Figure 7. MCP detector responsivity.

average of 1000 laser pulses, where each laser pulse triggers a separate photoionization and detection event. The trigger sequence was initiated by the Nd:YAG laser oscillator pulse which was used to trigger the molecular beam valve driver. The driver opened the pulsed valve and pulsed the sample gas towards the centerline of photoionization region of the time-of-flight mass spectrometer. The laser Q-switch pulse, which follows the oscillator pulse, was used to trigger the LeCroy DSO for capture of the detector signals. An example of the measured trigger sequence is shown in Figure 8. By measuring the elapsed times of the events occuring during the pulse sequence, the gas velocity can be estimated with reasonable confidence since the distance traveled (by the gas pulse) from the nozzle to the centerline of the TOFMS was measured (42mm) and the time required was 179 μsec. The calculated velocity, ν, is 235 m/sec. Haberland *et al.*[57] show that the velocity is related to the temperature,T, along the streamline of the expanding gas by the equation

$$c_pT_0 = c_pT + (\tfrac{1}{2})m\nu^2, \qquad (1)$$

where c_p is the specific heat at constant pressure, T_0 is the gas reservoir temperature (298 °K), m is the mass of the carrier gas (xenon), and ν is the measured velocity. For a monoatomic gas such as xenon the heat capacity, c_p, is given as (5/2)k, where k is the Boltzmann constant. Solving for T_0 gives a gas pulse temperature of $\approx$124 °K. At this temperature the vibrational and rotational temperature of the UF_6 are reduced.

When required, a Stanford Research Systems (SRS) gated integrator ("boxcar") could be used to acquire data as well. The "boxcar" was comprised of a SR280 system mainframe and display unit, a pair of SR250 gated integrators, a SR200 gate scanner, a SR235 analog processor, a SR245 computer interface, and the SR270 data acquisition program. The SRS "boxcar" system was especially useful for acquiring spectra while the wavelength was being slowly scanned. An example of the type of data which could be acquired with the "boxcar"

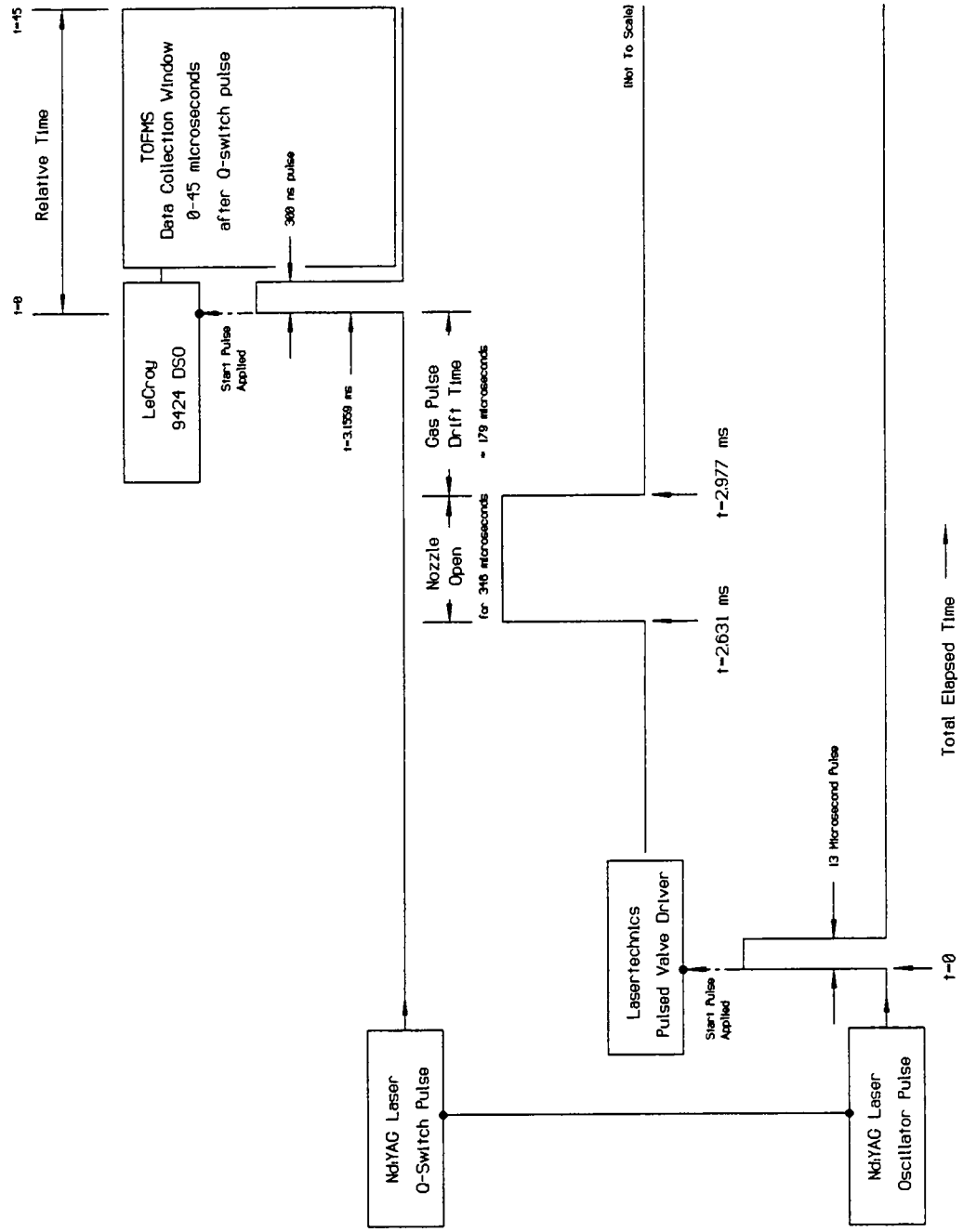


Figure 8. Trigger sequence.

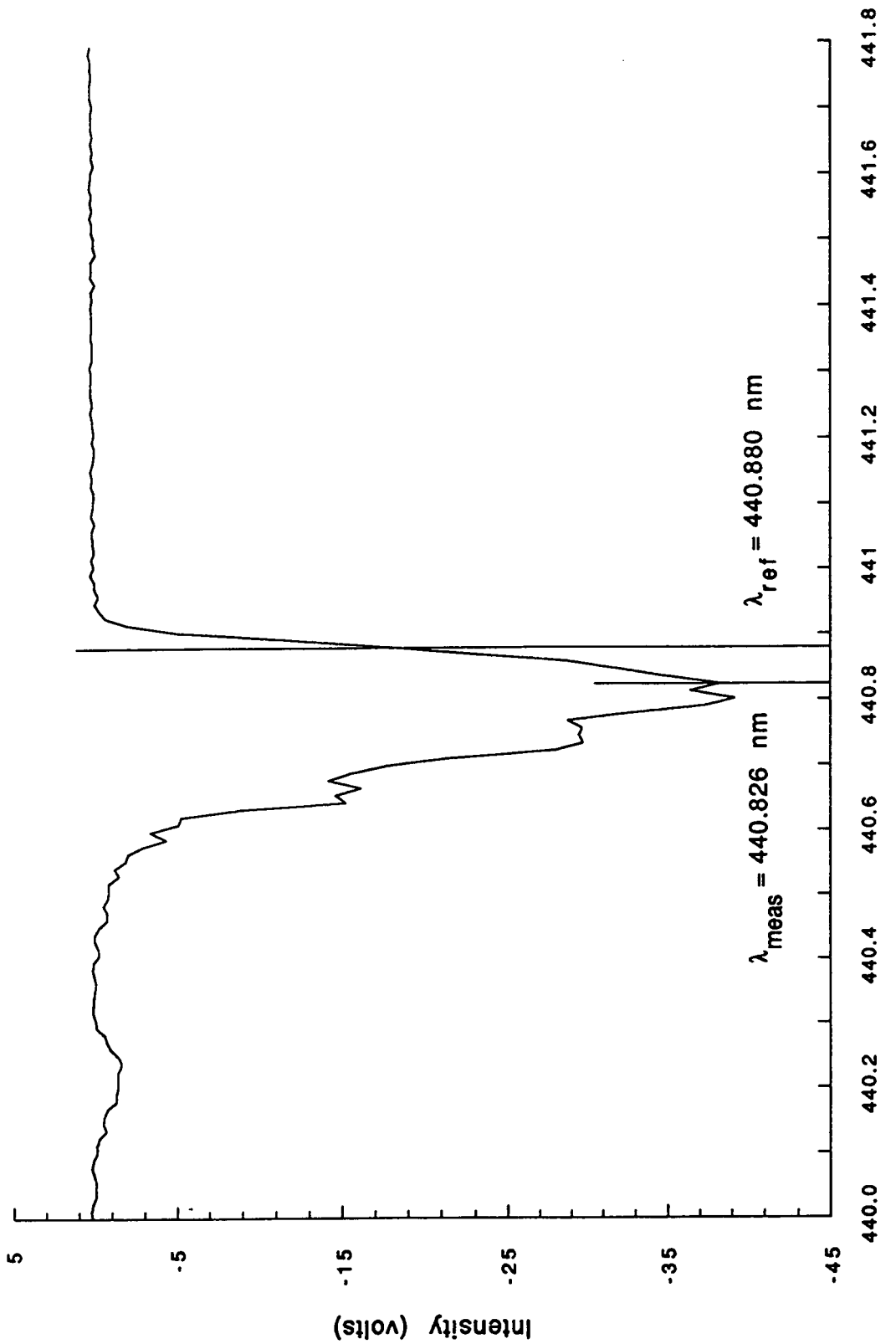


Figure 9. Dye laser calibration using xenon resonance.

is shown in Figure 9. In this figure, the calibration of the PDL-1 dye laser was confirmed by scanning the dye laser wavelength in the region of the three photon allowed $6s[3/2]_1$ resonance of xenon while the "boxcar" window was fixed on the $^{129}Xe^+$ photoionization signal. This resonance was employed for the (3+2) REMPI of xenon and the calculated wavelength for this transition was λ=440.880 nm. The wavelength dependence of the Xe^+ signal exhibits the well known AC-stark shift broadening to the short wavelength side of the resonance. This "power broadening" is very pronounced at high laser powers. The spectrum shown in Figure 9 was acquired at a relatively low power in order to minimize this broadening effect. For this case of low laser power, the agreement between the measured wavelength and the calculated value was quite satisfactory. Both the LeCroy "transient digitizer" and the SRS "boxcar" were interfaced to a Compaq 386/20e computer for local data storage and manipulation using LabCalc software (Galactic Industries). The Compaq 386/20e was connected to a local-area-network based on a VAXstation 3100 model 38 (Digital Equipment Corp.) for archiving the data at a central location while permitting manipulation and examination at remote locations. The important features of the MPI-TOFMS system utilized at the Oak Ridge K-25 Site is shown in Figure 10.

E. Photoelectron Spectrometer

The observation of the dominance of the multiply-charged U ions was quite surprising, so surprising in fact that the decision was made to verify them using a different apparatus. The second apparatus had a nearly identical laser system with the added advantage of deeper UV capabilities, but used a reflectron TOFMS rather than a linear TOFMS. The other very important advantage was the availability of an electrostatic energy analyzer (in the same vacuum chamber as the reflectron) with which photoelectron spectra could be obtained. The

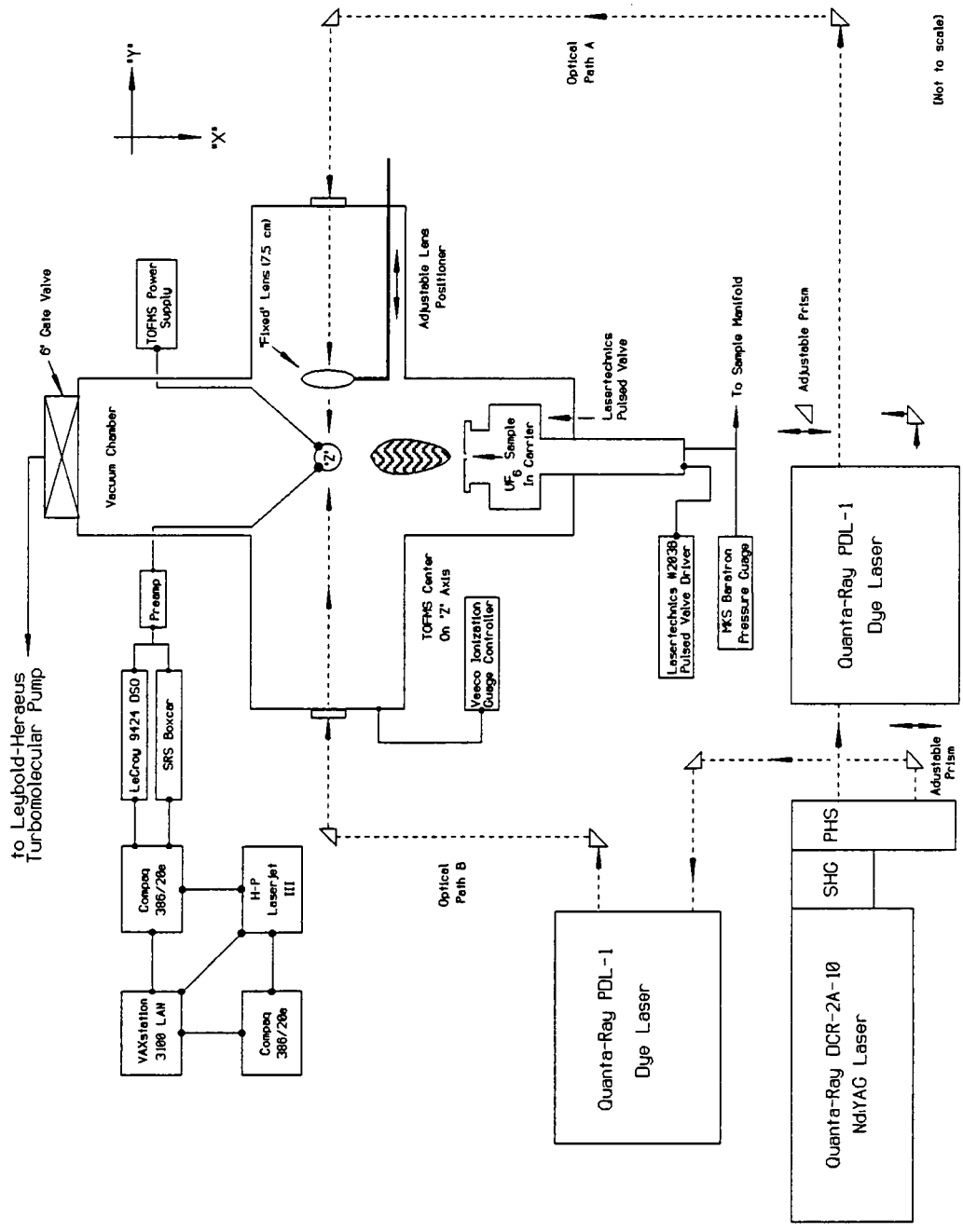


Figure 10. MPI-TOFMS experimental apparatus.

potential for complimentary data, in the form of photoelectron spectra, was a useful addition and the experiments were carried out accordingly. The photoelectron spectrometer (PES) system utilized in these experiments was located at the Oak Ridge National Laboratory as part of the Health and Safety Research Division (Chemical Physics Section) and managed by Robert N. Compton. Though the apparatus has been thoroughly described elsewhere it is summarized here for completeness.[58-60]

A pulsed laser system, an electrostatic energy analyzer (for the detection of electrons), a reflectron TOFMS (for the detection of positive or negative ions), a pulsed valve and detection electronics were the five basic components of the PES system. The laser system is virtually identical to the one employed in the aforementioned section B. A Quanta-Ray DCR-2A Nd:YAG laser, with a more variable repetition rate, was used to optically pump a Quanta-Ray PDL-2 pulsed dye laser. UV light pulses, other than the standard λ=266 nm fourth harmonic, were generated by using a Quanta-Ray WEX-1 wavelength extender to frequency double the PDL-2 output. The WEX could also be used to frequency mix the dye laser output with the Nd:YAG fundamental wavelength (λ=1064 nm). The resulting laser pulse was tightly focused in the sample region of the energy analyzer (and the TOFMS) using a short focal length lens. The sample gas, also a xenon/UF_6 mixture, was admitted into the same sample region orthogonal to the incoming laser beam via a Lasertechnics pulsed nozzle (model LPV with a model 203B valve driver). The reflectron TOFMS differs from a linear TOFMS in that the drift tube is folded (which permits compactness) and fitted with a grid biased to reflect the charged particles in the nearly opposite direction towards the MCP detector. The reflectron TOFMS is widely used to increase the mass resolution by compensating for the effects of the spread in initial velocity upon the arrival time distribution. In this particular case, the reflectron was used to obtain a resolution of $m/\Delta m \approx 300$ in a

small space.

The photoemitted electrons were passed through a three element einzel lens (at the entrance aperature) and detected by a double-focussing, 160° spherical sector electrostatic energy analyzer fitted with a MCP detector. The electrons can either pass into the entrance of the energy analyzer under their own velocity or be accelerated into the entrance aperture using a small "push" voltage. Since the electrons of all energies gain the same amount of energy (imparted by the "push" voltage), the energy spectrum of the electrons is simply shifted up by a constant amount. This is especially useful when the electrons are initially produced at low energies, as was observed to be the case for UF_6. For these experiments, the signals from the reflectron TOFMS were routed to a LeCroy 9410 DSO and could be captured and plotted on a Hewlett-Packard Colorpro plotter. The signal from the electrostatic energy analyzer was routed to an EG&G Princeton Applied Research #162 boxcar, stored and manipulated on a PC, and could be plotted on the Colorpro plotter. The important features of the MPI-PES system are shown in Figure 11. In addition to the previously mentioned capability of the PHS unit to internally alter the beam's polarization, waveplates could also be used to produce circularly polarized light by externally placing them in the beam path. Three zero-order, quarter waveplates (CVI, Inc.) were obtained which were anti-reflection (AR) coated for each of the three Nd:YAG laser harmonics. These waveplates permitted the comparison of the effects of linearly vs. circularly polarized light on the MPI signals for each of three wavelengths.

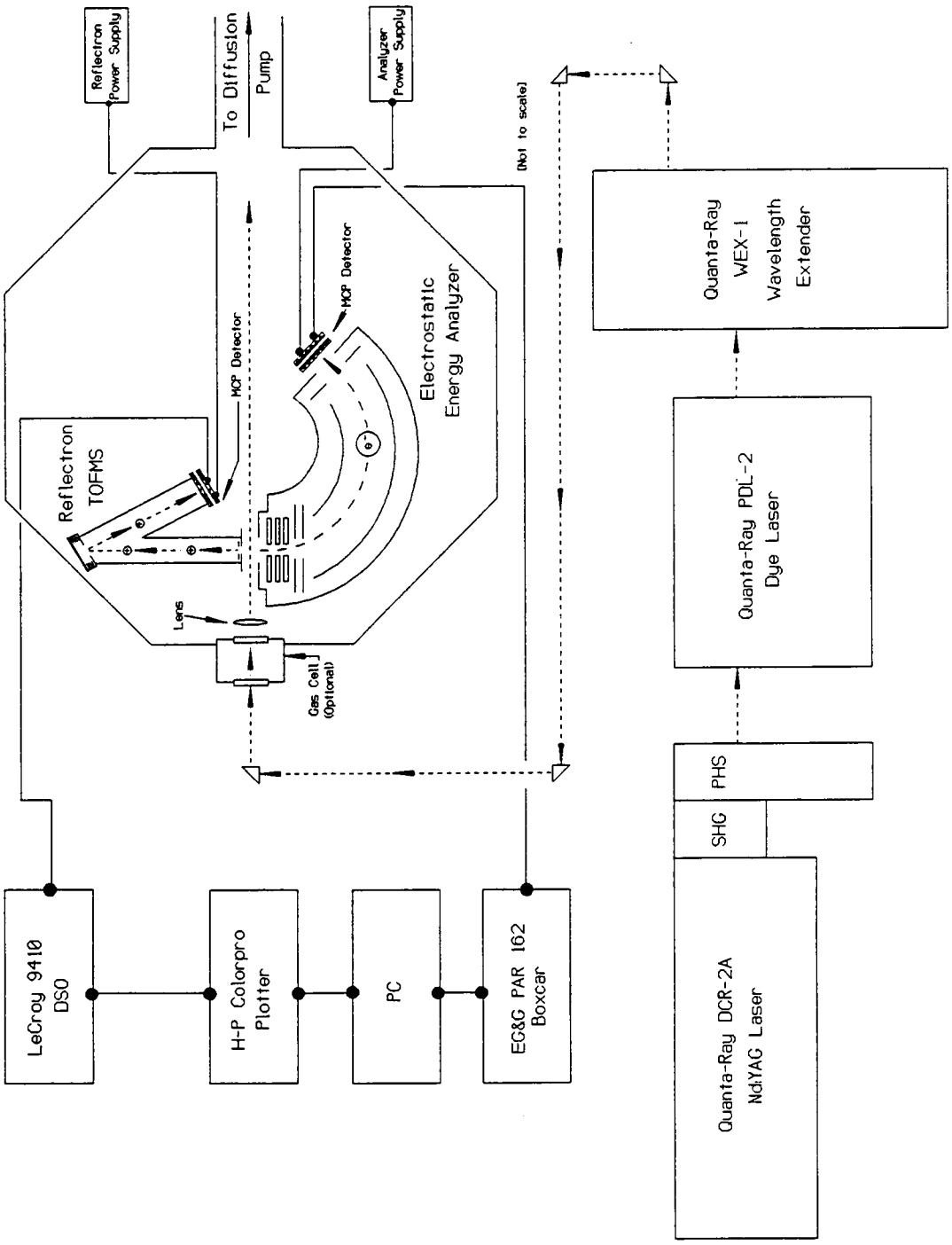


Figure 11. MPI-PES experimental apparatus.

CHAPTER III

RESULTS

A. Overview

This paper presents a detailed, systematic study of the positive ion mass fragments generated from UF_6 by single color, multiphoton ionization under a wide range of laser power and wavelength conditions. The data is presented in order of decreasing wavelength. Since one of the initial aims of the experiments was to determine the effectiveness of UV light for the MPI of UF_6, the data collection and treatment is extensive for results using λ=266 nm light. These results were the most interesting because of the extremely low powers with which data could be acquired. UV MPI should be the simplest scheme to understand since fewer photon absorptions are involved in the ionization. In addition to the Nd:YAG laser fundamental and its harmonics, MPI results were obtained using the PDL-1 dye laser for $\lambda \approx 440$ nm and $\lambda \approx 591$ nm. All MPI spectra shown were obtained using the apparatus described in chapter II, sections B, C, and D unless otherwise noted and all samples are 7.3% UF_6 in xenon unless stated otherwise.

B. MPI Results Using The Nd:YAG Laser

The MPI of UF_6 can be observed with the fundamental wavelength of the Nd:YAG laser (λ=1064 nm). Figure 12 shows the MPI mass spectrum obtained using this wavelength. As no published MPI spectrum of UF_6 using λ=1064 nm light has been located, this is believed to be the first of its kind. To achieve MPI at this wavelength requires using the highest output power available from the Nd:YAG laser (at this wavelength). In the case of Figure 12, the power density is estimated to be 7.6 x (10^{12}) W/cm^2 using the internally

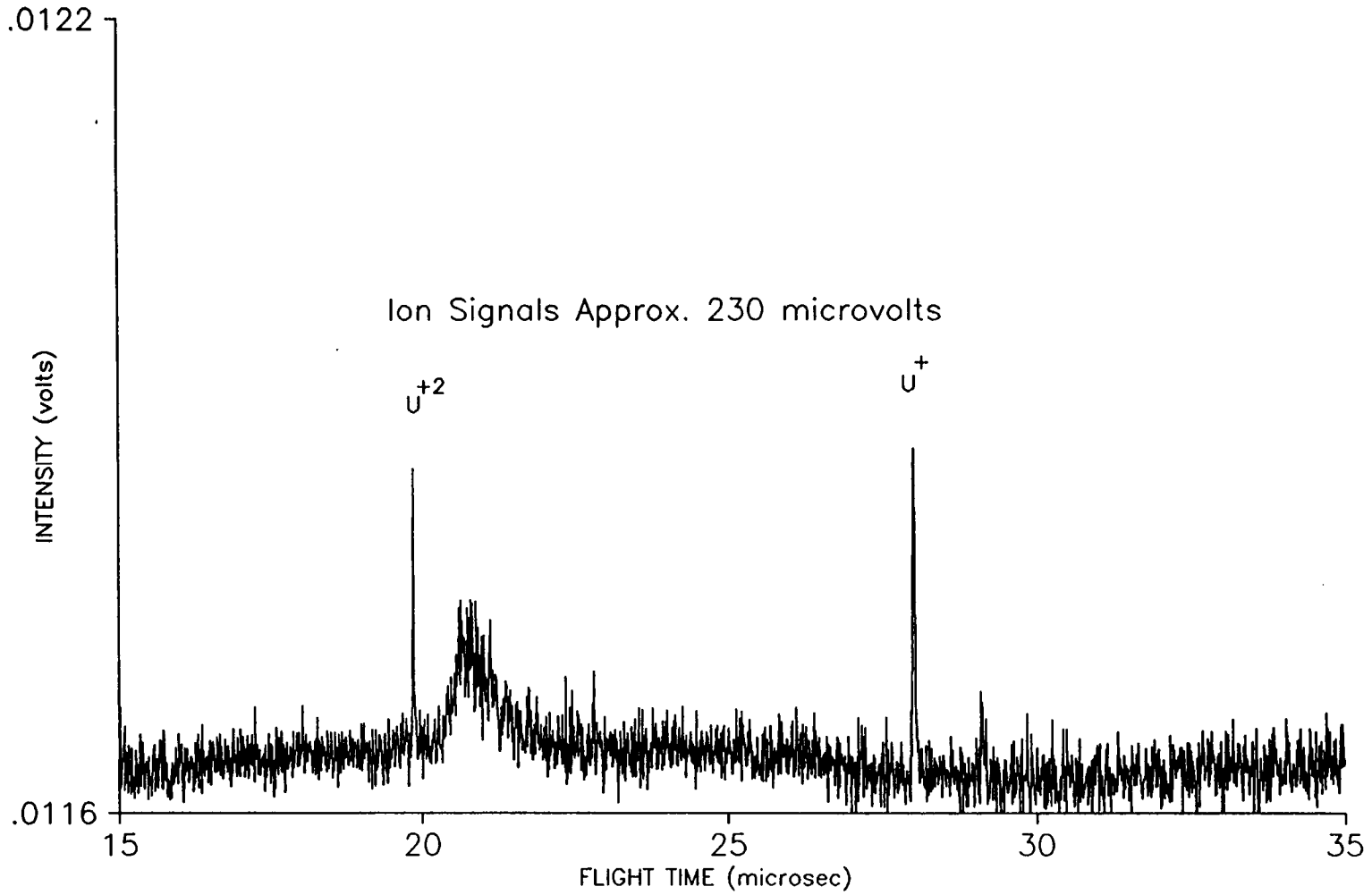


Figure 12. MPI mass spectra using λ=1064nm.

positioned 7.5-cm focal length lens. Even at these high powers the signal intensity is very low, only a few microvolts. The signal arising from U^{2+} and from U^{+} are clearly seen, but the signal originating in the mass region of xenon is unresolved indicating that xenon does not effectively undergo MPI at this wavelength, although Xe only requires 11 photons in order to produce Xe^{+}. The production of U^{2+} at this wavelength corresponds to the absorption of at least 44 photons.

In the case of data taken with λ=1064 nm the laser is operated at the full output power available and the shortest focal length lens used. Considerably more latitude in power levels are available when the second harmonic (λ=532 nm) of the Nd:YAG laser is used due to the focusing properties of the quartz "fixed" lens and the increase in absorption cross section for green light (vs. infrared). In Figure 13, the MPI mass spectra are shown in three dimensions. The measured ion signal intensity is along the z-axis, the ion flight time is along the x-axis, and increasing laser power is shown along the y-axis. For clarity, the spectra are evenly spaced as they are stacked along the y-axis. The power density range covered in this figure is 1.13 x (10^{12}) - 1.34 x (10^{13}) W/cm^2, which corresponds to a range of 50 - 600 mW exiting from the prism harmonic separator of the Nd:YAG laser. Notice that for the highest power density the signal arising from U^{2+} has saturated and MPI signals from Xe^{+} are observed. There is very little ion signal from UF_x^{+} fragments. The production of U^{2+} at this wavelength requires the absorption of at least 22 photons. It is also noted that the polarization of the incoming laser pulse does not alter the mass spectra. Vertically polarized light, which is parallel to the TOFMS drift tube, and horizontally polarized light, parallel to the gas pulse direction, both give the same results. These tests were performed to examine the potential effects of the ion draw-out field on the MPI. For example, if highly excited states were being field ionized by the draw-out field one would expect a dependence of the laser polarization

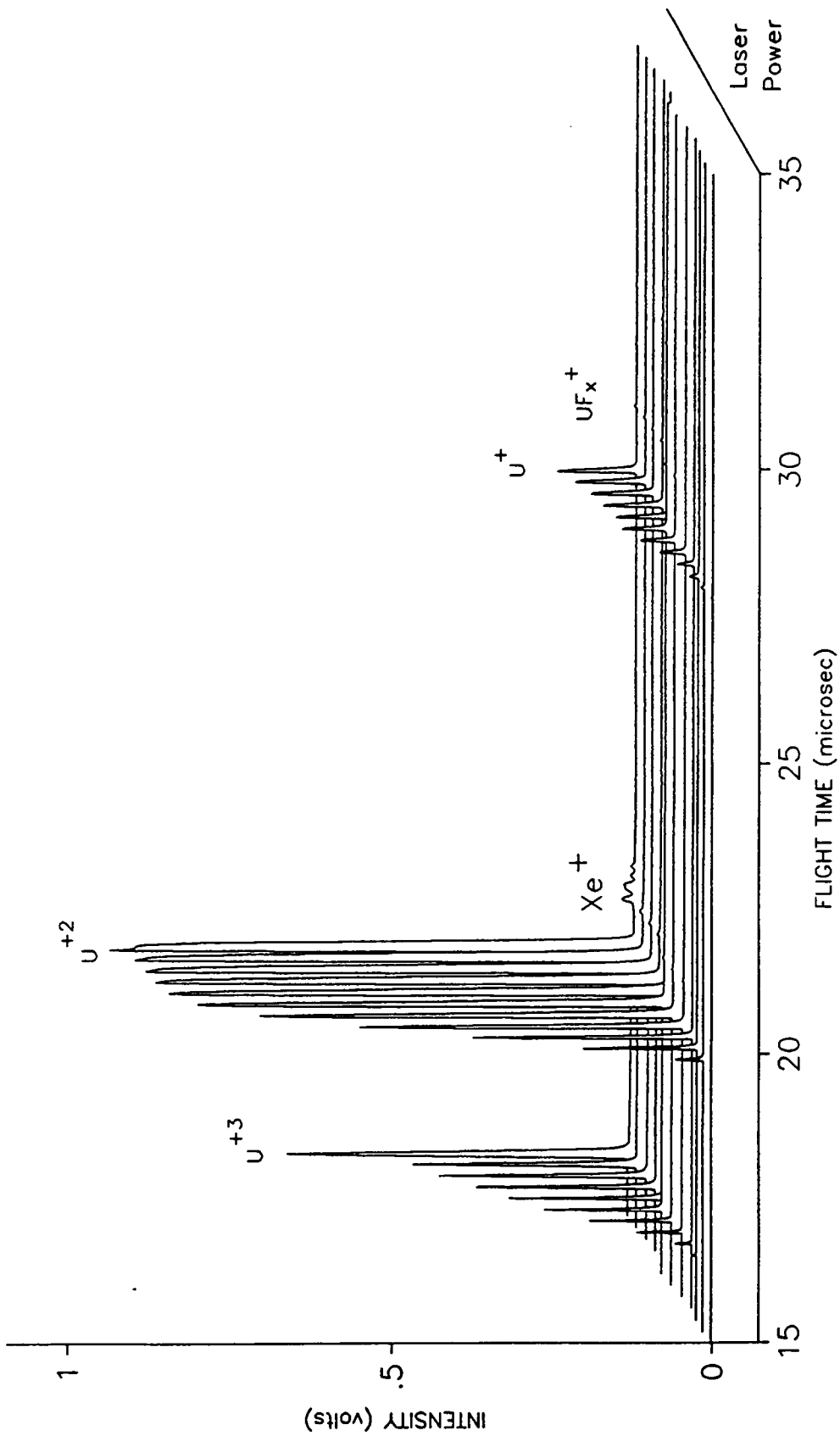


Figure 13. MPI mass spectra using λ=532nm.

on the draw-out field direction. The pressure in the vacuum chamber was typically 5.0 x (10^{-6}) Torr with a nozzle backing pressure of $\approx$ 18 Torr.

The next wavelength to consider is the ultraviolet third harmonic of the Nd:YAG laser, λ=355 nm. In Figure 14, the MPI data are shown for this wavelength. The power density range is calculated as 9.5 x (10^{10}) - 4.4 x (10^{12}) W/cm^2 which corresponds to an emitted laser power of 1.6 - 75 mW. The ion signal from U^{2+} begins to saturate at $\approx$ 8.5 x (10^{11}) W/cm^2, which corresponds to only 15 mW of emitted laser power. Typical sample pressures were 1.9 x (10^{-6}) Torr with a nozzle backpressure of $\approx$ 20 Torr. Note that the signal attributed to UF_x^+ fragments does not increase at low power densities and remains in a reasonably constant proportion to that of U^+ and U^{2+}. Again, the use of horizontally or vertically polarized light does not affect the resulting MPI mass spectra.

The fourth harmonic of the Nd:YAG laser corresponds to λ=266 nm. For the present applications, this wavelength was by far the most studied. It was previously pointed out (page 11) that interactions of molecules with high laser fields (> 10^{15} W/cm^2) is an area of great interest. Regrettably, the laser system used in this study is not capable of producing such power densities. In addition, if MPI product signal levels were commensurately greater at these higher laser power densities then detector saturation would become an unmanageable problem. Neither of these two circumstances proved to be problematic however, since ample ion signal levels are available at very modest laser power densities. This feature of the experiment provided opportunity to examine the number of photons absorbed during the MPI event without interference from the effects of detector saturation and of power broadening.

The presentation of the data begins with that taken using the internally mounted 7.5-cm lens (beam path A). Figure 15 shows the MPI mass spectrum obtained. As with the previous two figures, increasing laser power is shown along the y-axis. This (composite) spectrum is

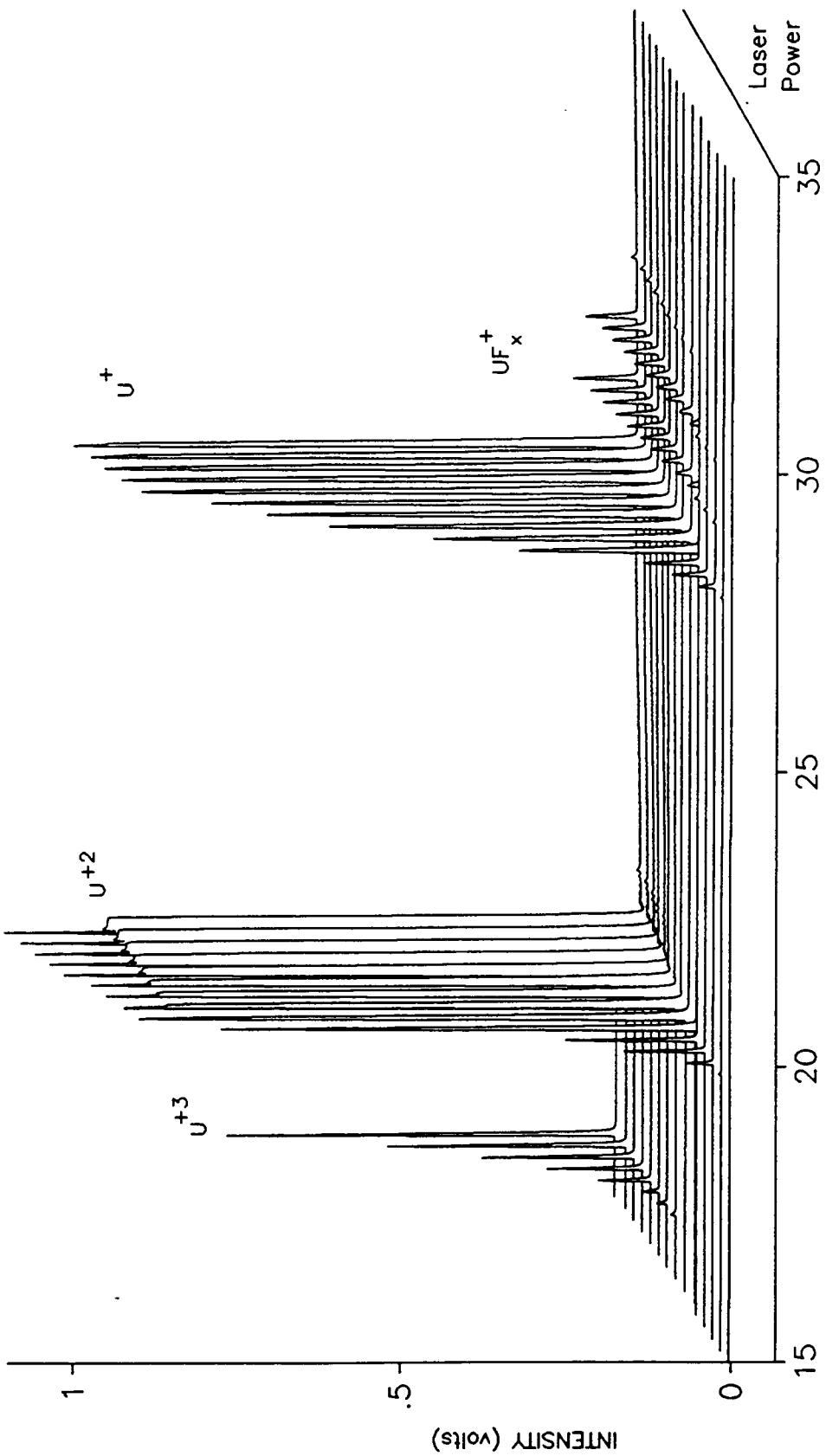


Figure 14. MPI mass spectra using λ=355nm.

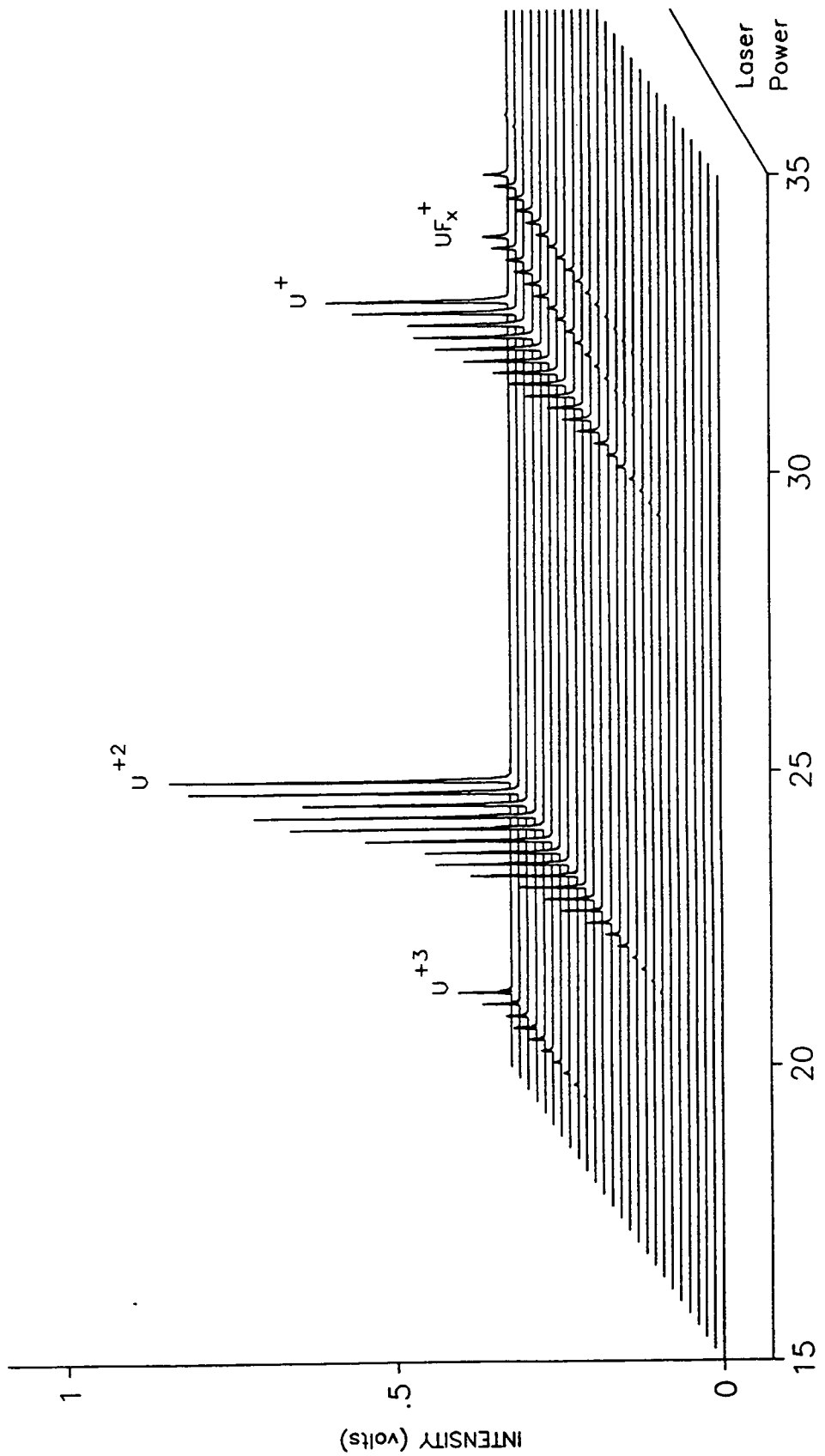


Figure 15. MPI mass spectra using λ=266 nm (7.5-cm lens).

acquired by adjusting the laser output power to a low, but stable, level using the laser oscillator lamp energy control and then further reducing the output power by appropriately adjusting the Q-switch delay. Normally, less that one milliwatt of output power is sufficient, and in this case the measured starting power was 500 μwatts. Each "slice" of the spectrum is acquired after the beam is uniformly attenuated by adding one quartz plate into the beam path. In this case a total of 24 quartz plates were added which produced a power density range of 8.92 x (10^9) - 6.33 x (10^{10}) W/cm^2, which has been corrected for reflective losses encountered in the beam path (e.g., prisms, window, and lens). The important points are that as the power density (in the sample focal volume) is reduced, all the ions present are progressively reduced in intensity in approximately the same ratio and the UF_6^+, UF_5^+, or UF_4^+ ions are not observed. Figure 16 displays the log-log plot of the ion signal vs. the laser power density for each species of U^{n+} (for n=1-3), where the slope, s, of the least squares fit to the points represents the approximate number of photons absorbed (per ion). Upon examination of this figure the reader is directed to the relationship between the slopes of U^+ and U^{2+}, and should notice that they appear to intersect at the lower power densities. At the higher power densities, however, they diverge with U^{2+} being the dominant ion. The slope of U^{3+} is close to that of U^+. Figure 17 shows the log-log plot of the ion signal vs. power density for each of the UF_x^+ (for x=1-3), and clearly shows that the slopes for UF^+ and UF_2^+ are almost identical. Again, the slope, s, of the linear least squares fit to the data is approximately the number of photons absorbed per fragment. Typical vacuum chamber pressure was 3.5 x (10^{-6}) Torr with a nozzle backing pressure of $\approx$ 19 Torr. At these power densities, the slope of the log-log plots for all ions were far less than that expected from the energetics involved. Saturation of many of the transitions is evident.

As the laser was operated near its minimum power output for the above described data

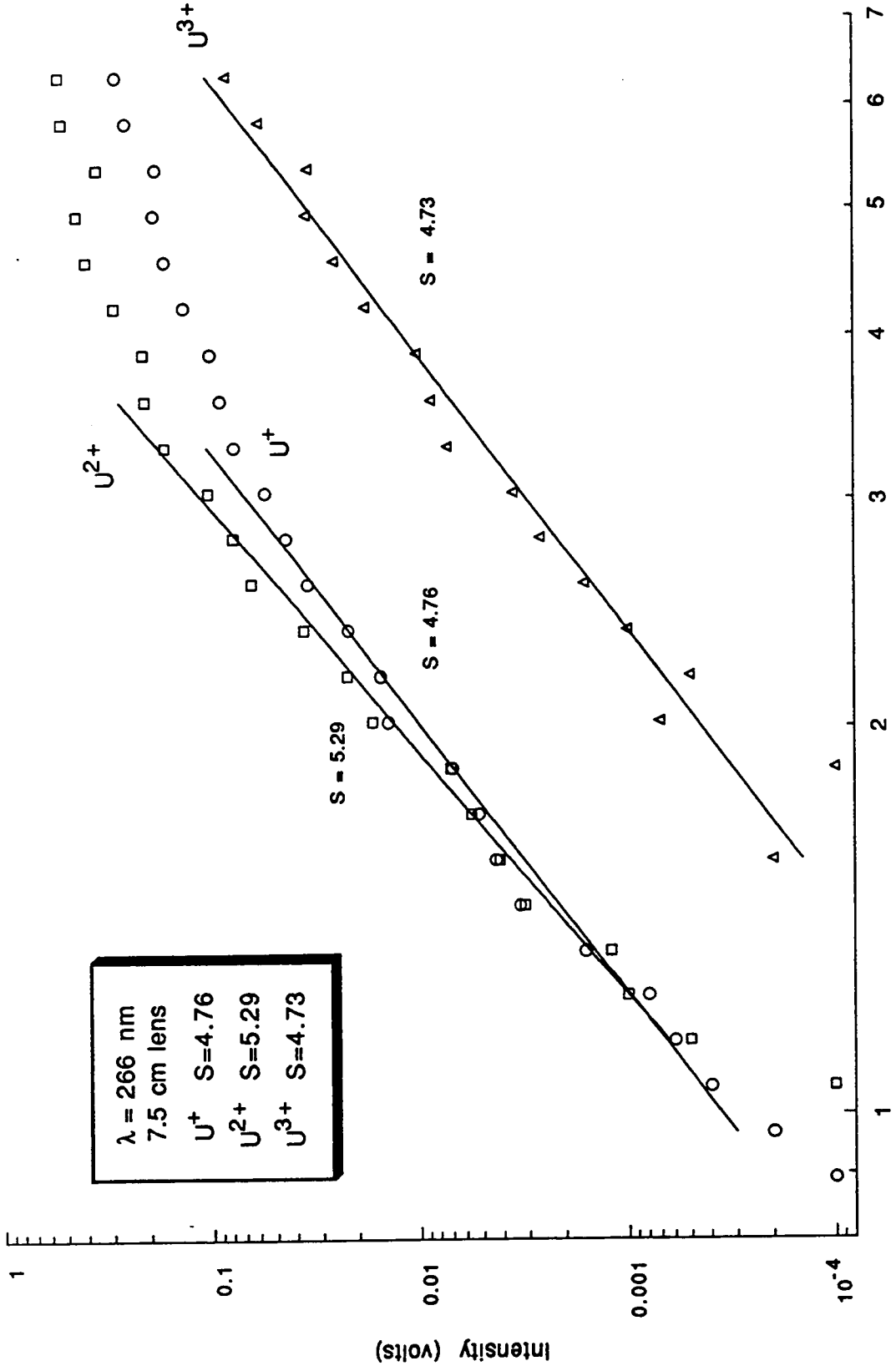


Figure 16. Slope of signal vs. intensity for U^+ (7.5-cm lens).

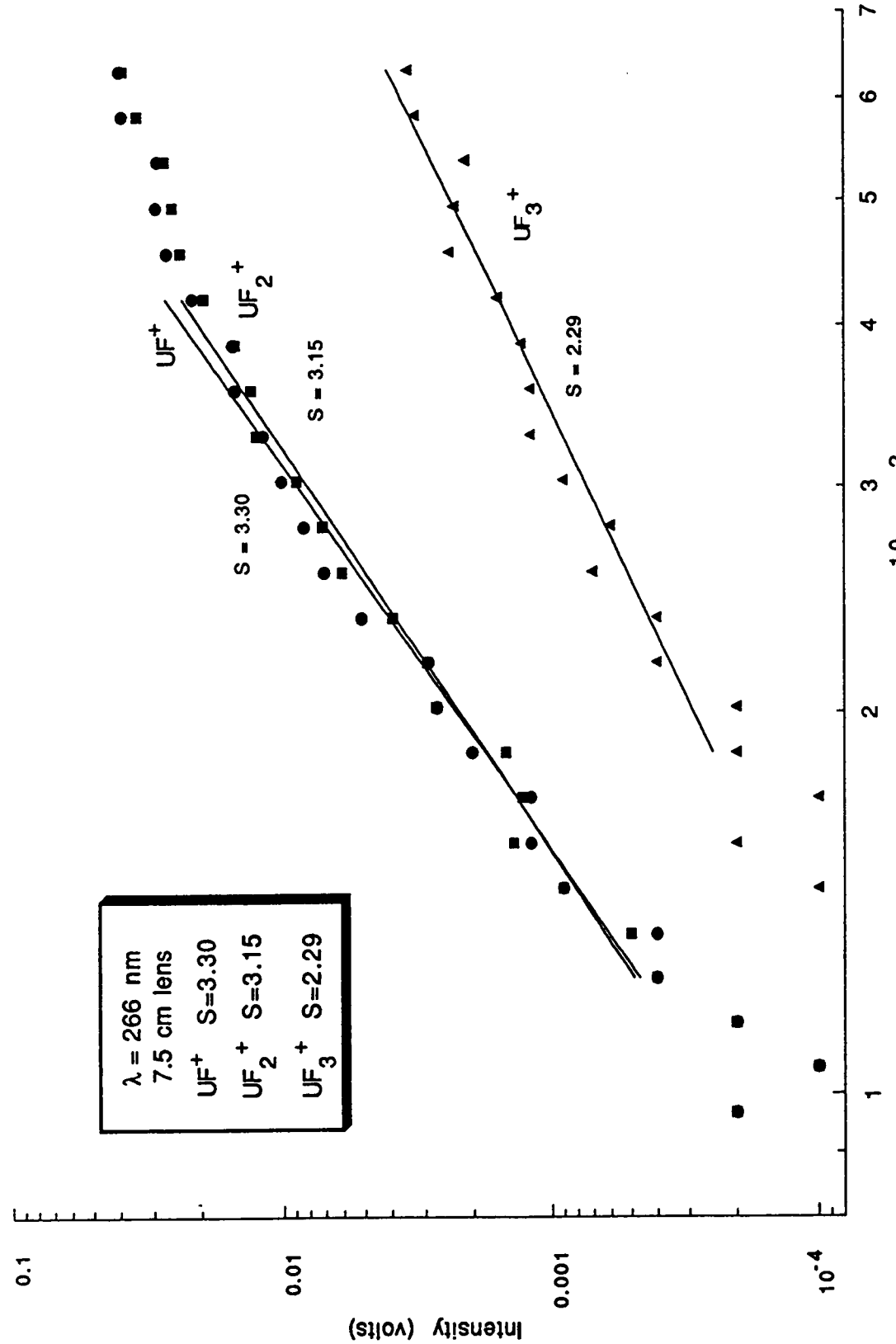


Figure 17. Slope of signal vs. intensity for UF_x^+ (7.5-cm lens).

set, further reductions in the laser power density must be achieved by using longer focal length lenses. The net effect of the longer focal length is to increase the focussed spot size in the sample region, thereby reducing the power density. Figure 18 shows the MPI mass spectrum using the 35-cm focal length lens, placed in beam path B. The use of 20 quartz plates produced a power density range of 1.17 - 5.99 x (10^9) W/cm^2. As the power is decreased the ratios of ion intensities is approximately constant and the parent ion is not observed; therefore, the basic features of Figure 15 are preserved, with one important exception. The log-log plot for U^{n+} of the ion signal vs. power density for this set of spectra is shown in Figure 19, with the calculated slopes. The reader is directed to note an important difference between these slope calculations and those of Figure 16. For this data set, at the low power densities, the calculated slopes (where S_{LP}=slopes calculated for spectra at low power) show that U^+ is the dominant ion and that this slope does intersect with that of U^{2+}. Indeed, it can be seen that in the region of $\approx$2.25 x (10^9) W/cm^2, the intensity relationship of the dominant ion is reversed. Subsequently, at higher power densities the U^{2+} ion now is the dominant ion and the resulting slopes (where S_{HP}=slopes calculated for spectra at higher powers) have become essentially parallel. Figure 20 shows clearly the change in the intensity relationship between the two dominant ions, U^{2+} and U^+, which was indicated by the changes in the slopes as shown in the previous figure. The upper trace is the MPI spectrum taken when the beam is attenuated to a power density $\approx$2.65 x (10^9) W/cm^2 and the lower trace is taken when the beam is attenuated to a power density $\approx$2.25 x (10^9) W/cm^2. Even though the calculated power densities are nearly identical, at the lower power level the U^+ ion is now more intense than the normally dominant U^{2+} ion. The discussion will return to this important feature later. In Figure 21 the log-log plot for the UF_x^+ ions is shown and those slopes calculated. The basic features of the slopes of the UF_x^+ ions from Figure 17 are

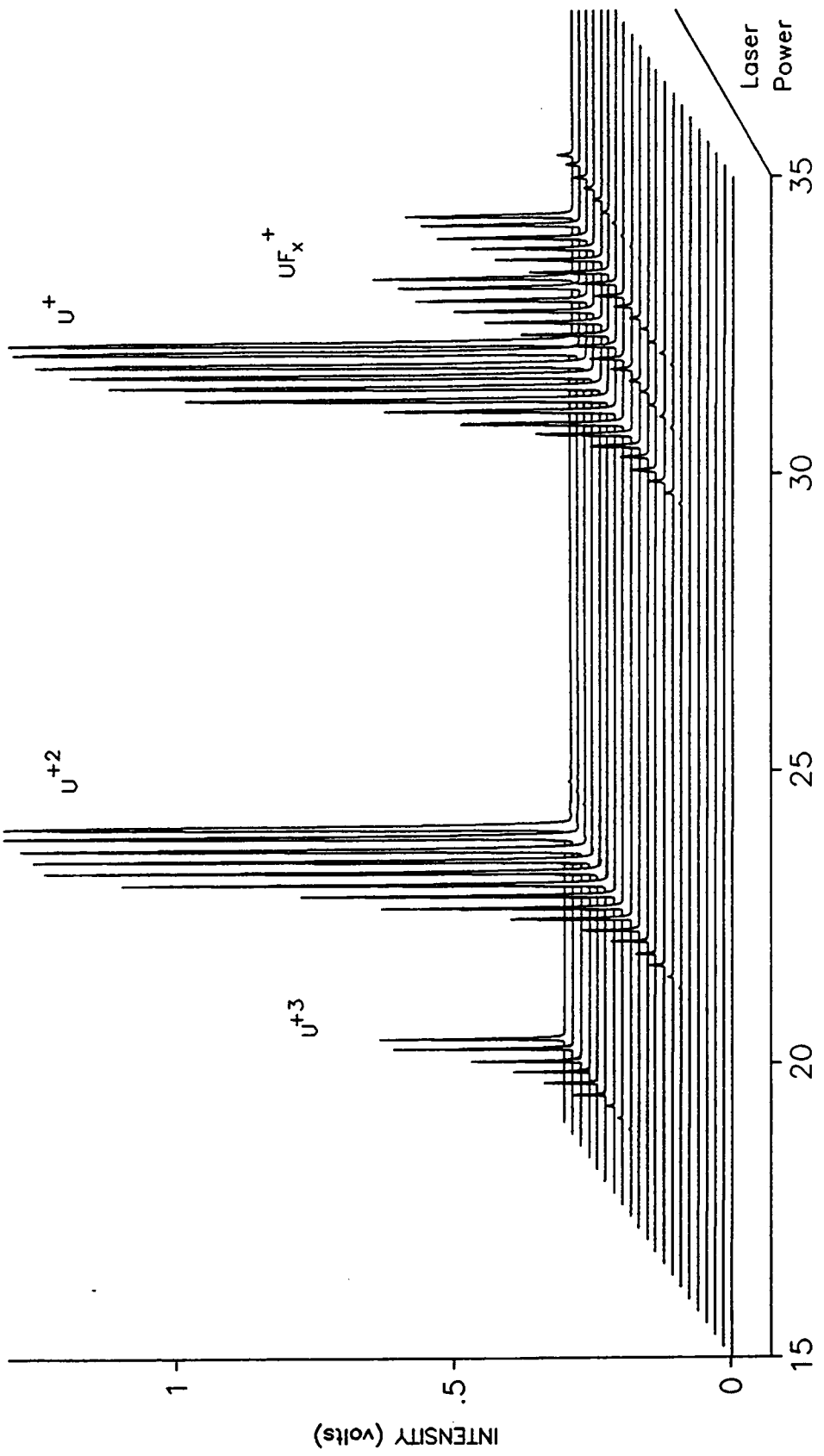


Figure 18. MPI mass spectra using λ=266 nm (35-cm lens).

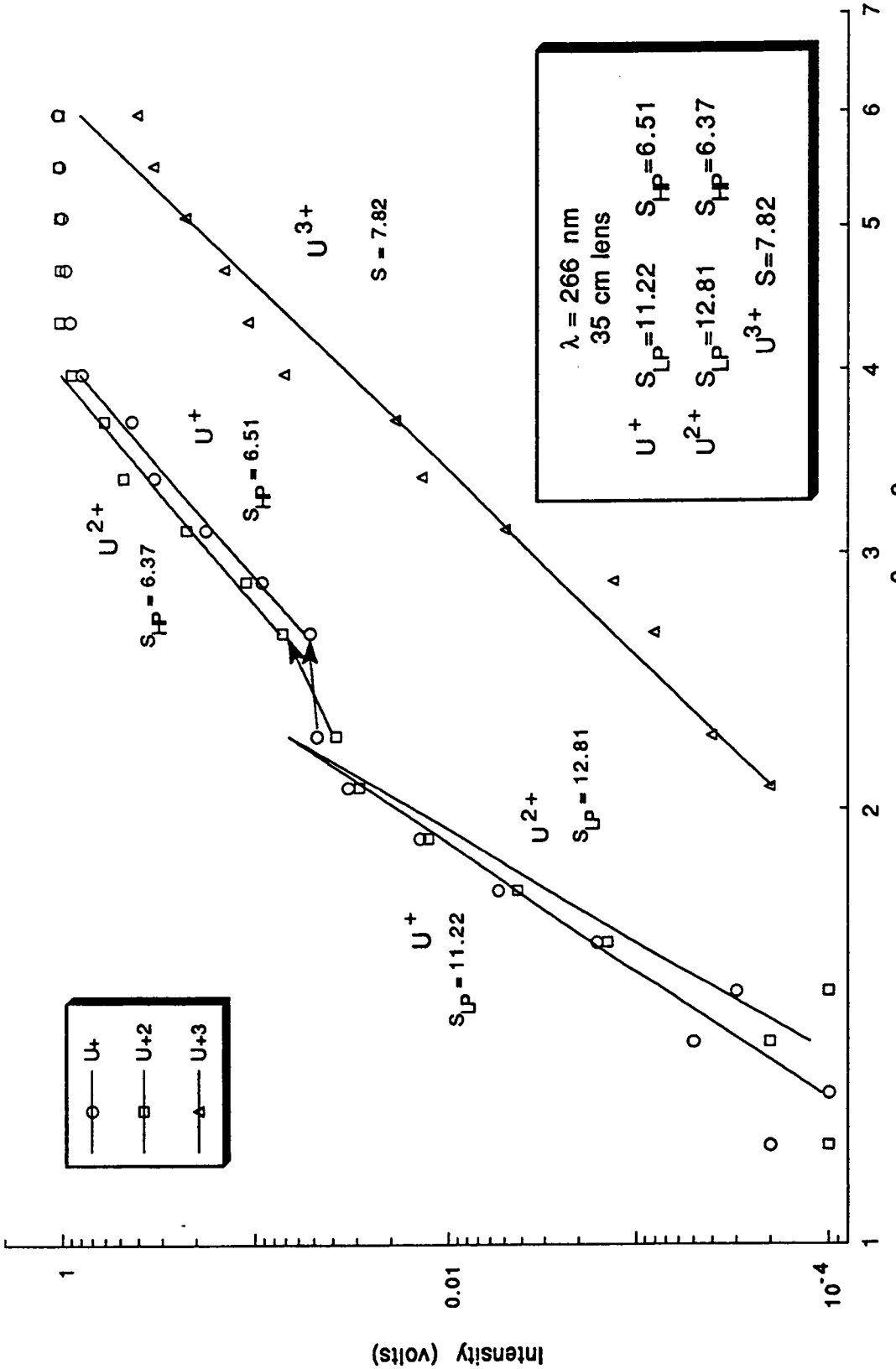


Figure 19. Slope of signal vs. intensity for U^{n+} (35-cm lens).

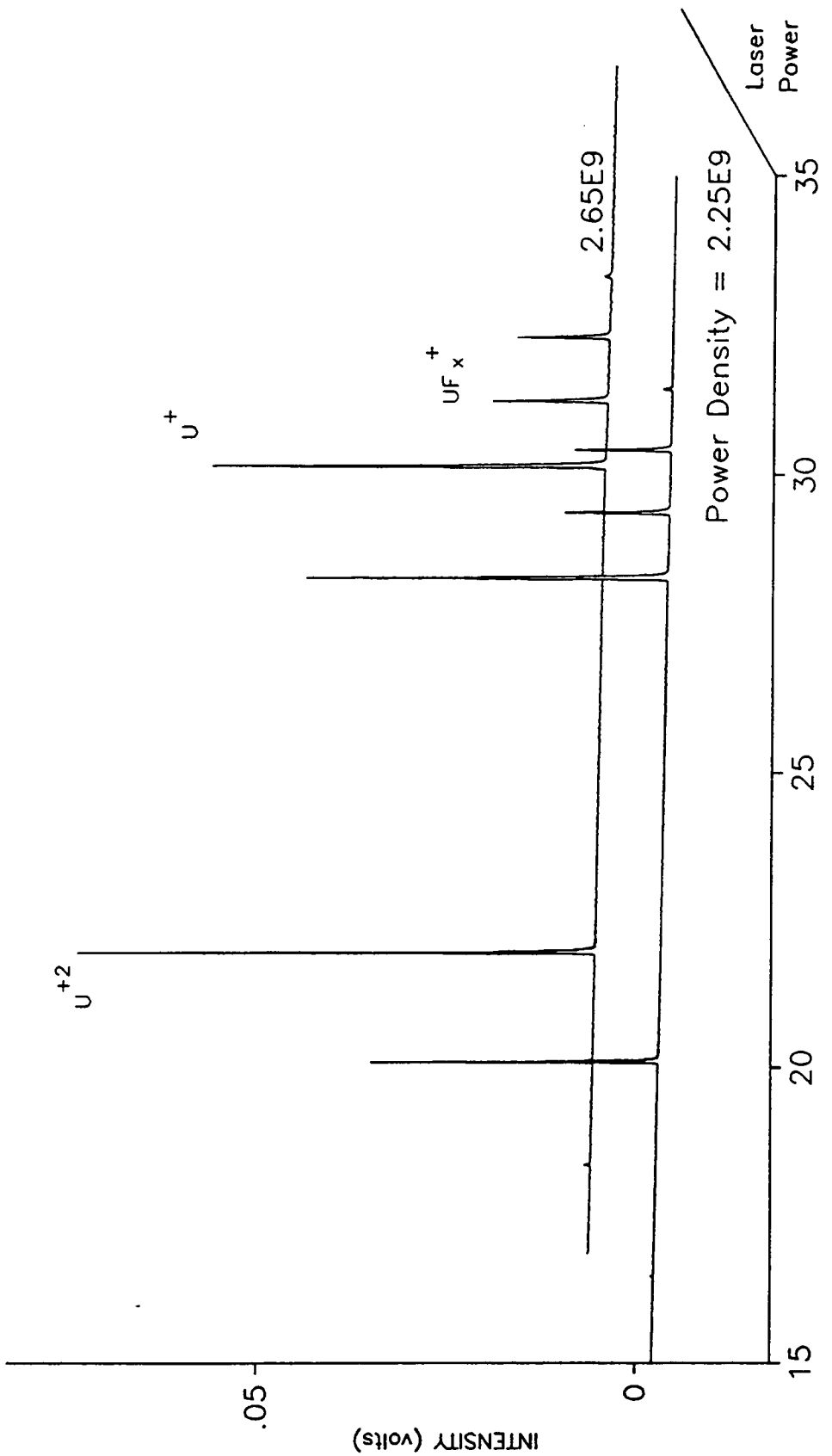


Figure 20. Reversal of the dominant ion intensities.

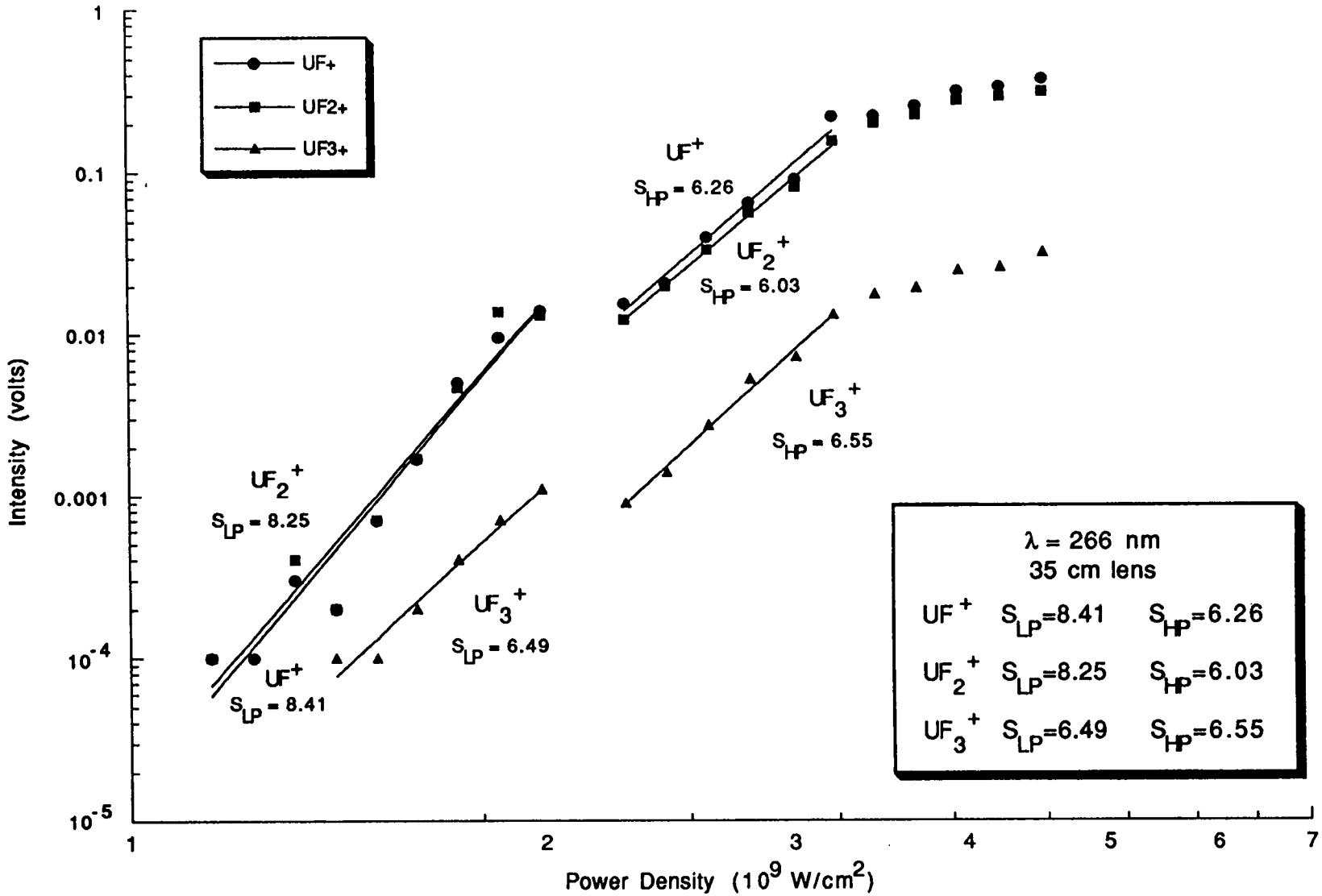


Figure 21. Slope of signal vs. intensity for UF_x^+ (35-cm lens).

preserved here, that is, the slopes for UF^+ and UF_2^+ are essentially equivalent and that for UF_3^+ is approximately parallel to them. For these spectra, typical vacuum chamber pressure was 2.4 x (10^{-6}) Torr with a nozzle backing pressure of $\approx$ 24 Torr.

The final set of spectra using λ=266 nm was acquired using the 50-cm lens in beam path B, and represents the lowest power densities examined for this wavelength. Figure 22 shows the MPI mass spectrum over the power density range covered by this lens, which was 9.85 x (10^8) - 3.09 x (10^9) W/cm^2. A total of fourteen quartz plates were used. Figure 23 shows the log-log plot of ion signal vs. power density and the corresponding slope for each U^{n+} ion. The slopes clearly show U^+ to be the dominant ion at these lower powers, but that the reversal of the intensity relationship with the U^{2+} ion occurs at $\approx$2.25 x (10^9) W/cm^2, as was shown in Figure 19. Figure 24 represents the slope calculations for each UF_x^+ ion, and their relationship to each other is the same as described for the low power slope values of Figure 21. The typical pressures in the vacuum chamber for these experiments was 1.9 x (10^{-6}) Torr with a nozzle backing pressure of $\approx$ 22 Torr. The three sets of experimental results can best be compared by examining each set of slopes. Figure 25 shows the slope values for the U^+ ion, Figure 26 compares the slope values for the U^{2+} ion, and Figure 27 represents the slope values for the U^{3+} ion. It should be noted that neither the polarization of the incident laser pulse, parallel or perpendicular with respect to the ion draw out field, nor the choice of carrier gas has a noticeable effect on the MPI mass spectrum. MPI spectra of neat UF_6 is likewise similar. An interesting note concerning the data acquired with this UV light is that no mass peaks corresponding to F^+ or U^{4+} were observed at these power densities. Figure 28 is the MPI mass spectrum which corresponds to the most intense "slice" of Figure 15. The mass peaks attributed to U^{3+}, U^{2+}, U^+, UF^+, and UF_2^+ are clearly observed, and to a lesser degree that of UF_3^+. By magnifying the y-axis and moving down the x-axis to shorter flight

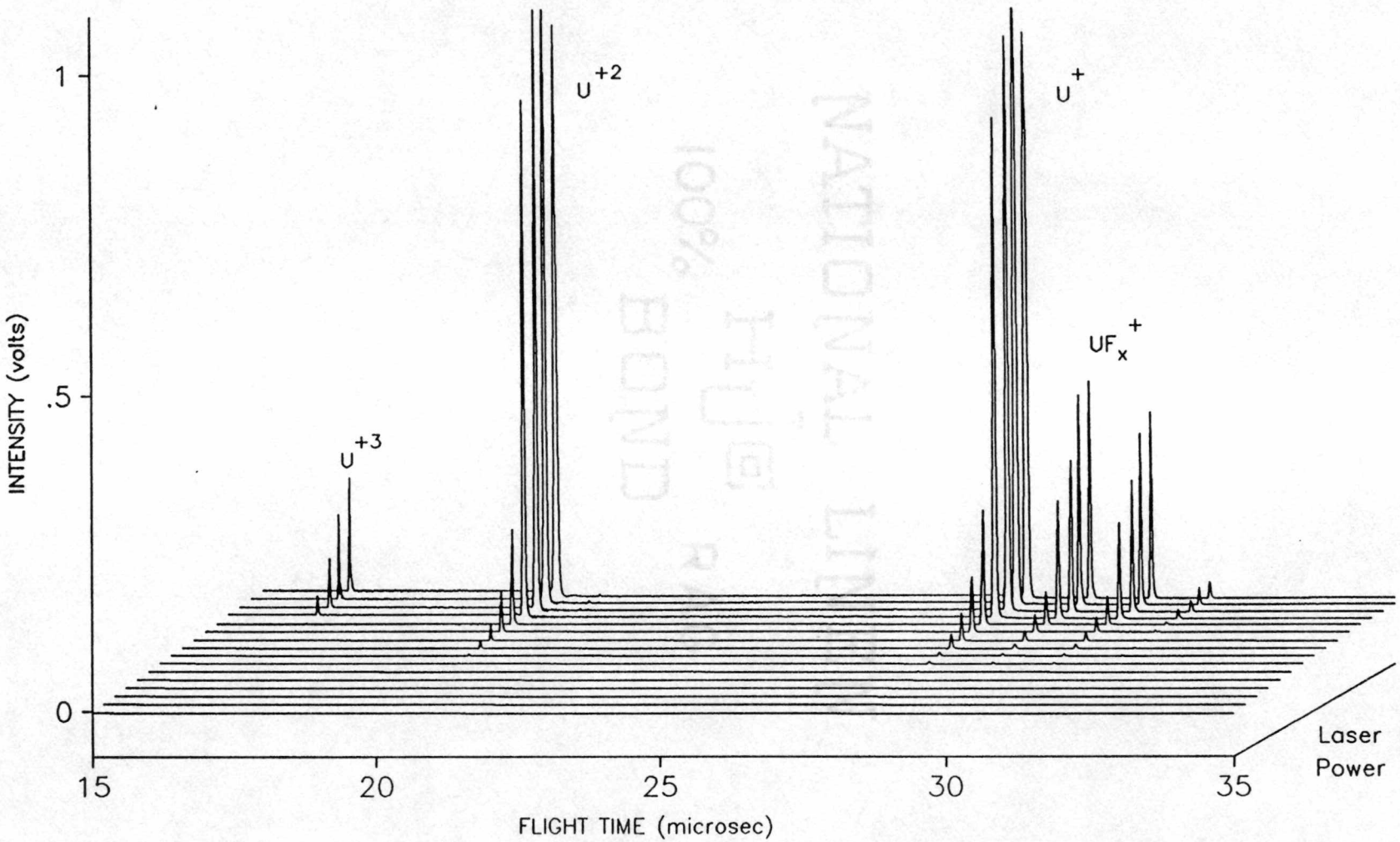


Figure 22. MPI mass spectra using λ=266 nm (50-cm lens).

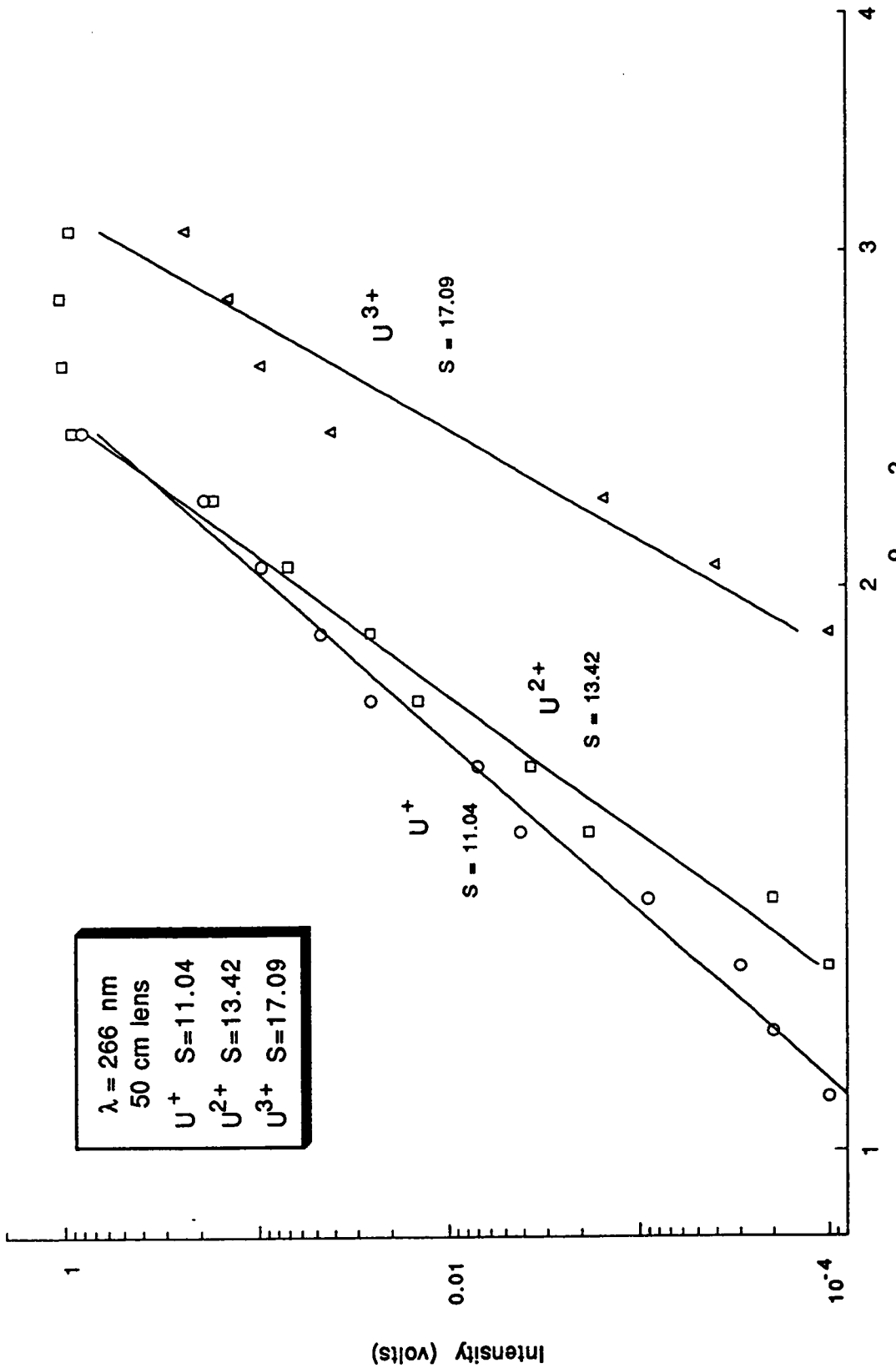


Figure 23. Slope of signal vs. intensity for U^{n+} (50-cm lens).

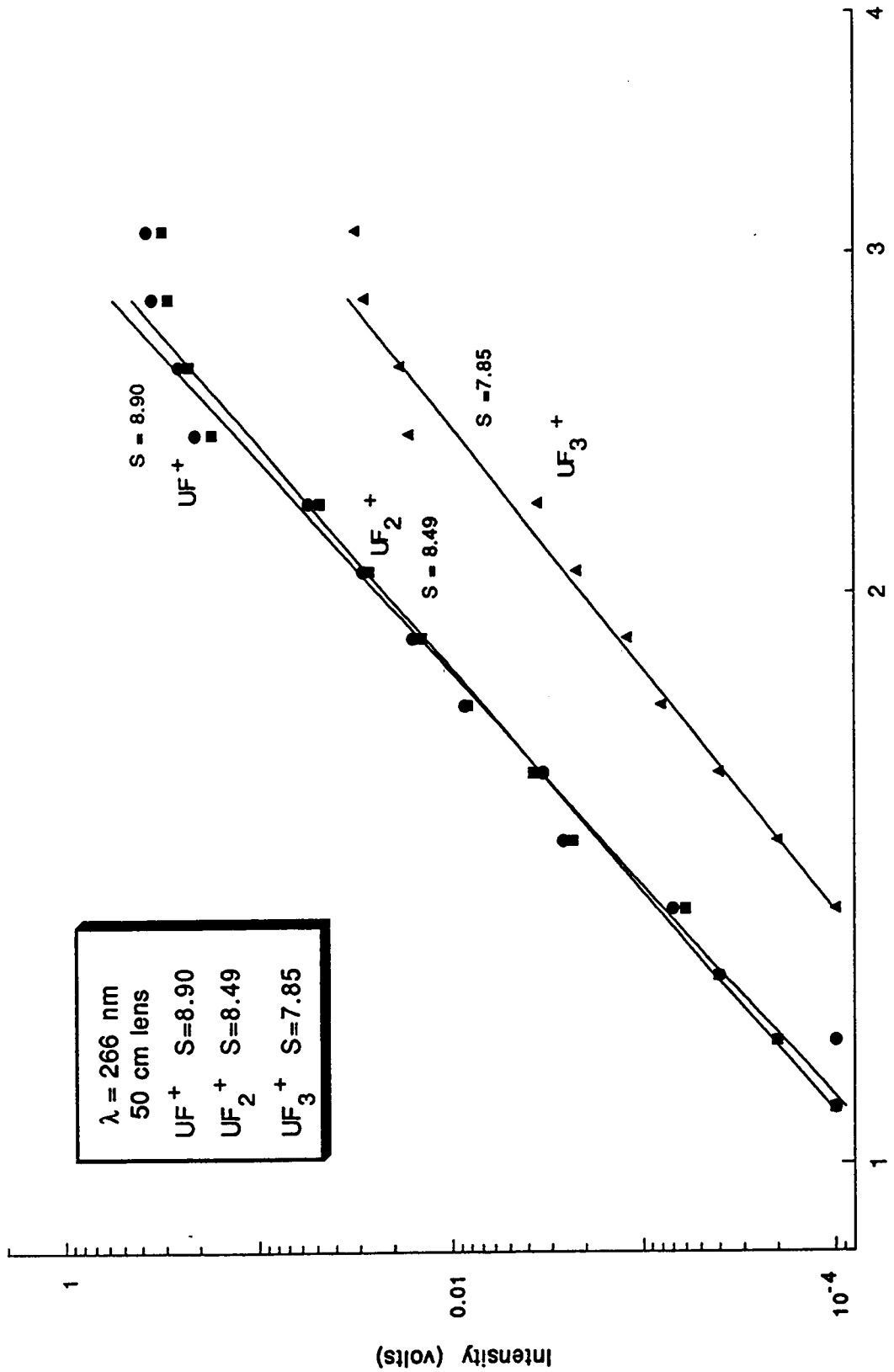


Figure 24. Slope of signal vs. intensity for UF_x^+ (50-cm lens).

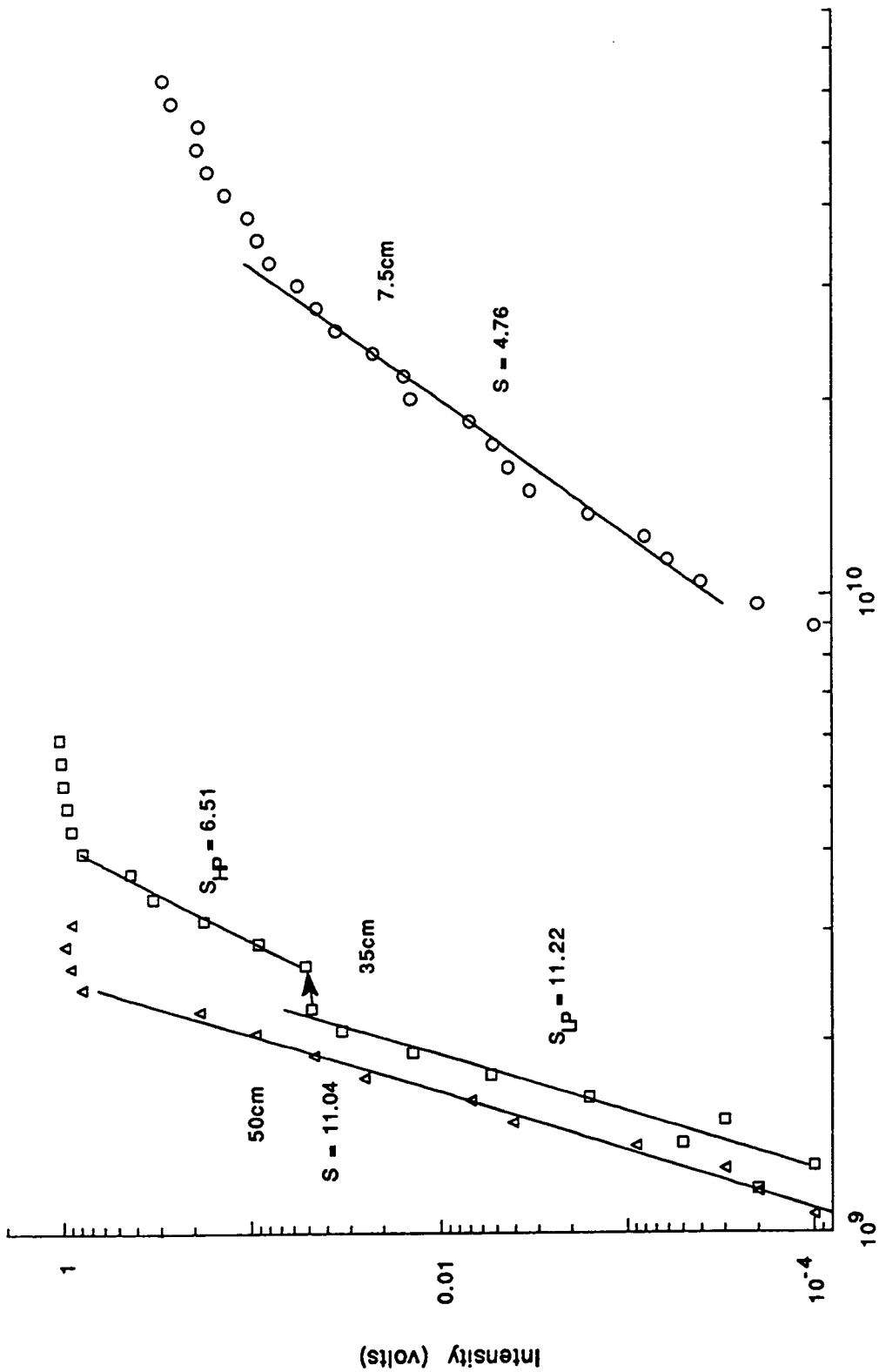


Figure 25. Combined slope data for U^+.

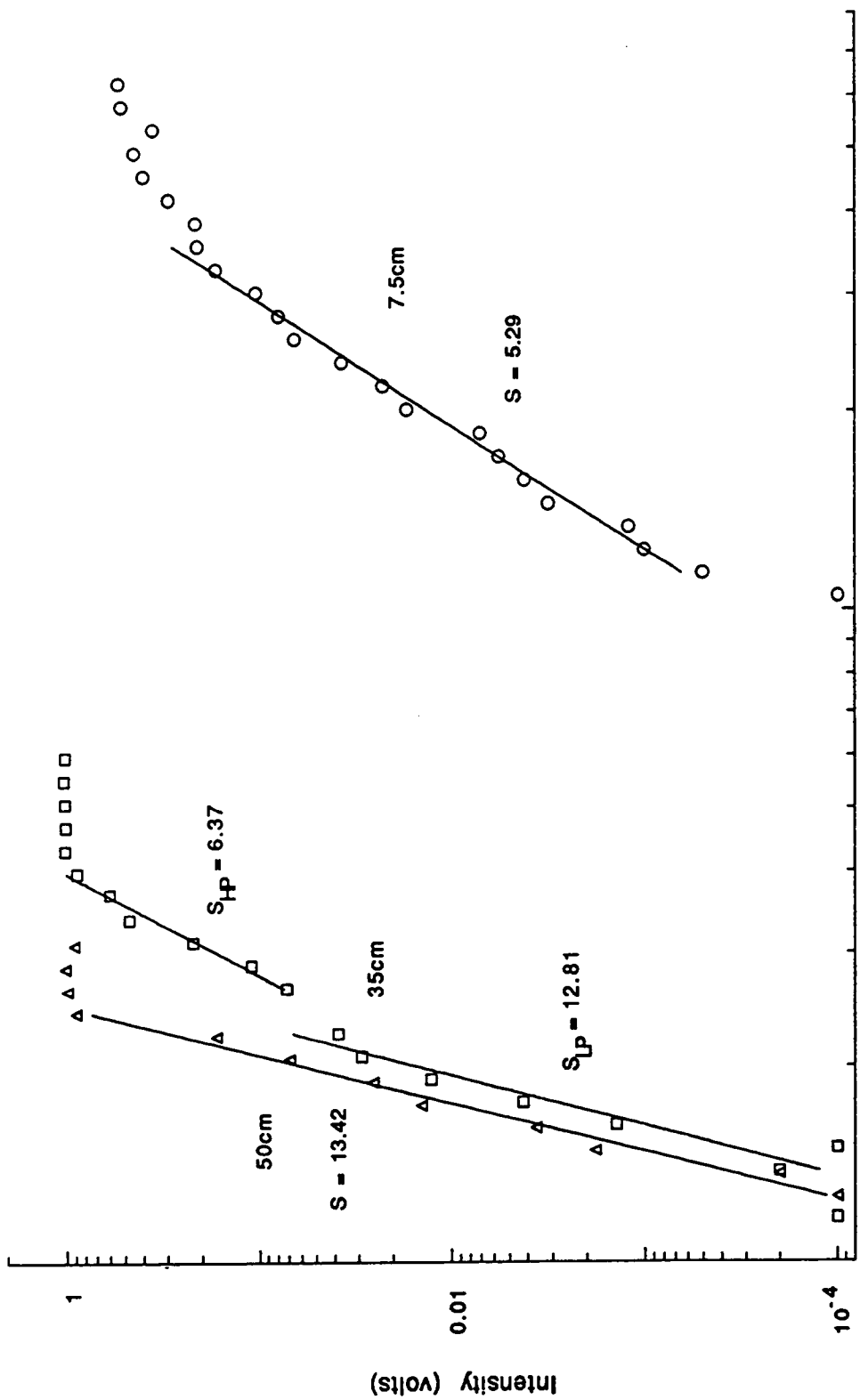


Figure 26. Combined slope data for U^{2+}.

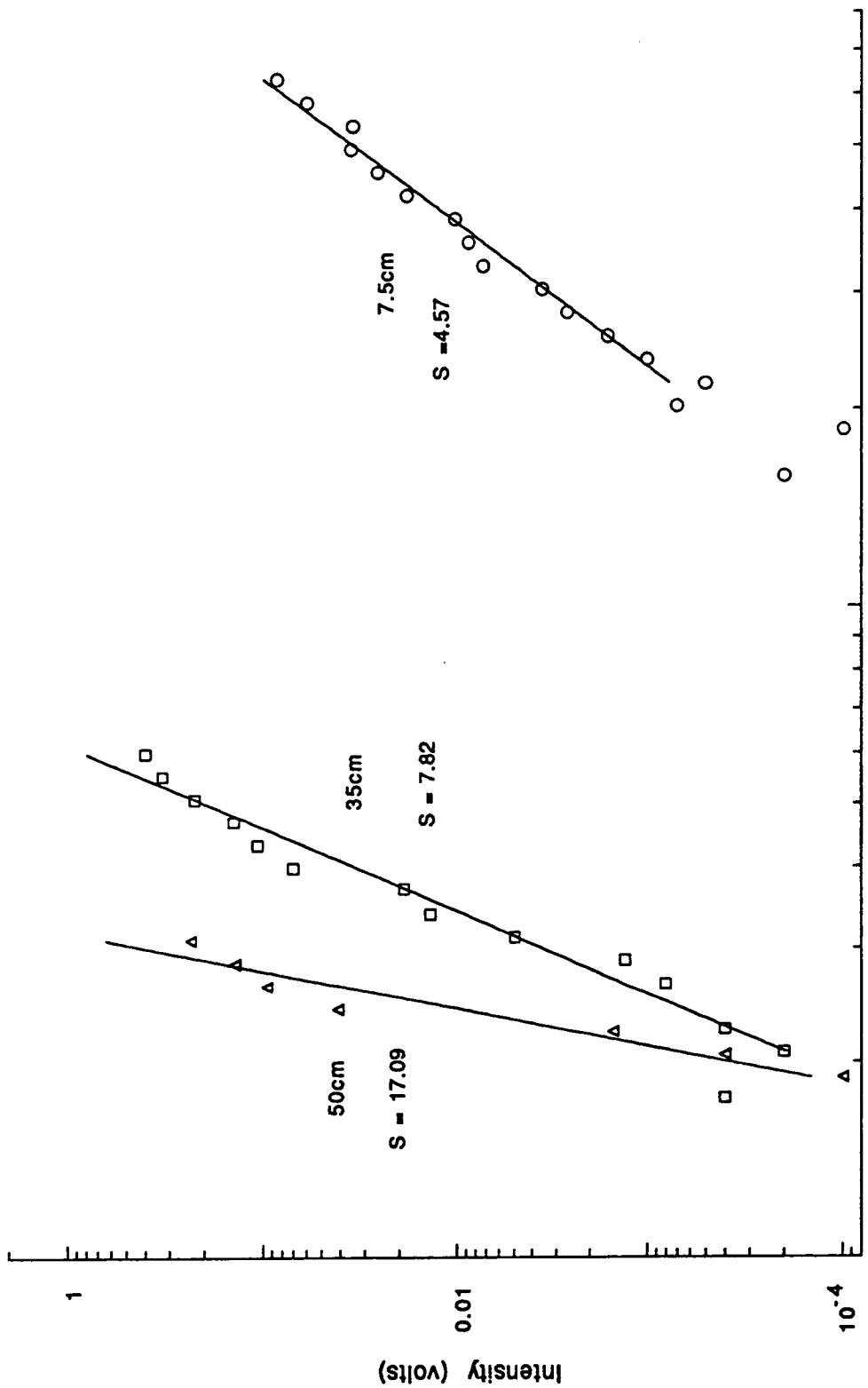


Figure 27. Combined slope data for U^{3+}.

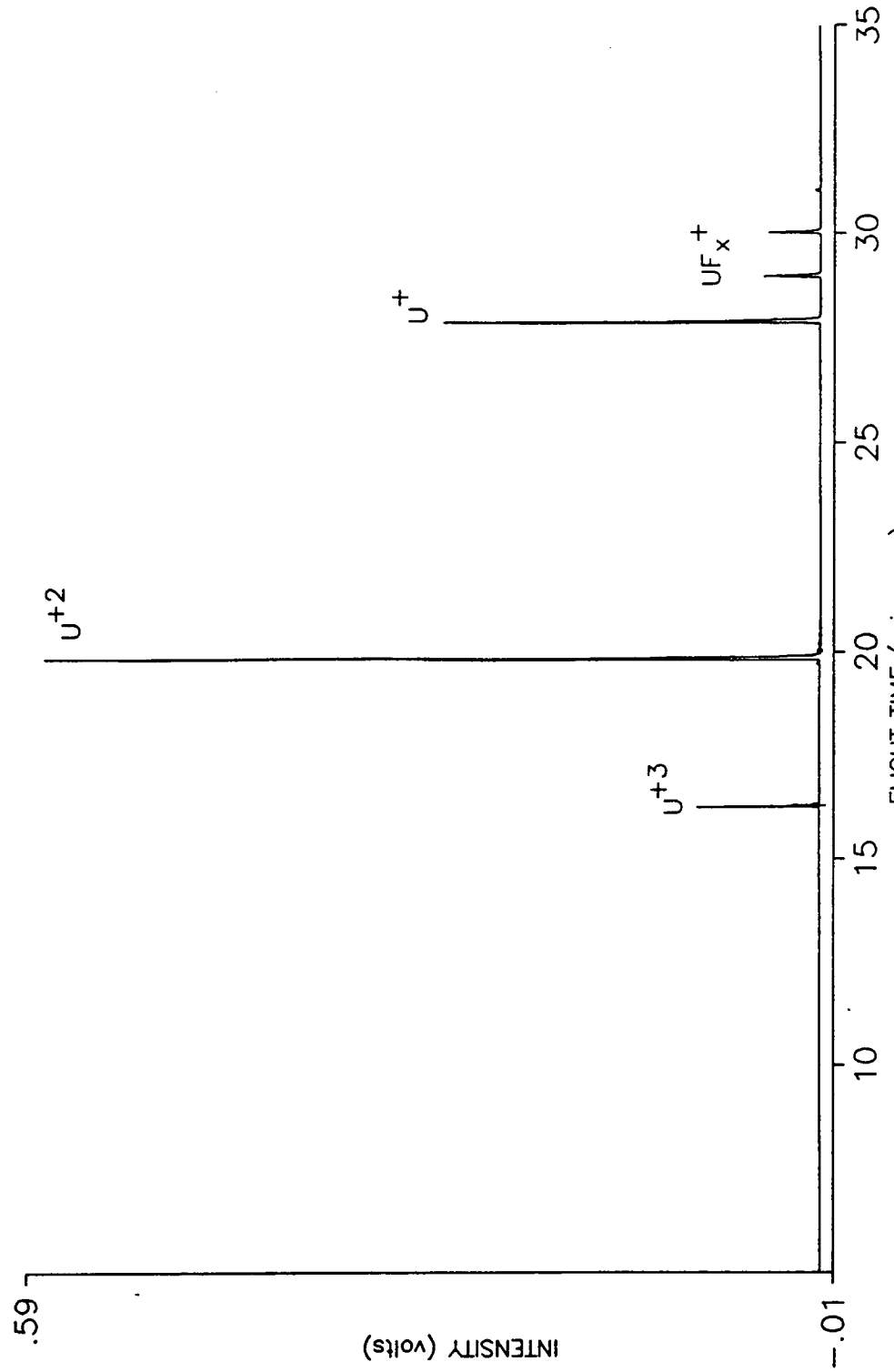


Figure 28. MPI mass spectra using λ=266 nm, single "slice".

times (5 - 15 μsec), the areas of the mass spectrum where features arising from F^+ and from U^{4+} can be inspected. In Figure 29 this magnified area is shown for each ion. There is no detectable signal from either of these two species as can be seen by examining the squared areas of the figure. Notice that the ion signal from the ^{235}U isotope is detected in its singly charged state by magnifying the x-axis from 27.4 - 31.4 μsec, as shown in Figure 30. In Figure 31, the region of 15.9 - 19.9 μsec is magnified such that the ^{235}U isotope is clearly seen in its doubly charged state and can also be distinguished in its triply charged state. Since the isotope ratio, ^{238}U:^{235}U, is 713:1 for this sample's assay, it is perhaps remarkable that it can be detected at all.

C. MPI Results Using The Dye Laser

The dye laser was used to obtain results in two areas of the visible spectrum. One was the yellow region around λ=591.5 nm, due to its well known strength as a resonant transition for uranium atoms.[61, 62] The second was the blue region around λ=440 nm, due to its use as a (multiphoton) resonant transition for xenon. Though originally intended to be used only for troubleshooting the MPI-TOFMS apparatus, it was learned that blue light was also effective in photoionizing UF_6; hence, it is included here.

Compton *et al* has previously reviewed the MPI characteristics of xenon and the use of λ=440.88 nm light in the (3 + 2) REMPI process for xenon.[36] As the only real criteria for chosing a carrier for UF_6 in these experiments was that it be nonreactive with the apparatus and with UF_6, the local expertise with xenon made it the logical choice. Though the MPI of UF_6 with blue light can be done with or without the xenon carrier gas, the results of the UF_6/Xe mixture are shown for the purpose of demonstrating the relative strength of the MPI process in UF_6. Figure 32 shows a wavelength scan from λ=440.0 - 442.2 nm, which covers

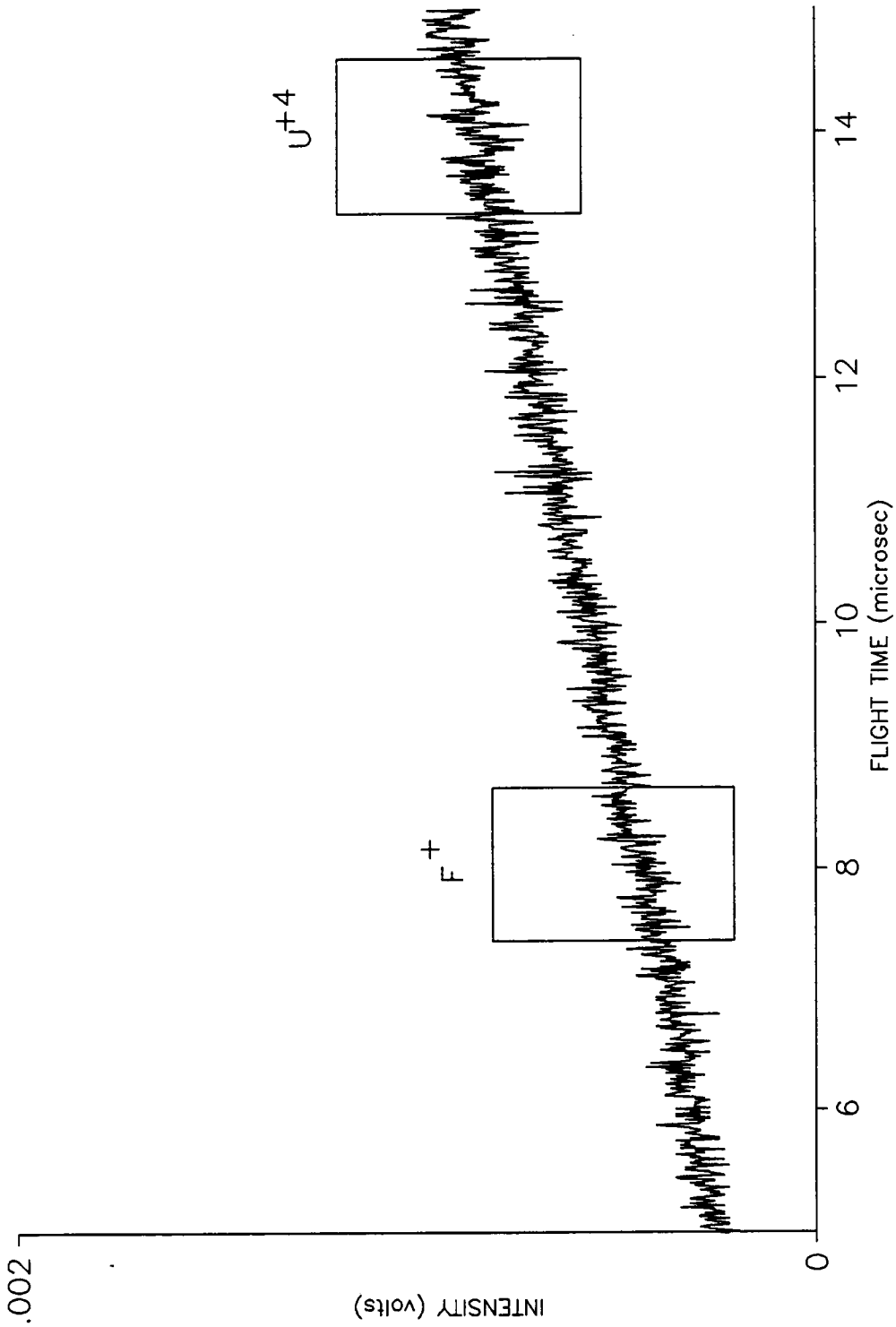


Figure 29. Magnification of TOF region: 5 - 15 μsec (from Fig. 28).

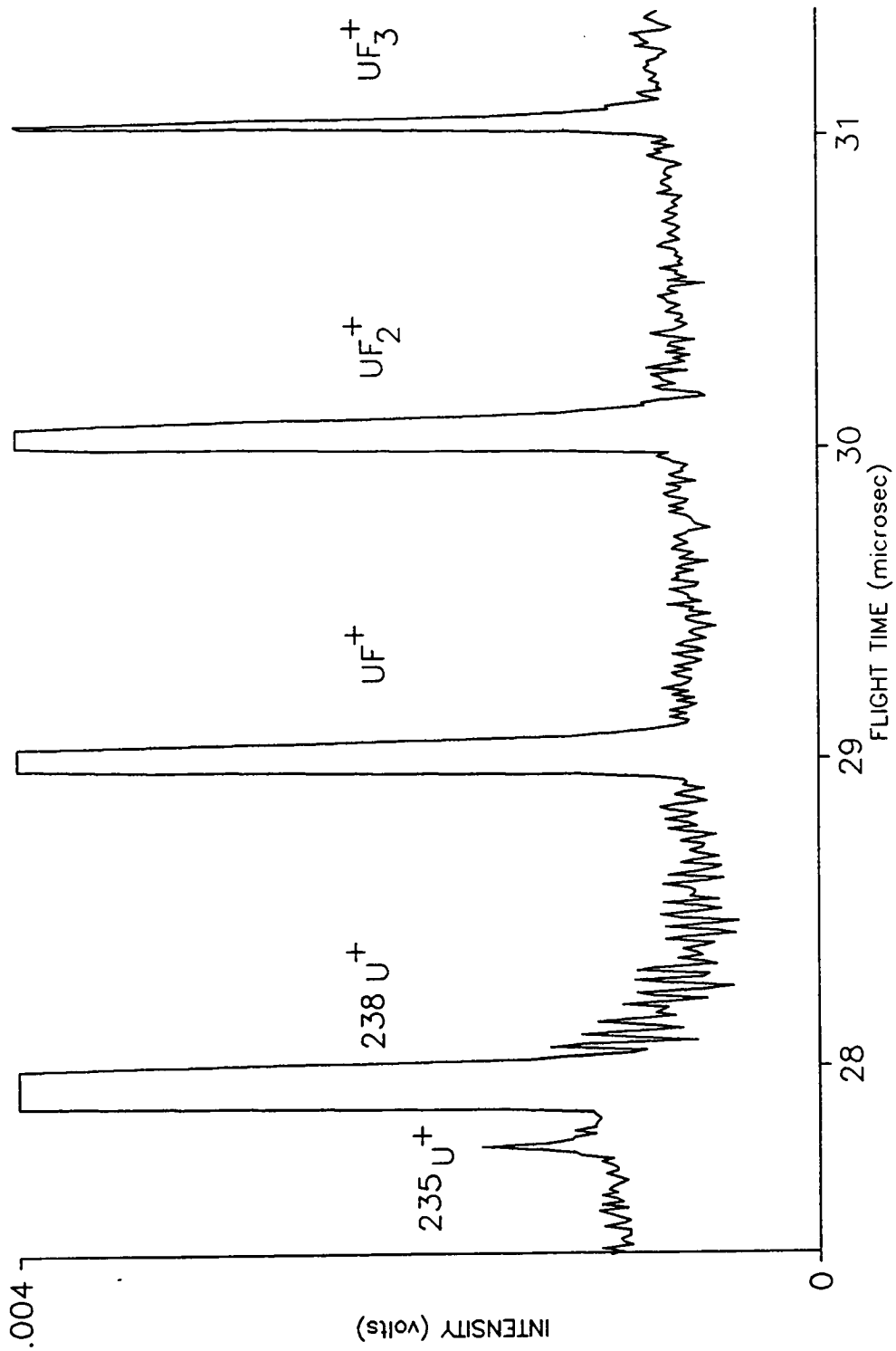


Figure 30. Magnification of TOF region: 27.4 - 31.4 *μsec* (from Fig. 28).

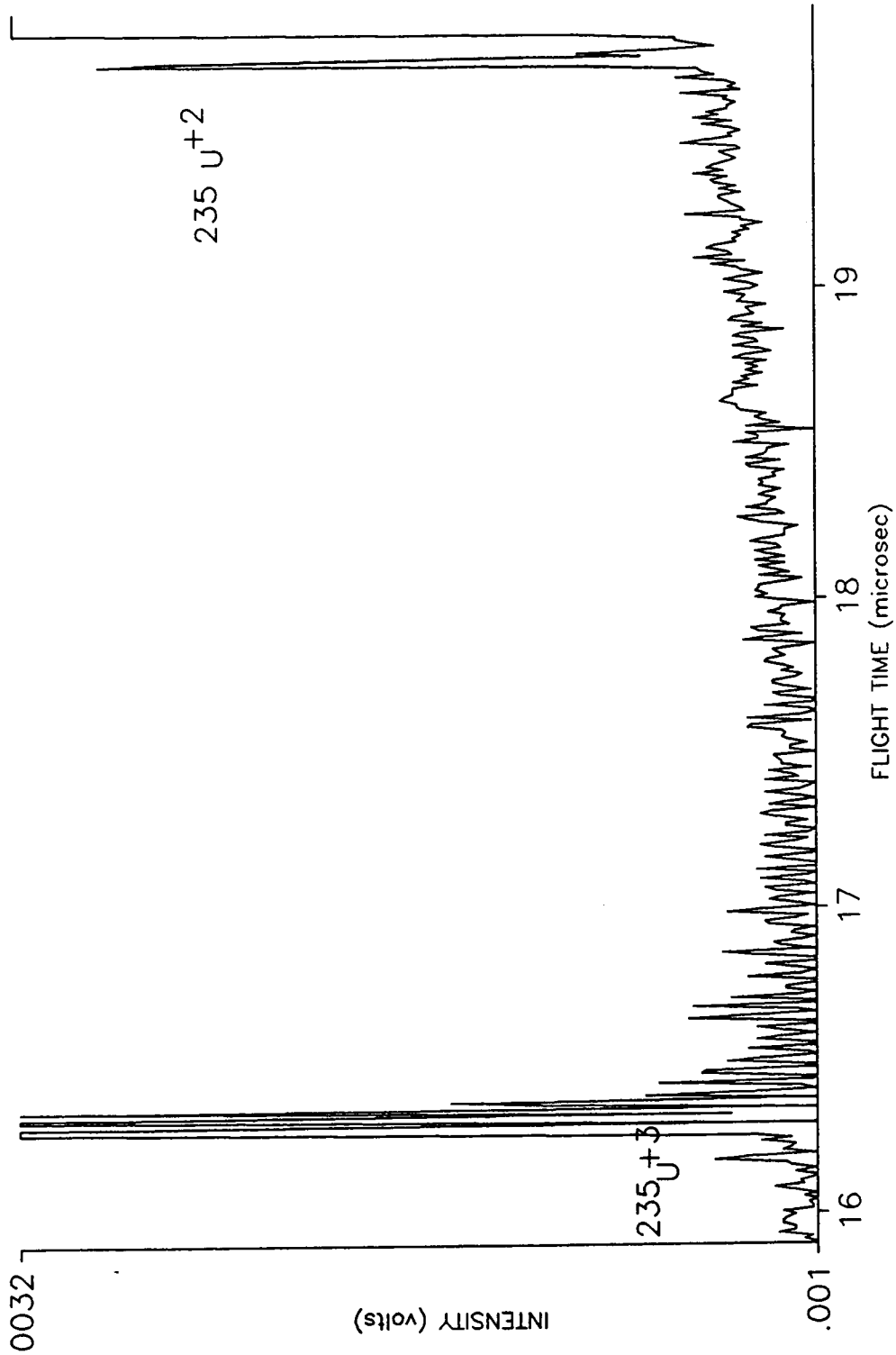


Figure 31. Magnification of TOF region: 15.9 - 19.9 μsec (from Fig. 28).

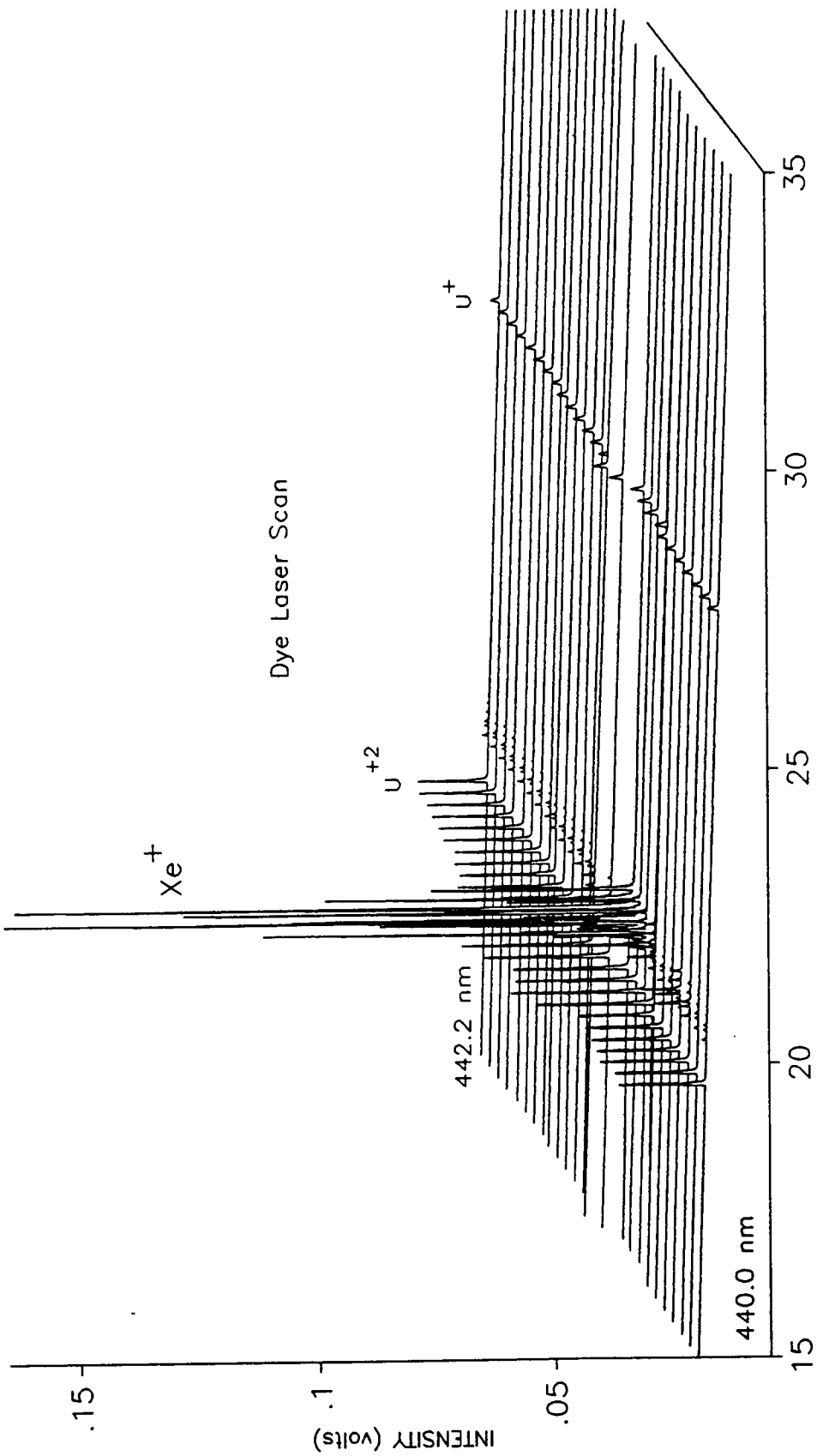


Figure 32. Wavelength scan of the "blue" xenon resonance.

the three photon allowed resonance of the $6s[3/2]_1$ state of xenon. Each slice of the MPI composite spectrum represents a dye laser step of 0.083 nm. There are two important features in this figure. First when the xenon transition is in resonance, notice that the (presumed) nonresonant MPI process in UF_6 gives a signal which is within an order of magnitude of the (3 + 2) REMPI signal intensity from xenon, even though the gas mixture is 92.7% xenon! Secondly, notice that as the laser is tuned over the transition wavelength, the signal intensity for U^{2+} increases slightly. This is an interesting, but not reproducible effect.

A complete range of power density studies were not performed for the yellow dye laser light, instead the yellow wavelengths were used to attempt to find a resonance enhancement in the MPI mass spectrum that would positively identify the presence of the U atom (a product of neutral ladder climbing, see Figure 1). Controlled wavelength scans were performed over the full tuning range (λ=588 - 607 nm, for 20 mW minimum output power at the extremes) of the Kiton Red laser dye. In spite of the fact that the U^+ signal is described as "strongly tunable" with many transitions in the wavelength region λ=570 - 600 nm, no resonance enhancement due to the interaction of yellow laser light with UF_6 was observed.[63] However, there are some notable differences between spectra obtained with λ=591 nm light and those obtained with λ=266 nm light. In a fashion identical to the previous composite spectra which have been shown, Figure 33 shows the MPI mass spectra obtained using the 7.5-cm lens and successive quartz plate attenuation. A total of 18 quartz plates were used to give a power density range of $3.12 \times (10^{11})$ - $1.35 \times (10^{12})$ W/cm^2. The initial dye laser output power was 62 mW at λ=591.5 nm. Two features are immediately noticeable, as compared to data acquired with λ=266 nm. The ion signal (for U^{2+}) is approximately 5 times smaller even though the power density is about 150 times larger and

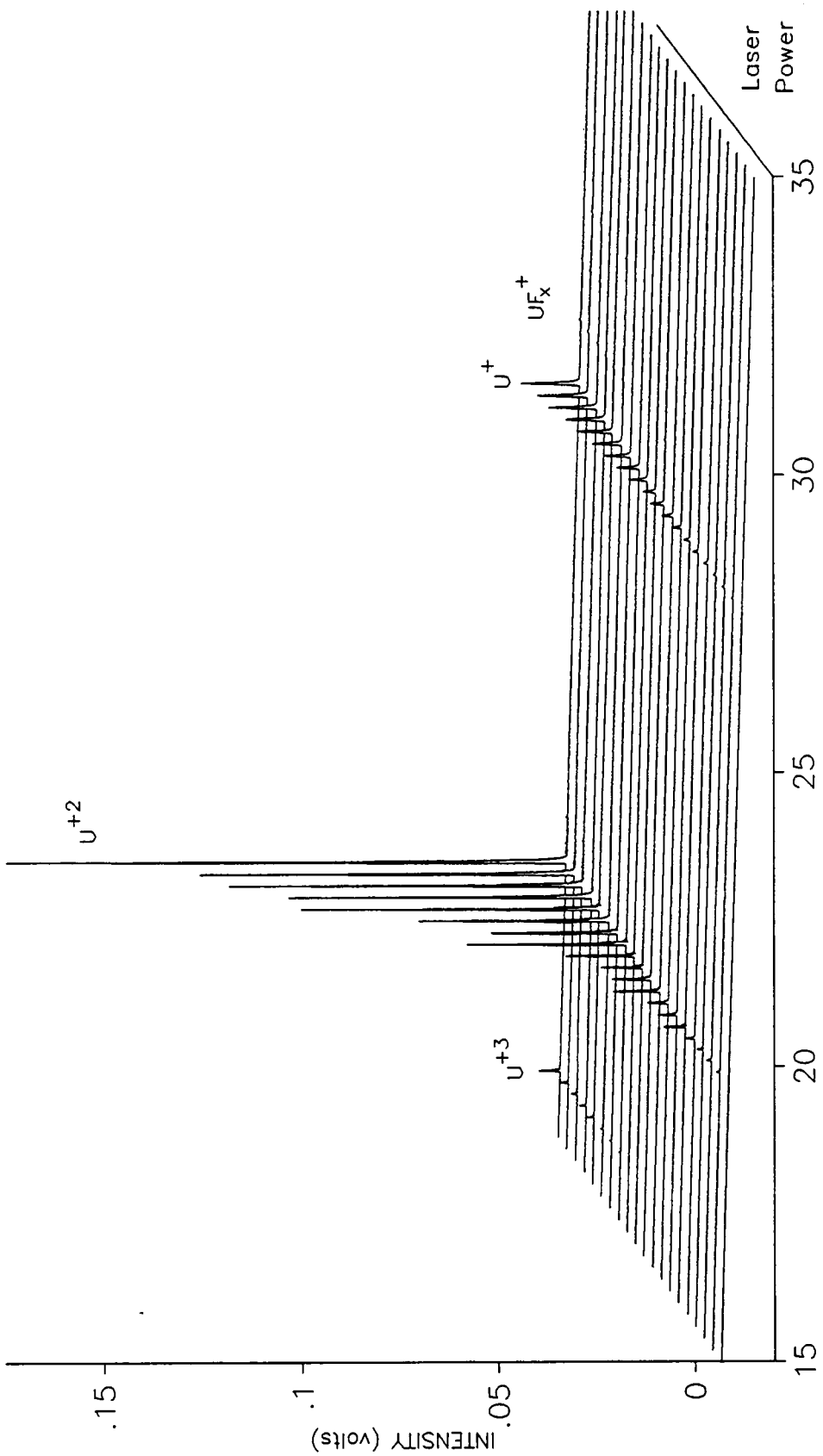


Figure 33. MPI mass spectra using λ=591 nm, low power.

there is virtually no ion signal arising from the UF_x^+ fragments. One must look more carefully to observe the other differences. Figure 34 shows a MPI mass spectrum taken using a dye laser output power of $\leq$ 200 mW and the major features are very typical of spectra acquired using the yellow laser pulses. Note the relationship of the ion intensities, i.e., $U^{2+} > U^{3+} >> U^+$ and that there are new features in the region of 21 μsec flight time. In Figure 35, the spectrum of Figure 34 has been magnified by $\approx$20X. Under these conditions, new features can be examined. The ions UF^+, UF_2^+, and UF_3^+ are observed, with the intensity of the UF_2^+ diminished in relation to the ions on either side of it. A packet of closely spaced ions, in the region of the Xe^+ isotopes, can be seen as well as the multiply charged isotopes of uranium, $^{235}U^{3+}$ and $^{235}U^{2+}$. For the first time, U^{4+} is clearly seen at what must be described as a fairly modest power level. These new features bear closer examination. The 27 - 32 μsec region of the spectrum has been magnified by another $\approx$10X to produce the view in Figure 36. Noteworthy in this figure is the absence of $^{235}U^+$, the diminished intensity of UF_2^+, and the extremely weak feature in the flight time region where UF_4^+ would be expected to occur. This evidence for the UF_4^+ ion has only been noted for this yellow wavelength, and clearly is extremely weak in intensity. Figure 37 is the central portion (19.3 - 21.3 μsec) of Figure 35 which has been magnified by $\approx$3X. This view shows clearly the $^{235}U^{2+}$ ion, the UF^{2+} ion (m/e=128.5), and the $^{129}Xe^+$, $^{131}Xe^+$, $^{132}Xe^+$, $^{134}Xe^+$, and $^{136}Xe^+$ isotopes. The UF^{2+} ion is only observed when the UF_2^+ ion displays the corresponding decrease in intensity. In Figure 38, the leftmost region of Figure 35 has been magnified by $\approx$3X also. In this view the $^{235}U^{3+}$ ion, the U^{4+} ion, and F^+ can be seen, though the latter two are extremely weak.

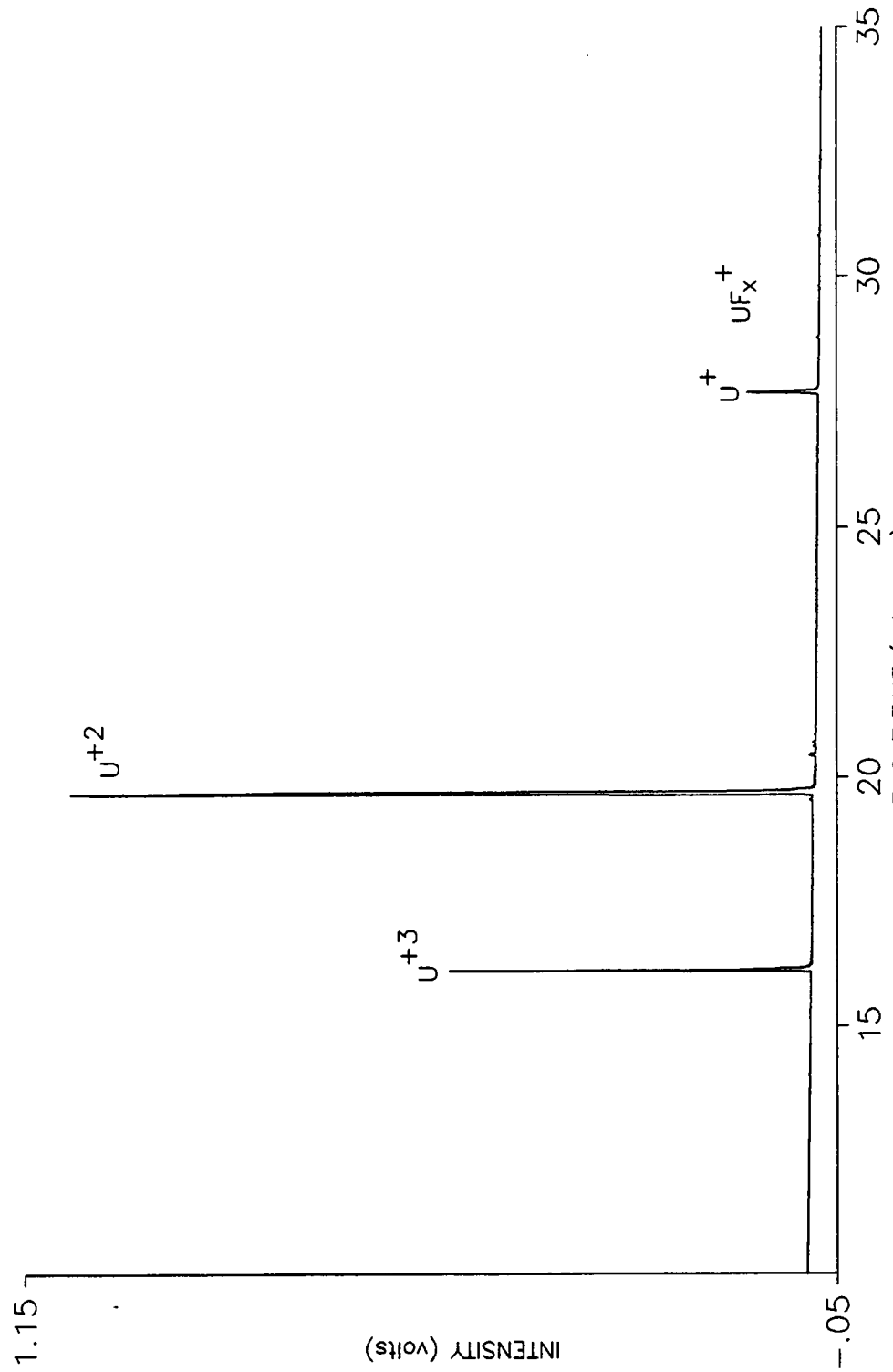


Figure 34. MPI mass spectra using λ=591 nm, high power.

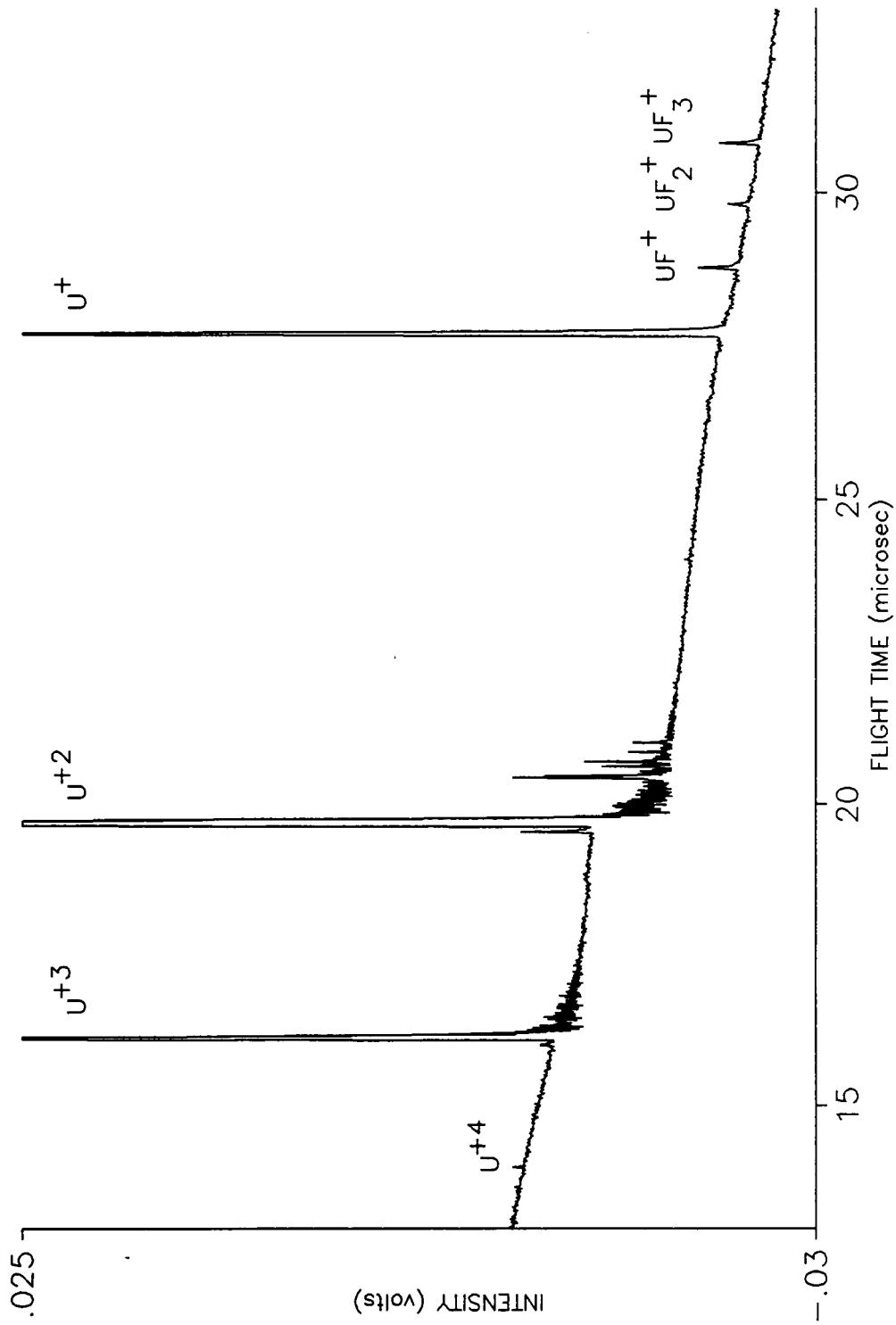


Figure 35. Magnification of Figure 34 by 20X.

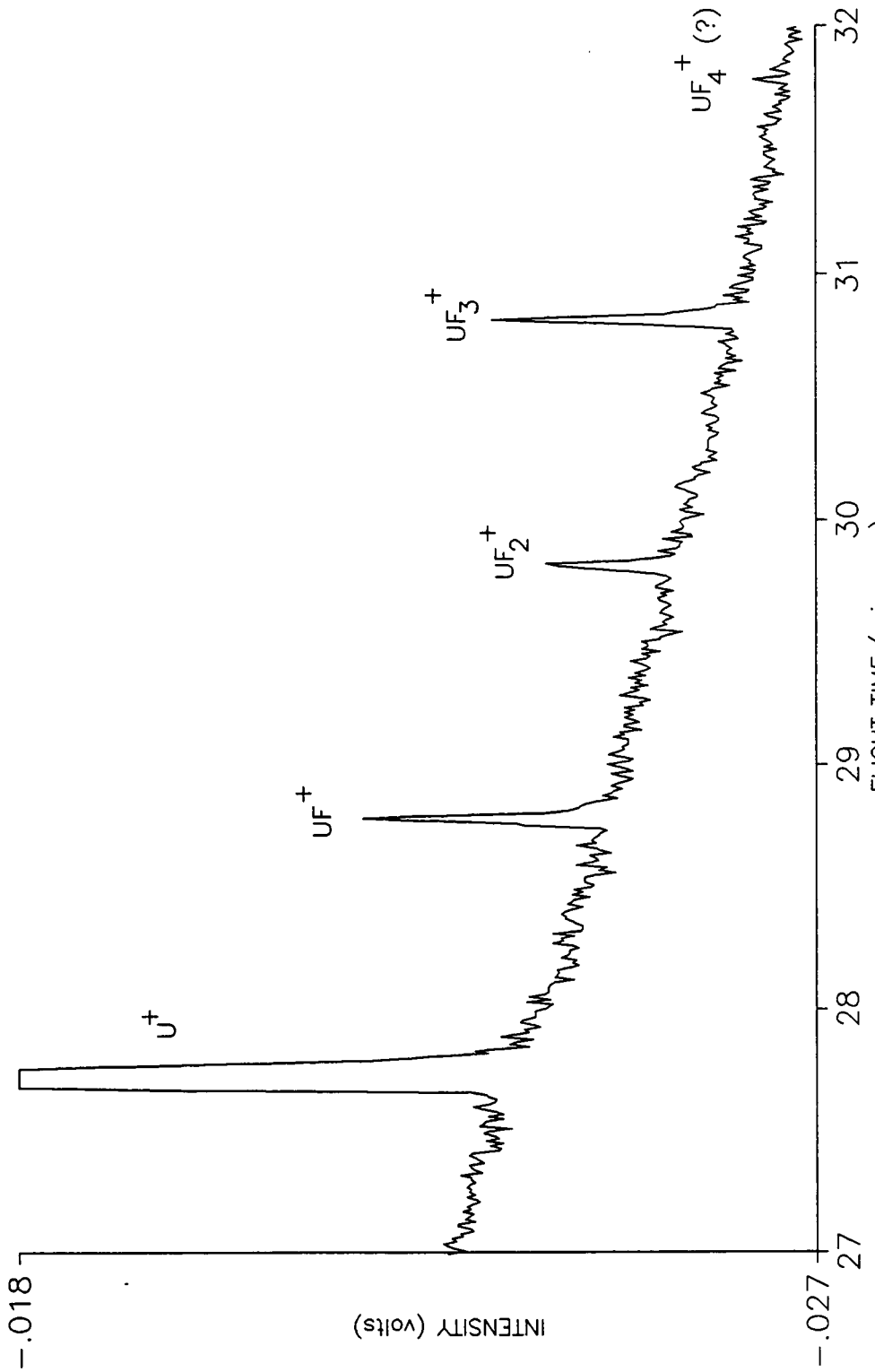


Figure 36. Magnification of TOF region: 27 - 32 *μsec* (from Fig. 35).

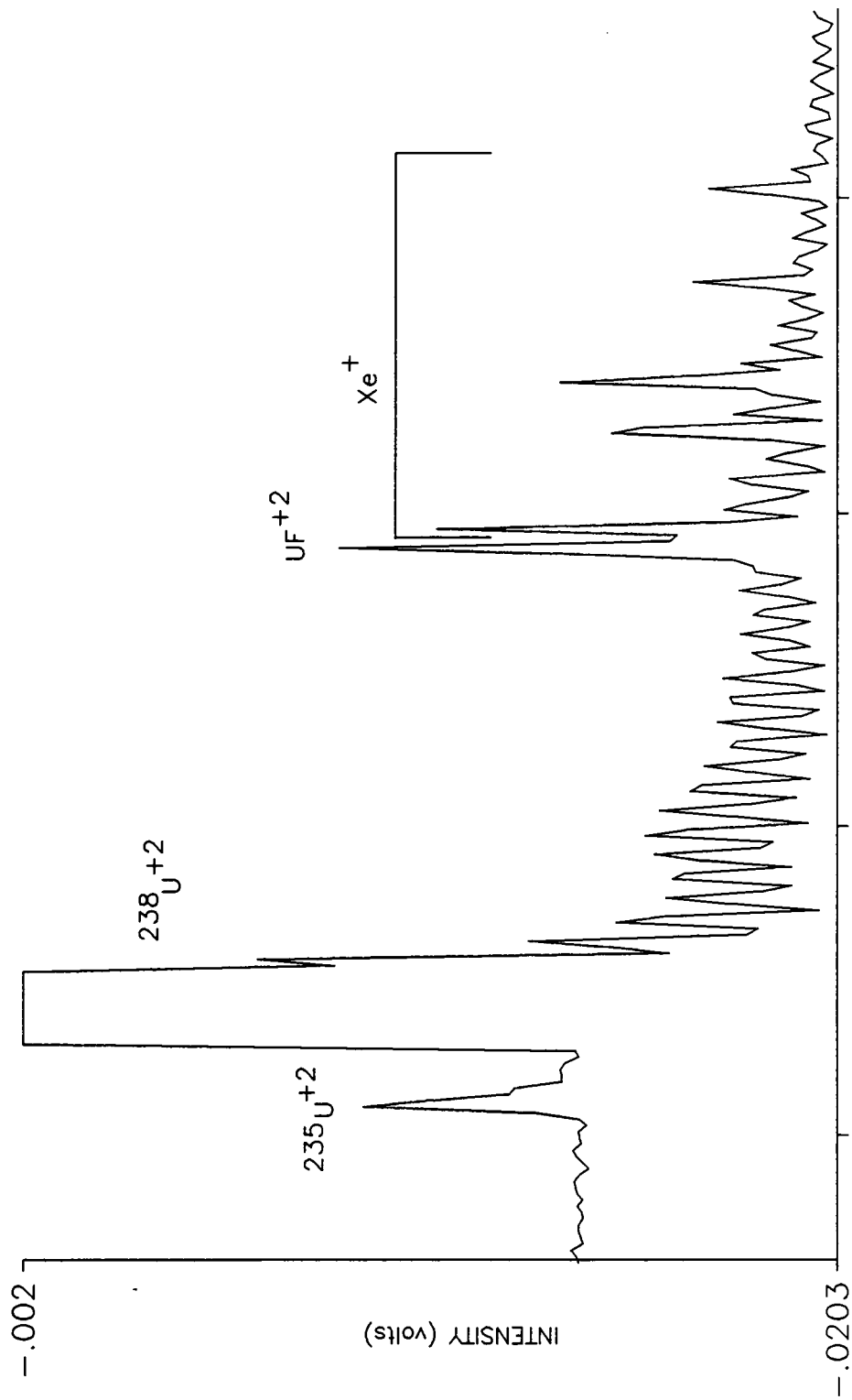


Figure 37. Magnification of TOF region: 19.3 - 21.3 μsec (from Fig. 35).

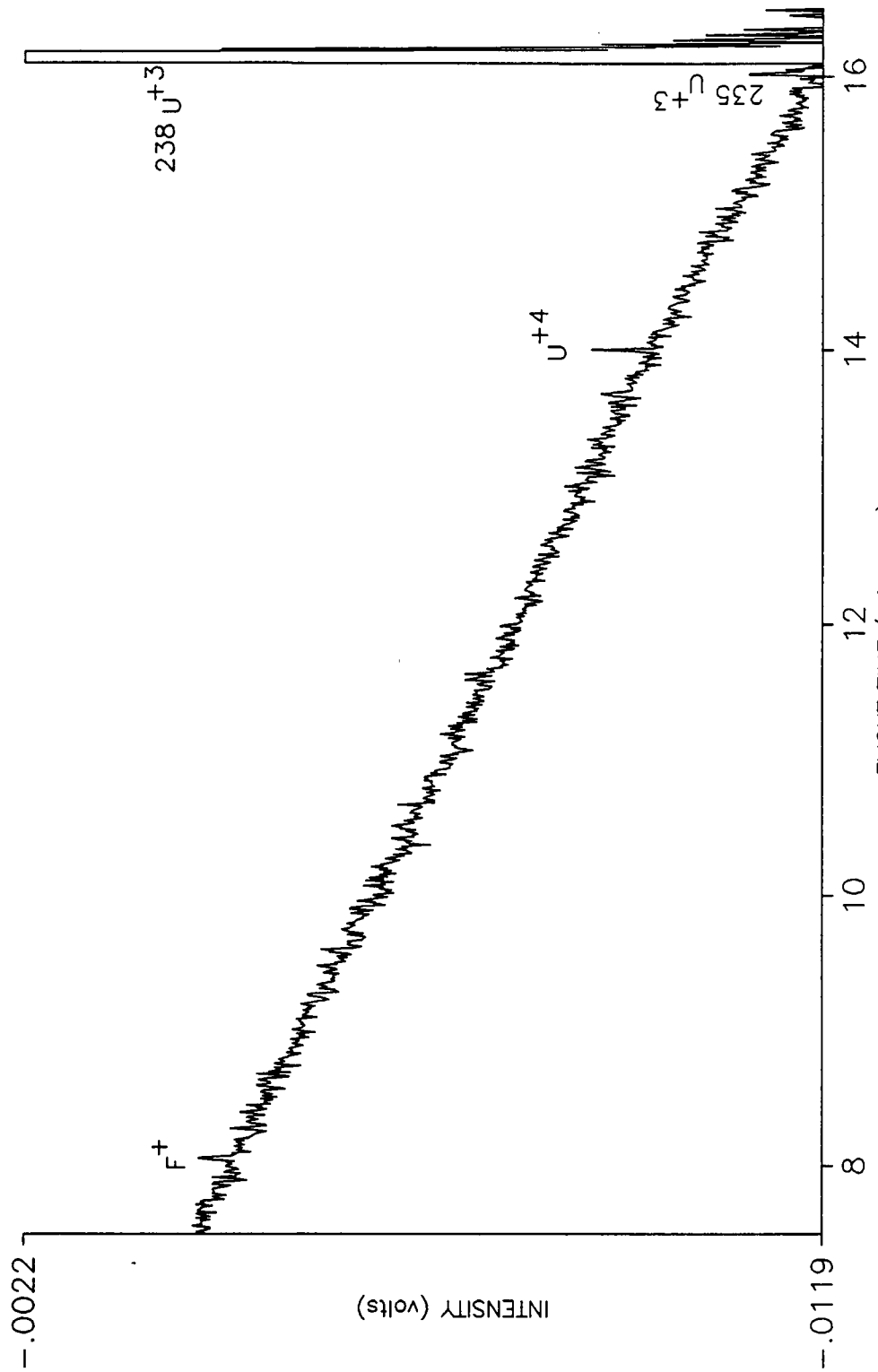


Figure 38. Magnification of TOF region: 7.5 - 16.5 μsec (from Fig. 35).

D. MPI and Photoelectron Results Using The PES System

The MPI-PES system (shown in Fig. 11) provided an excellent opportunity to not only confirm the unexpected results of this experiment, but to acquire complimentary photoelectron spectra of UF_6 undergoing MPI. The opportunity to use tunable UV laser pulses, of shorter wavelength than the fourth harmonic of the Nd:YAG laser, was also advantageous. Figure 39 shows the MPI mass spectrum acquired using the reflectron TOFMS and λ=225 nm laser pulses from the WEX. The spectrum is convincing evidence for the reproducibility of the experiment. Similar results were obtained with each of the harmonic wavelengths as well. More interesting are the photoelectron spectra which were acquired in the apparatus. Figure 40 shows the kinetic energy of the photoejected electrons from the MPI of UF_6 using λ=266 nm light. Only "slow" (energies less than 1 eV) electrons were observed. Figure 41 shows the analagous results when using λ=355 nm pulses and Figure 42 depicts the MPI-PES results when λ=532 nm light is used. Note that the scatter arises from the space charge effects that perturb the electrons due to the higher laser fields needed for MPI at this wavelength. Not only is xenon an excellent mass calibrant for a TOFMS, it serves as an excellent calibrant for an electrostatic energy analyzer as well. Having shown that UF_6 can undergo MPI at the wavelength, λ=440.88 nm, the standard mixture of UF_6 in xenon can be photoionized together to give a spectrum which contains the photoelectrons from both species. Figure 43 shows one such result and clearly indicates the characteristic photoemitted electrons from xenon along with the slow electrons for UF_6. It is also possible to observe negative ions such as F^- in either the reflectron or the energy analyzer, but no negative ions were detected in any of these experiments. It is a straightforward procedure to obtain and compare the differences in ion signal intensity when using linearly (horizontally or vertically) polarized light versus the intensity when using circularly polarized light (obtained using

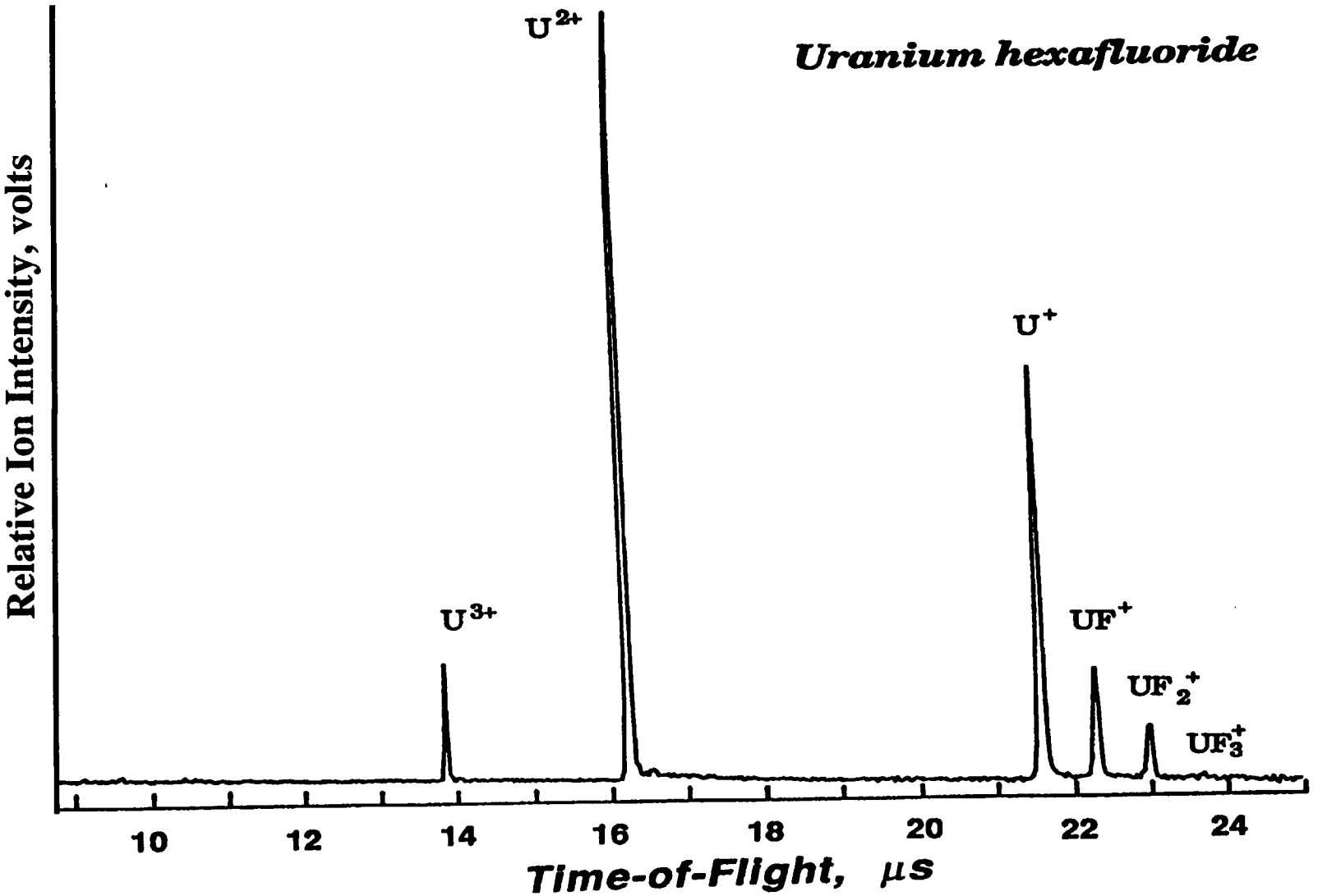


Figure 39. MPI mass spectrum using MPI-PES apparatus.

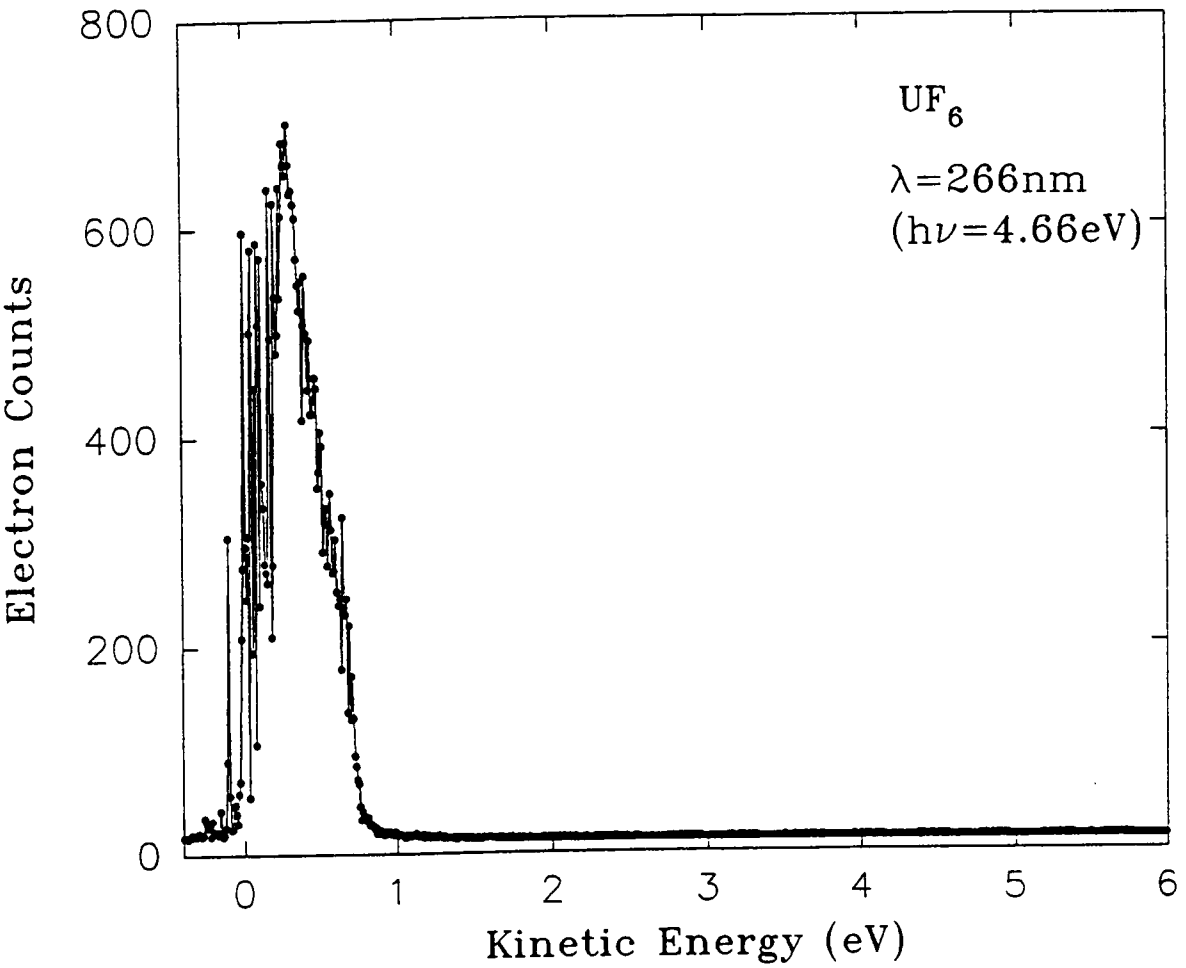


Figure 40. Photoelectron spectrum of UF_6 using λ=266 nm.

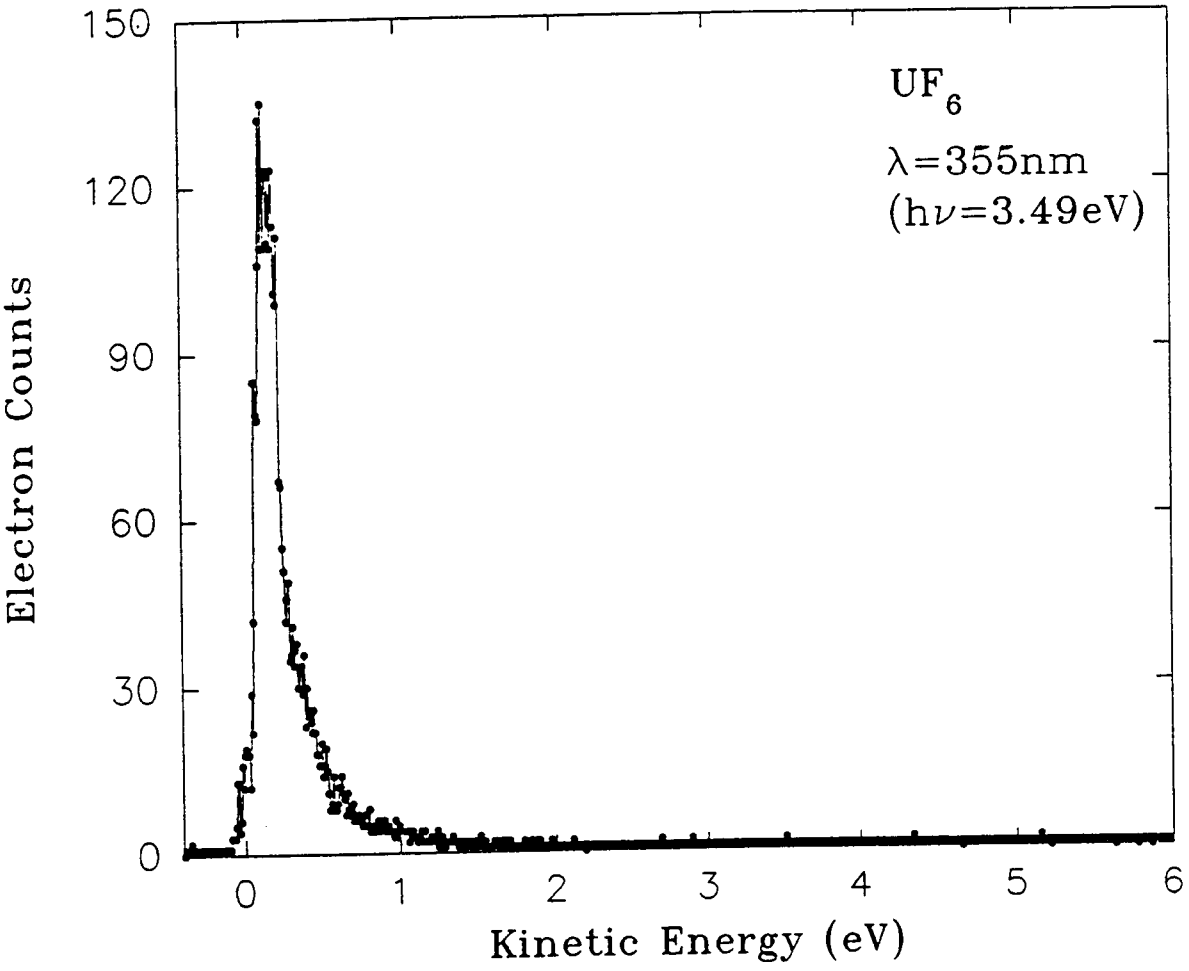


Figure 41. Photoelectron spectrum of UF_6 using λ=355 nm.

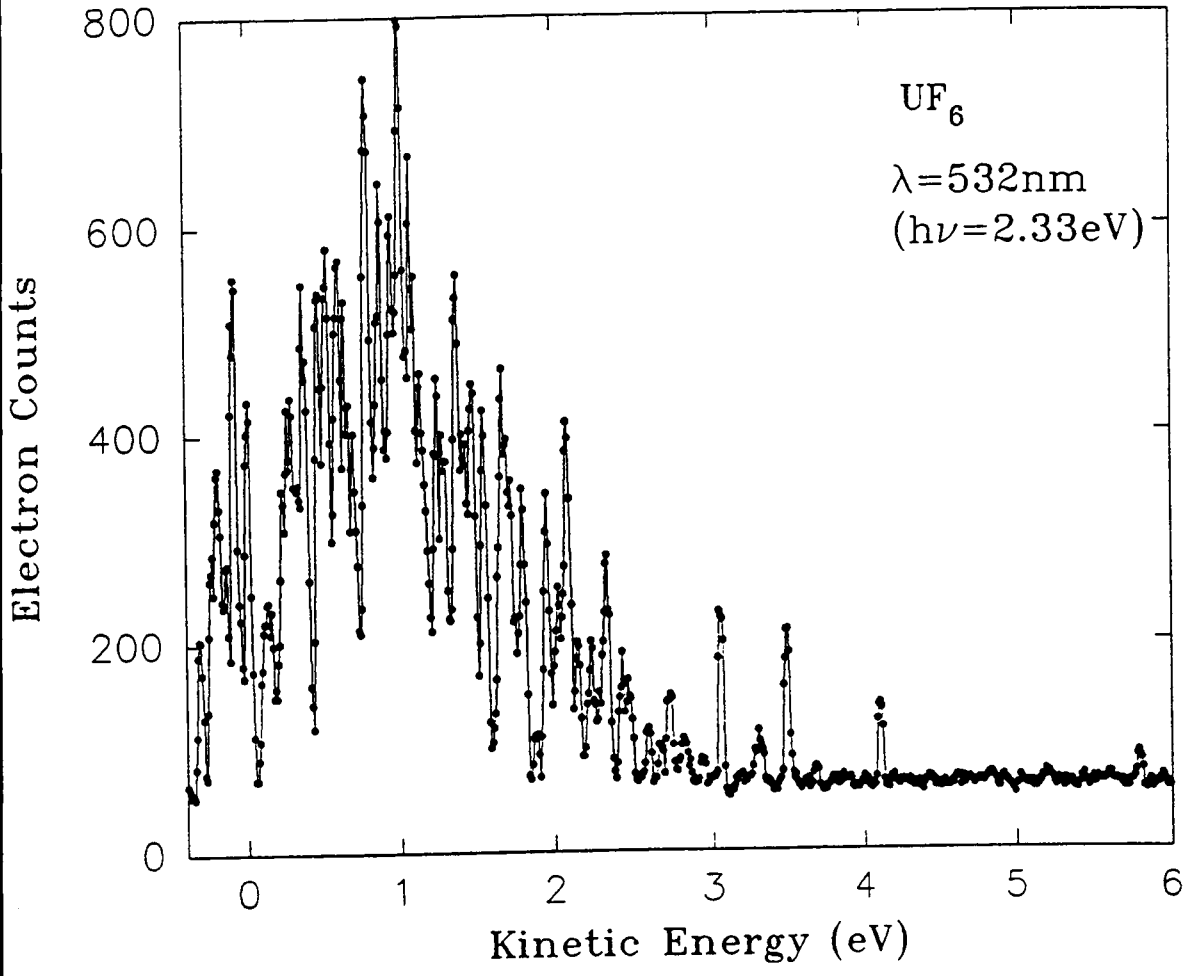


Figure 42. Photoelectron spectrum of UF_6 using λ=532 nm.

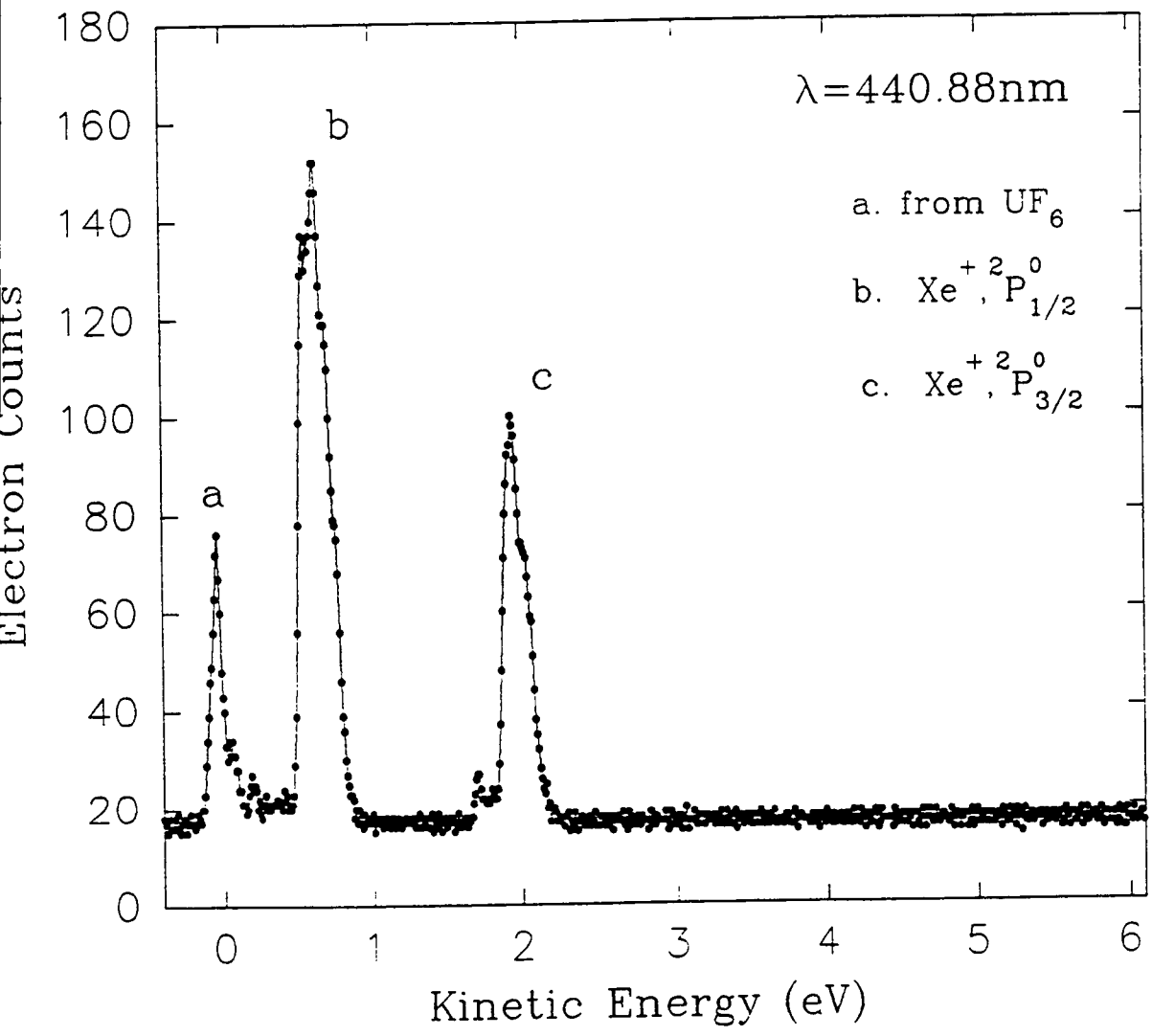


Figure 43. Photoelectron spectrum of UF_6 and xenon using λ=440.88 nm.

quarter waveplates). This comparison was done for each harmonic wavelength of the laser and no substantial differences in the signal ratios were noted. Figure 44 shows the ion signal ratios obtained when using λ=266 nm light.

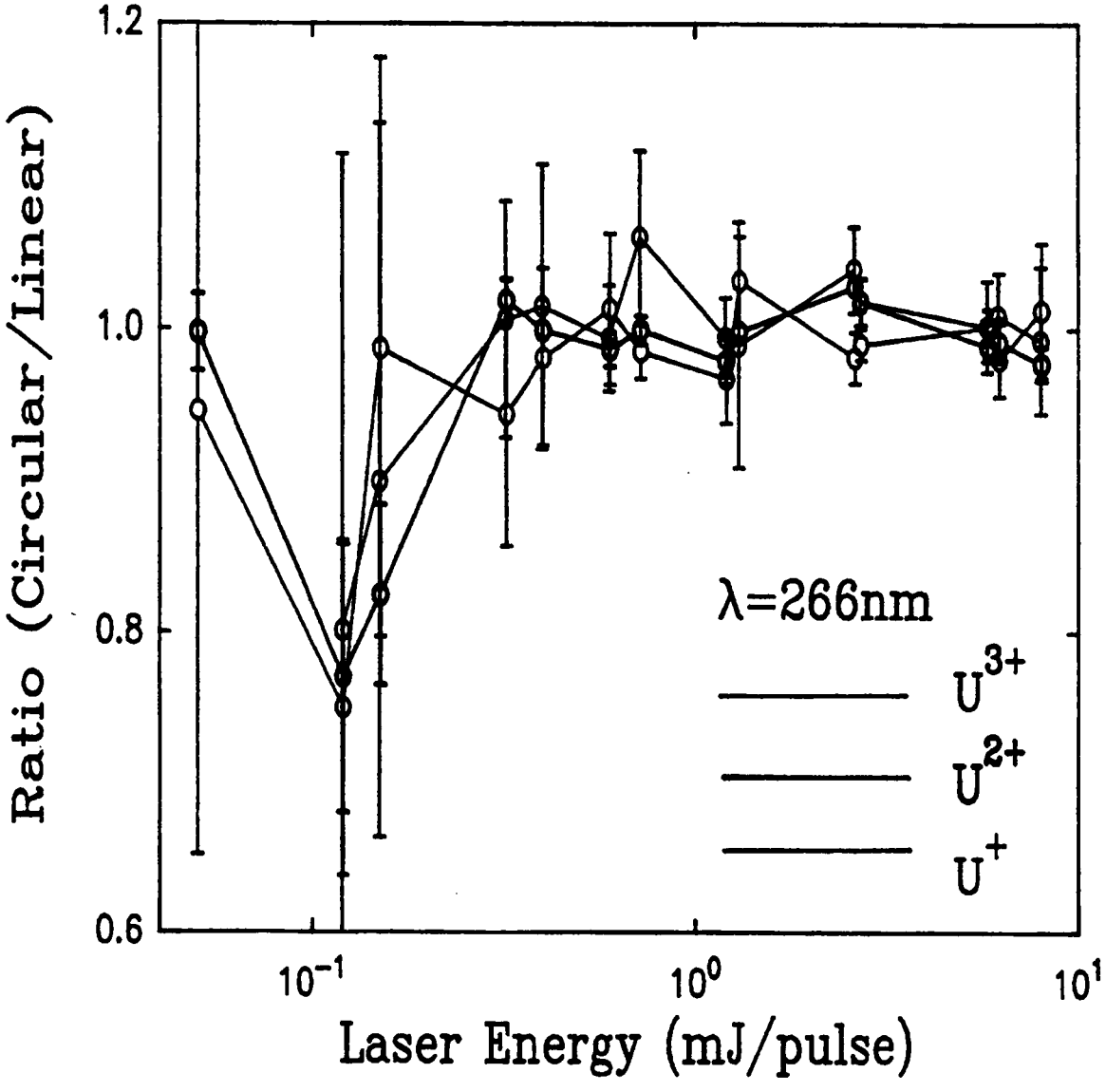


Figure 44. Ion signal ratios for circular and linear polarizations.

CHAPTER IV

DISCUSSION

One of the principal objectives of these experiments was to determine a wavelength(s) with which UF_6 could be effectively and efficiently photoionized using a pulsed laser. The very first experiments involving laser MPI of UF_6 indicated that this system is indeed remarkable. The ease with which atomic ions were produced was striking. The fact that multiply charged uranium atoms (U^{2+}, U^{3+}) were more intense than U^+ was unprecedented. The initial studies of Wittig *et al.* had also pointed to this unusual property of UF_6.[47-49] It was clear that a more in-depth understanding of the MPI mechanisms which might be at work was required.

The "classic" representation for the MPI of a molecule is shown in Figure 1 where MPI can proceed through the "neutral ladder" and/or the "ionic ladder". The ionic ladder can be eliminated from further consideration by virtue of the data contained in the three-dimensional spectra shown in Figures 15, 18, and 22. These spectra show clearly that at decreasing power densities, the signal intensities of the UF_x^+ fragments do not increase relative to U^+ or U^{2+} and the parent ion is not observed even at low powers. If this mechanism were operative, then at sufficiently low laser powers the UF_x^+ ion fragments with high (>4) values for x would be observed. The formation of UF_5^+ in particular, would be expected to dominate at low powers. Up-pumping through the ionic ladder depletes these populations at high power and results in populating the upper levels (x<3) and eventually U^+, from which the U^{n+} ions originate. No data obtained in these experiments support the ionic ladder climbing mechanism. The difficulty now is to examine the data for clues as to whether the neutral ladder is responsible for the MPI. Unfortunately, the detection of the neutral fragments

directly is very difficult, which greatly complicates matters. It is possible to detect the formation of neutral uranium atoms by using resonance ionization spectroscopy (RIS) as was described in the Results (section C). If uranium atoms are being formed in multiphoton dissociation (i.e., the neutral ladder) which leads to U^+ ions by nonresonant or resonantly enhanced MPI then one would expect the U^+ ions to be more intense than U^{2+}. This does not seem to be the case. Perhaps the most surprising observation is the fact that MPI signals for UF_6 are as intense as the resonantly enhanced multiphoton ionization (REMPI) of Xe, although many more photons are involved in the MPI of UF_6 than the 5 photons required to ionize Xe. These observations lead us to suggest a new mechanism for MPI, namely MPI involving superexcited states via a "giant resonance".

To properly examine the details of these experiments, one must refer again to Figure 3 (page 10); however, Figure 3 as drawn is not to scale and as such is inadequate. Additional details are required concerning the various energy levels of the different regions of the ladders. Many of these values are available from the literature, but some must be estimated (or calculated). To correctly scale the energy levels of the neutral ladder requires knowing the F_xU-F bond energies. These have been determined by Lau and Hildenbrand and are tabulated in Table I.[64] To scale the levels of the ionic ladder requires the ionization energies for the various UF_x species of interest. Table II contains a listing of the ionization potentials and the electron impact appearance potentials for these species, as compiled from Hildenbrand[65] and from Lau and Hildenbrand.[66] In addition, as U^{n+} ions are of primary interest, atomic ionization potentials are required as well. Table III lists the pertinent values, both measured and calculated, as given by Carlson *et al.*[67] A final resource is Table IV which lists the energies (in eV) for the wavelengths used in these experiments. With these data the energetics of Figure 3 can be more precisely depicted, and the minimum energy requirements

TABLE I

F_xU-F Bond Energies

Bond	Energy (eV)
F_5U-F	3.07
F_4U-F	4.24
F_3U-F	6.37
F_2U-F	6.41
FU-F	5.85
U-F	6.71

TABLE II

UF_x Ionization Energies

Species	Precursor	IP (eV)
UF_6^+	UF_6	14.00
UF_5^+	UF_6	14.20
UF_5^+	UF_5	11.29
UF_4^+	UF_6	17.5
UF_4^+	UF_4	9.96
UF_3^+	UF_3	7.05
UF_2^+	UF_2	6.2
UF^+	UF	6.0

TABLE III

Atomic Ionization Potentials		
Species	Precursor	IP (eV)
F^+	F	17.4
U^+	U	6.19
U^{2+}	U^+	(11.63)
U^{3+}	U^{2+}	(18.09)
U^{4+}	U^{3+}	(30.9)

( ) = Calculated value.

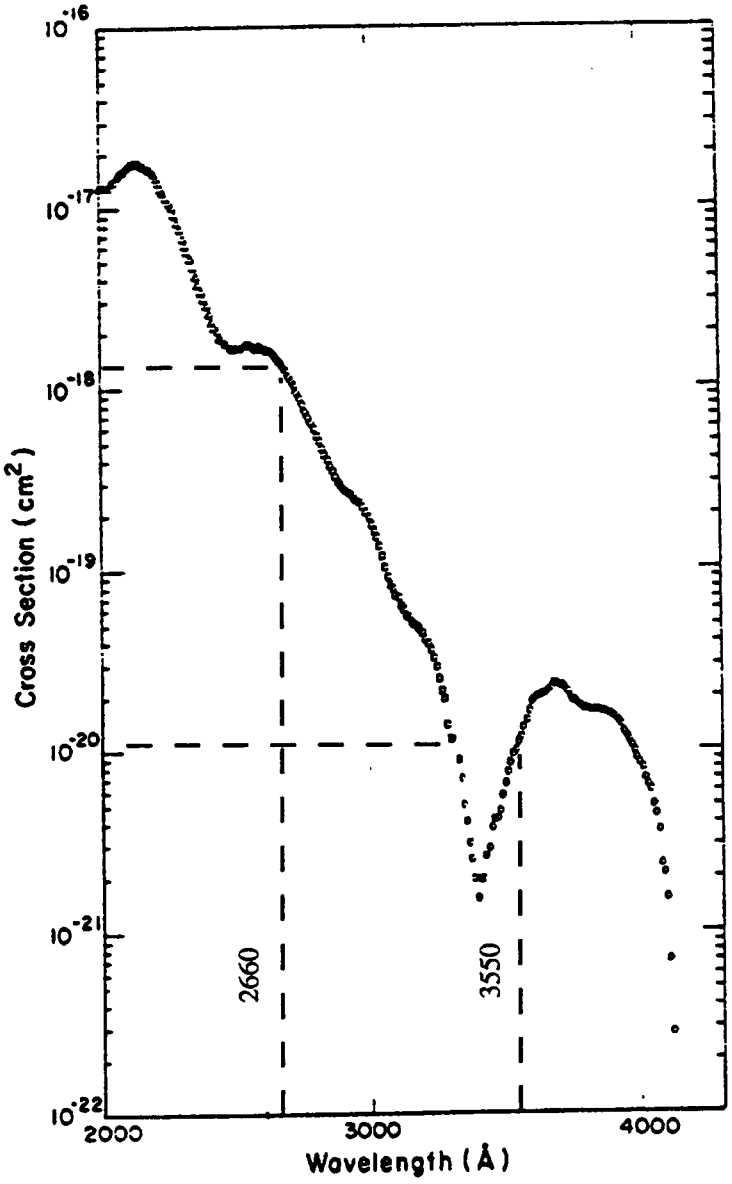
TABLE IV

Photon Energies	
λ (nm)	Energy (eV)
1064	1.17
591	2.10
532	2.33
440	2.82
355	3.49
266	4.66

of the hypothesized superexcited state, UF_6^{**}, can now begin to be estimated. However, information is still required concerning the atomic levels of uranium and the energy of the giant resonance.

The number of energy levels in neutral atomic uranium is enormous and is listed as 92,000 with an average density of 15 lines per Angstrom.[68,69] In a previous laser excitation experiment in UF_6, Allison has recorded the emission of photons using a focused laser. Allison had observed as many as 440 emission lines, half of which were attributed to U neutrals and the other half from U^+.[27] For the purposes of this discussion it is only necessary to note that this enormous number of energy levels creates a very dense manifold of states in going from U to U^+. It is expected that the energy region between U^+ and U^{2+} will likewise have a very dense manifold of states. The final piece of spectral data needed to complete the puzzle, starts with the absorption spectrum of UF_6 which covers the region λ=200 - 420 nm.[70] The UV absorption spectrum of DePoorter and Rofer-DePoorter is reproduced in Figure 45. The wavelengths of the third and fourth harmonics of the Nd:YAG laser have been indicated for qualitative comparisons of the absorbance cross section, σ. Srivastava *et al.* obtained the electron energy loss spectra for UF_6 and by correlating their results to those of DePoorter and Rofer-DePoorter (see Fig. 45), were able to derive the photoabsorption cross sections for the region λ=206.7 - 43.5 nm.[71]

Large atoms whose outer electrons are partially shielded from the attractive force of the nucleus by the presence of *d* and/or *f* electrons are described as experiencing the lanthanide contraction. Connerade has described how the screening of the outer electrons causes the atomic potential energy curve to change from a single well, to that of a double well.[72] The outer region of the double well is influenced by the magnitude of the screening and as such describes the diminished, long-range Coulombic attractive forces. The inner region posesses

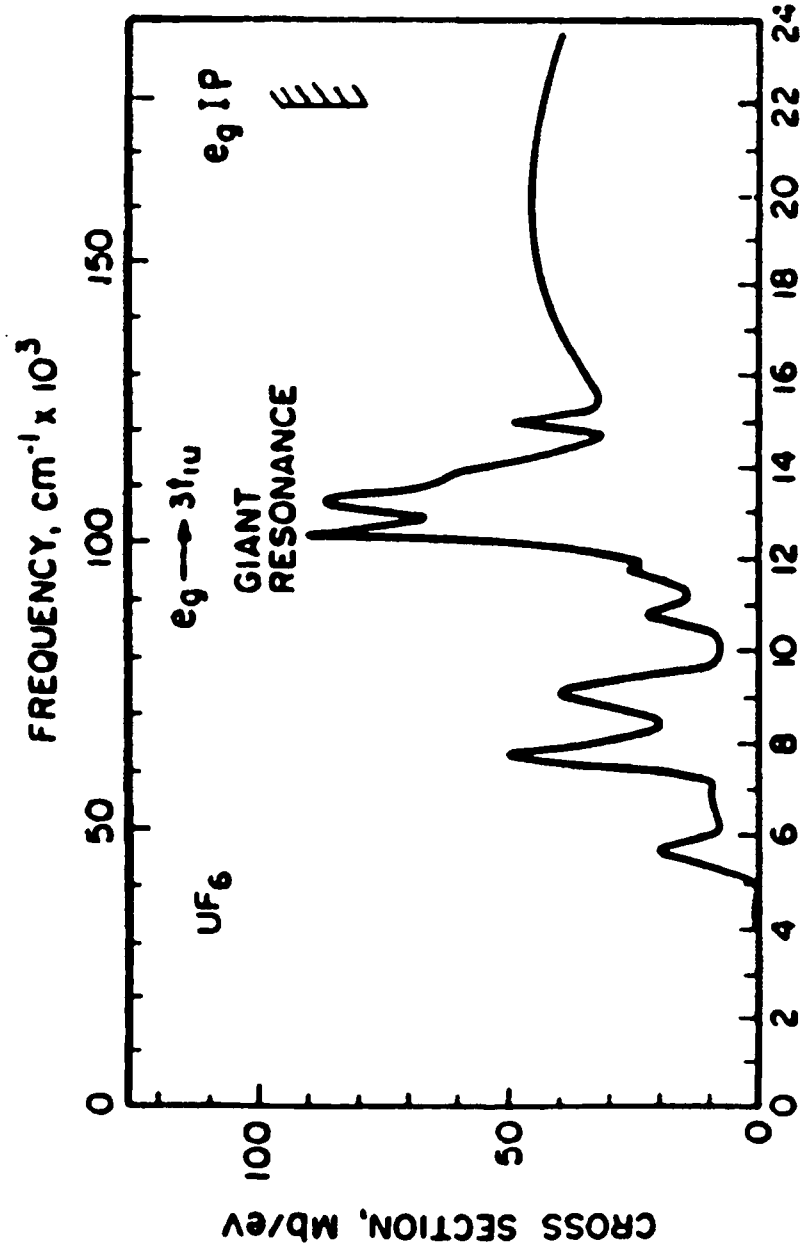


From Reference 70: G. L. DePoorter and C. K. Rofer-DePoorter, Spectros. Lett. 8, 521 (1975).

Figure 45. UV absorption spectrum for UF_6.

a potential well which is acted upon by the strong, repulsive centrifugal forces. For this short-range, inner well to acquire a new bound state it must be pulled down from the continuum (i.e., a *f* orbital). Indeed, the wavefunction of the excited electron can become resonantly localized in this inner well and require longer than the normal time to escape. The spatial overlap between the initial (*d*) state and final (*f*) state wavefunction can posess gigantic oscillator strengths, hence the name "giant resonance". Robin has also described the type of $nd \rightarrow f$ transition and the general characteristics for its manifestation in polyatomic molecules, particularly UF_6.[73] Recognizing the correlation between the absorbance features in the spectrum of Srivastava *et al.* (see Reference 71), Robin identified the giant resonance in UF_6 in the region between 12 - 14 eV. One key feature which permits $d \rightarrow f$ giant resonances in a polyatomic molecule are the presence of an unoccupied antibonding valence shell orbital of *f* symmetry, high molecular symmetry, and occupied valence molecular orbitals of *d* symmetry from which the excitation can originate. The octahedral UF_6 molecule fits this case perfectly. The electronic configuration of the valence shell of uranium is $5f^3 6d 7s^2$. When bonded to six fluorines by transferring the electron density to the F atoms, the net effect can be described as inserting a set of empty *f* orbitals between the occupied *d* molecular orbitals and *p* (in this case) ligand orbitals.[74] In fact, relativistic bonding calculations show that for the case of charge transfer transitions from the ligand to the central atom, only $(F\text{-}2p) \rightarrow (U\text{-}5f)$ are possible because the *f* orbitals were emptied during bonding.[75] The spectrum of the giant resonance in UF_6 is reproduced in Figure 46. Note that the giant resonance is the most intense one ($\approx$ 12 -14 eV) and lies just below the ionization limit. The less intense ones are described simply as "molecular resonances" for the purpose of this discussion.

Having now collected all the necessary details, Figure 3 can be reconstructed (to scale)



From Reference 73: M. R. Robin, Chem. Phys. Lett. 112, 33 (1985).

Figure 46. "Giant Resonance" in UF_6.

to show the relationship of the superexcited UF_6^{**} system to the other mechanism participants. Using the data from Tables I-IV and taking the values for the molecular and giant resonances directly from Figure 46, one can now construct Figure 47. Since most of our discussion involves the simplest (fewest number of photons) case of λ=266 nm excitation, we show the incremental energies for $nh\nu$ (in groups of 3 = n). Figure 47 uniquely permits the reader to compare all three mechanisms within the reference framework of the molecular resonances and the number of photons absorbed, n. By way of explanation, starting from the left edge of the figure, the molecular resonances are taken directly from Figure 46, the photon energy from Table IV, the F_xU-F bond energies from Table I, the UF_x ionization energies from Table II, and the atomic ionization potentials from Table III. The doubly charged UF_x fragments are added to the right edge although no ionization potential data are available for these. However, as the exact values for these energies are not crucial to the discussion, the approximation is not a fatal one.

One must now closely examine the data and attempt to determine if the energy level diagram correctly represents the experiment. Beginning with the results from λ=266 nm with the 7.5-cm lens from Figure 16, the slopes for U^{n+} are all $\approx$ 5. Clearly from the energy diagram of Figure 47, n must be greater than 15 in order to produce U^{3+}. As stated in chapter III, saturation effects are evident at these power densities. The important feature of this figure is that the slopes for U^{2+} and U^+ intersect at low powers, i.e., U^+ being more intense at low power. The corresponding slopes for the UF_2^+ and UF^+ are equivalent, suggesting that both ions have a common precursor. Next consider the low power data acquired with the 50-cm lens (see Figures 23 and 24). In the region below 2 x (10^9) W/cm^2, the U^+ ion intensity is greater than that of the U^{2+}, albeit not by very much. The slope of the U^+ ion is $\approx$ 11, but energetically only 9 photons would be needed to produce the ion.

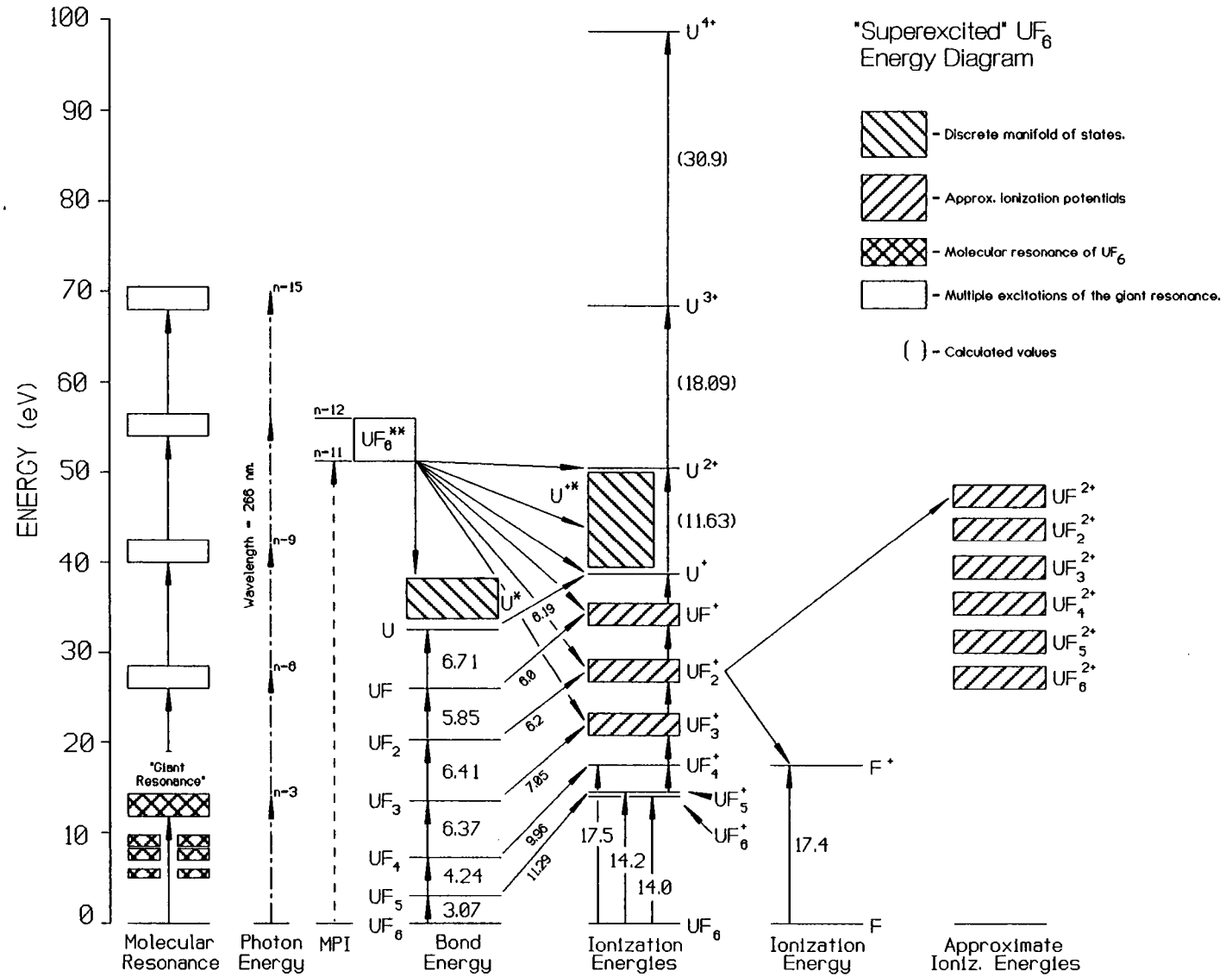


Figure 47. "Superexcited" UF_6 energy diagram.

The slope of the U^{2+} ion is $\approx$ 13, but only 11 photons should be required. The slope for the U^{3+} ion is $\approx$ 17, but only 15 photons would be required for its production. Note that this assumes reasonably accurate calculated IP values (see Table III). Notice also that the slope values for the UF_x^+ ions are approximately 2 photons higher than the energy levels predict. Now let us consider the data taken with the 35-cm lens. For the U^{n+} ions, the low power slopes (S_{LP}) display the same behavior as those of the 50-cm lens, except that there is a plateau in the data at $\approx$ 2.25 x (10^9) W/cm^2. Beyond these power levels, the higher power slopes (S_{HP}) are essentially identical. These comparisons can be more easily made by considering Figures 25 and 26. In the region of low power, the slope for the U^{2+} ion is consistently 2 photons higher than for U^+; however, 3 photons of this wavelength would be required to span the energy difference between U^+ and U^{2+} (shown as 11.63 eV). The observation that both ions experience this plateau in the 35-cm lens slope data strongly suggests that both species are experiencing saturation of a mutual, lower-lying energy level. The giant resonance could satisfy that condition since it is lower in energy than either U^+ or U^{2+}. Since all of the spectra presented show ion signals for U^+ and U^{2+}, even at the lowest powers, then it cannot be assumed that all of the population of the doubly-charged ion comes solely from the up-pumping of the population of the U^+ level. Recall from the introductory remarks that a characteristic of the superexcited mechanism is that the ions are produced in approximately the same ratios regardless of laser power. This certainly applies to these data. As drawn in Figure 47, the threshold for the UF_6^{**} state is at n = 11 photons ($\approx$ 51 eV), which would be the minimum energy required for dissociation into the U^{2+} and U^+ levels. Several dissociation channels are depicted in the figure. Dissociation channels, based on the data obtained, which are available are those to the U^{2+} state, an excited state manifold shown as U^{+*}, the U^+ level, an excited state manifold shown as U^*, the UF^+ level, the UF_2^+ level,

and the UF_3^+ level. As no atomic resonances for U were observed then one must presume that either neutral uranium atoms are not produced by dissociation or the population is too small to observe. The major dissociation channels will be those most closely matched in energy with the UF_6^{**} molecule, and they are U^{2+} and U^+. These data strongly indicate the existence of the superexcited state corresponding to an 11 photon transition, or a (3 + 8) REMPI process via the giant resonance.

For the purposes of this hypothesis, acceptance of the role of the giant resonance is comparatively secure. If the concept of the experimentally observed giant resonance playing a role in the MPI of UF_6 is feasible, then the n = 11 (or 12) photon process is converted to an n = 3 + 8 (or 3 + 9) REMPI process. Although precise, mathematical calculations for the transition probabilities of this MPI event are not available, they are not necessary to envision the problem. By invoking the giant resonance as a real intermediate step in the MPI of UF_6, then intuitively the magnitude of the transition probability has increased relative to that of an n = 11 (or 12) MPI process. But is this single resonant state alone enough to explain the superexcited state? The answer is probably not. The giant resonance alone increases the magnitude of the transition probability if it is employed as a resonant state (for n = 3); however, one then has to consider the difficulty in absorbing 8 or 9 more photons for the second step to the superexcited state which lies at $\approx$ 51 eV. Recall that the case of λ=266 nm is the simplest case because it has the fewest number of photons involved. For the case of λ=1064 nm, the first transition to the giant resonance requires 12 photons, and the second step requires a minimum of 32 photons. A 32-photon, one-step transition is difficult to accept. To span the almost 40 eV energy gap between the giant resonance and the superexcited state (as represented in Figure 47) must involve other intermediate levels. At this point there are two routes to explore. The first and most obvious route is to ask if

there are other, more energetic molecular resonances in UF_6. In Figure 46, the energy scale of the data ends at 24 eV; consequently, this question cannot be answered with the available data, though the region from 24 - 74 eV would now be very interesting to examine. This is a possibility that also cannot be ruled out, since Connerade *et al.* have described a very high lying state at $\approx$ 100 eV in both UF_4 and atomic U.[76] The second route is to question the possibility of multiple excitations of the giant resonance. These multiple excitations are analogous to overtones in conventional vibrational spectroscopy or to harmonics in electronic spectroscopy. This may seem difficult to accept at first glance, but one need look no further than the experimental studies done on surface plasmons to see that integral multiples of some characteristic energy can and do occur.[77,78] Plasmons are energy quanta associated with oscillations of electrical charge (in condensed matter, e.g., metals). In a recent publication by Connerade and Dietz, in their discussion of multielectron ionization of atoms one finds that they equate resonant collective motions (of electrons) with plasmons.[79] Since plasmons and giant resonances both involve oscillations of electrons, the reader perhaps is not quite so far out on the limb by accepting the idea of "overtones" of the giant resonance. Returning to the features of Figure 47, the integral multiples of the giant resonance, in this experiment, occur for each set of three photons at λ=266 nm. For descriptive purposes, they are termed "molecular plasmons". If this concept is utilized then the question of the relative magnitudes of the transition probabilities becomes less intimidating, since now the picture suggests superexcited ladder climbing in discrete steps via these molecular plasmons. The data has shown that at the lowest observable powers the U^+ and U^{2+} ions are the dominant features, consequently the energy level of the molecular plasmon which corresponds to n = 12 must be one which is easily reached, inferring large oscillator strengths between the initial and final states. Given that these power densities are lower, by a factor of $\approx 10^4$, than most reports

of multiply charged ions and given the small population of UF_6 molecules in the sample volume, the actual oscillator strengths may be exceptionally large. Recall from Figure 32 that the MPI signals from UF_6 are comparable to the REMPI signals of xenon despite the differences in excitation mechanisms.

Returning to the problem of rejecting the neutral ladder mechanism, there are some rather straightforward arguments which may be made. For up-pumping through the neutral ladder, at some point there will be an appreciable population of U atoms and yet when scanning the dye laser in the region of strong atomic U resonances, no resonance enhancement is observed. This alone is not conclusive though, because given the expected density of states one could make the arguement that every wavelength was in resonance and the effect just could not be distinguished. If atoms were produced then the resulting MPI PES spectra would contain discrete energetic electrons characteristic of the uranium atom. Instead, the PES results at all wavelengths examined show the same results, "slow" electrons. Also for the case of the MPI of an atom, the use of linearly polarized light should produce much larger ion signals (especially for large n) than those produced using circularly polarized light. The results shown in Figure 44 show that there is essentially no differences in the ion signals produced using either polarization of light. This effect has been discussed by Carmen and Compton[80], as well as by others. Noting from the spectra shown throughout this discourse, the ratios of the UF_x^+ ions are always approximately constant. This implies two things. First, for there to be UF_x^+ present in the spectrum at all, then extensive ladder switching must be occurring (equally) for all the intermediate UF_x fragments. For the UF_x^+ fragments to maintain their near constant ratio relationship then not only must the ladder switching occur at a steady rate, but the uppumping of the ionic ladder must occur at a steady rate such that none of the lower levels become depleted. This is a combination of unlikely

events. The fact that UF^+, UF_2^+, and UF_3^+ all have approximately the same power dependence ($\approx$ 9) suggests that the the multiple (three) excitation of the giant resonance corresponding to n = 9 may be responsible. Different ions that come from a common photochemical precursor will have the same power dependence. A final argument against neutral ladder climbing can be made by qualitatively examining the effect of the Franck-Condon principle. In Figure 47 (and Figures 1 and 3) the neutral ladder climbing is represented with vertical arrows stacked on top of each other. This does not imply that a favorable Franck-Condon overlap exists between these fragments. In fact, the converse is more likely to be true when energetic photons (i.e., not IR photons) are used with a pulsed nozzle. When cooled to the calculated temperature of $\approx$ 124°K by the pulsed nozzle expansion, approximately 80% of the molecules will occupy the 10 lowest-lying vibrational states.[18] The ground vibrational state will contain about 28% of the population. Upon cooling, the excited stretching modes are depopulated more rapidly and contain negligible populations at this temperature. Any populated, excited modes are likely to be the bending modes.[81,82] Contributions to the transition probabilities from "hot bands" is greatly diminished. In addition, the large relative increase in bond energies proceeding up the ladder from UF_6 indicates a shortening of the U-F bond distance and subsequent shift in the equilibrium coordinates with respect to the initial coordinates of the ground state UF_6 molecule. The net result is that the excited state vibrational wave function may have negligible values in that region.[83]

Though the spectral features are essentially identical for all the wavelengths used, there are some subtle differences between the λ=266 nm and λ=591 nm results. In examining the λ=266 nm data in Figures 29 - 31, notice that the ^{235}U ion is observed in its singly, doubly, and triply charged states, but no signals from U^{4+} or F^+ are observed. There is also a

relatively consistent contribution from the UF_x^+ ions. In the case of the λ=591 nm data, shown in Figure 33, for the lower power regime, the $U^{2+} >> U^+$, and there are virtually no signals from UF_x^+. If one examines the higher power spectrum of Figure 34, one observes that $U^{2+} > U^{3+} >> U^+$ with almost no UF_x^+ ions observed. Figures 35 - 38 are magnifications of the regions of Figure 34 which are of interest. Notice from these spectra that signals arising from F^+ and from UF^{2+} are seen when a corresponding depletion of signal for UF_2^+ is observed, relative to the adjacent UF^+ and UF_3^+ ion signals. The most plausible explanation is that UF_2^+, has undergone dissociation itself and this is indicated in Figure 47. The postulated difference in energies between UF_2^+ and UF^{2+} means that some up-pumping of the UF_2^+ fragment must be occuring. Also, note that U^{4+} is observed as the signals from U^{3+} increase. This is another strong indication that some up-pumping may be occuring. Finally, note that a trace of signal which could be attributed to UF_4^+ is now seen. To achieve the same level of the superexcited state ($\approx$51 eV) requires 25 photons be absorbed, but it also requires that 6 photons be absorbed to reach the giant resonance. This first step would certainly be less efficient than when using λ=266 nm. The possible explanation for the results obtained from using λ=591 nm light is that the superexcitation of UF_6 does not completely progress to the same high energy level as with λ=266 nm light. Instead, some lower level of excitation may dissociate into fragments which are themselves up-pumped. The much larger signals of the U^{2+} ion suggests that the primary dissociation channel may be into the U^{+*} manifold, where the longer wavelength photons have an excellent chance of encountering a resonance enhancement which produces more U^{3+} and U^{4+}. It is highly probable that the UF_2^+ fragment is itself undergoing MPI, a not too surprising conclusion.

The original work on this topic, by Wittig and coworkers in 1981,[47-49] has many similarities, and an important difference. In their experiments they employed an effusive

source for UF_6, although they describe the process as "collisionless". In the experiment herein a 7.3% mixture of UF_6 in xenon was used in a pulsed nozzle expansion to produce pressures which were an order of magnitude lower; consequently, by comparison this experiment was "more collisionless". In addition, to further reduce the probabilities of ion collisions a large extraction field was used to immediately remove the ion from the TOFMS focal volume. It is noted that as the experimental apparatus used by Wittig evolved to one which more closely matched the one employed in this study, their MPI data more closely resemble the current data.

It is interesting now to look back at the experiments on $Fe(CO)_5$ by Duncan *et al.*[43] In his discussion he points out that even near the photoionization threshold, the Fe^+ signal is dominant despite the fact that the appearance potential for the parent ion, $Fe(CO)_5^+$ was twice as low in energy. His results on $Cr(CO)_6$ and $Mo(CO)_6$ were similar. Engelking had later described that in the MPI of iron carbonyl, atomic iron was produced.[45] He also discussed that the MPI of iron is either so strongly saturated that resonance enhancement is not important to ionization or that the iron is produced in electronically excited states within one photon step of ionization. Even though iron carbonyl is an example of a highly symmetric molecule which posess a heavy central atom (i.e., a metal) in a fully coordinated ligand "cage", the previously described constraints on the orbital symmetries eliminate it from the consideration of having a giant resonance. The purpose of including it in this discussion is only to illustrate the utility of PES measurements for the identification of atoms in MPI experiments. In a series of papers, Nagano *et al.* showed conclusively that atomic iron was present as a product of the MPI of $Fe(CO)_5$ by detecting and assigning the photoelectrons ejected from both Fe atoms and excited Fe atoms.[84-87]

As a final comment, consider again the experiment of Rhodes and coworkers (see

Reference 50) where they observed the U^{10+} ion. The power density is given as $\approx 10^{14}$ W/cm^2, and this is certainly an important experimental difference. More important, however, is the fact that by using the ArF^* laser photons (λ=193 nm) they could reach the giant resonance with less photons, since $n = 2$ instead of 3. In the context of this discussion this is the most important difference due to the suspected strength of transition via the giant resonance. The obvious added benefit is that each step of the multiple excitations only requires 2 photons, instead of 3, so that the gain in the transition probability manifests itself at each step of the excitation. If this can be accepted as an advantage, then their experimental results on UF_6 are hardly surprising.

CHAPTER V

CONCLUSIONS

This dissertation presents a comprehensive experimental study of the multiphoton ionization of uranium hexafluoride. The results of these experiments suggests a new mechanism of ionization which strongly implicates what have been termed "giant resonances" in molecules. The role of the giant resonance in MPI processes has not been previously described and originates in this study. The evidence provided strongly indicates that the traditional neutral ladder and ionic ladder MPI mechanisms are not operative under these conditions, but instead it is possible to excite UF_6 to one or more highly excited, or "superexcited" states. The primary dissociative channels for this state appear to be the production of U^{3+}, U^{2+}, U^{+}, and most probably excited states of U and of U^{n+} ions, which may then undergo up-pumping themselves. It is rather probable that any wavelength of light would be able to effect a resonant transition in the dense, power-broadened manifold of excited states. The observation of slow electrons resulting from the MPI of UF_6 is taken as further evidence for the following dissociative decay:

$$UF_6^{**} \rightarrow U^{n+} + 6F + ne^{-}. \qquad (2)$$

The decay of a superexcited state is expected to produce slow electrons as a result of equipartition of energy. The absence of discrete fast electrons together with the fact that linearly and circularly polarized light give the same ionization rates strongly argues against the production of U atoms (i.e., the neutral ladder). It cannot be said with absolute certainty that there are no uranium atoms present after the dissociation of UF_6^{**}, but it can be said with reasonable assurance that there cannot be a substantial population of them. The general characteristics of the giant resonance in polyatomic molecules are the presence of unoccupied

antibonding valence shell orbitals of *f* symmetry, high molecular symmetry, and occupied valence molecular orbitals of *d* symmetry. The octahedral UF_6 molecule fits this case perfectly. The fluorine bonding greatly perturbs the electron density surrounding the central uranium; and thus, plays a major role in the occurence of the giant resonance by "emptying" the *f* orbitals on the uranium atom. Given that in its cooled state, stretching vibrations are reduced to near their ground state the net effect is to hold the central atom motionless, with respect to the fluorine atoms. Under these conditions the central atom may actually act as a "photon sink", whereby the threshold for $d \rightarrow f$ electron excitations is actually lower than the thresholds for energy redistribution through the molecule via rovibronic chaos. The exact excitation mechanism is not yet fully understood, but the reported giant resonance, having an energy of 12 - 14 eV, must surely play an important role. Multiple excitations of the giant resonance may be operative, and verifying the existence of such overtones presents future experimenters with an interesting problem.

Future directions for this experiment could follow many paths. Robin (see Reference 73) predicts a giant resonance with energy 13.5 eV in tungsten hexafluoride and this could be investigated with an experiment such as this one. Performing a nonresonant MPI experiment on uranium atoms would be expected to give very different results since the molecular resonances, and their overtones, are absent. Operating on the presumption that 44 photons can be absorbed, as was indicated by the λ=1064 nm results, then formation of the U^{6+} ion should be possible using λ=266 nm pulses provided the power density is sufficient and detector saturation can be avoided. The fact that these experiments can seemingly be done with any wavelength creates opportunities to obtain important new results using shorter laser pulses and higher powers.

LIST OF REFERENCES

References

1. F. Weigel, "Uranium and Uranium Compounds," Encyclopedia of Chemical Technology, 3rd ed., Vol. 23, John Wiley & Sons, New York, N.Y., 1983, pp. 502-547.

2. J. Bigeleisen, M. G. Mayer, P. C. Stevenson, and J. Turkevich, J. Chem. Phys., 16, 442 (1948).

3. T. G. Burke, D. F. Smith, and A. H. Nielsen, J. Chem. Phys., 20, 447 (1952).

4. J. Gaunt, Trans. Faraday Soc., 49, 1122 (1953).

5. H. H. Claassen, B. Weinstock, and J. G. Malm, J. Chem. Phys., 25, 426 (1956).

6. B. Weinstock and G. L. Goodman, Adv. Chem. Phys., 9, 169 (1965).

7. H. H. Claassen, G. L. Goodman, J. H. Holloway, and H. Selig, J. Chem. Phys., 53, 341 (1970).

8. D. P. Armstrong, R. J. Jarabek, and W. H. Fletcher, Appl. Spectrosc., 43, 461 (1989).

9. K. L. Kompa and G. C. Pimentel, J. Chem. Phys., 47, 857 (1967).

10. L. B. Asprey and R. T. Paine, Inorg. Synth., 19, 137 (1979).

11. J. L. Lyman and R. J. Jensen, J. Phys. Chem., 77, 883 (1973).

12. J. L. Lyman, R. J. Jensen, J. Rink, C. P. Robinson, and S. D. Rockwood, Appl. Phys. Lett., 27, 87 (1975).

13. R. V. Ambartzumian, N. P. Furzikov, Yu. A. Gorokhov, V. S. Letokhov, G. N. Makarov, and A. A. Puretzky, Opt. Commun., 18, 517 (1976).

14. R. V. Ambartzumian and V. S. Letokhov, Acc. Chem. Res., 10, 61 (1977).

15. A. M. Ronn, Scientific American, May 1979, pp.114-128.

16. J. J. Tiee and C. Wittig, Opt. Commun., 27, 377 (1978).

17. P. Rabinowitz, A. Stein, and A. Kaldor, Opt. Commun., 27, 381 (1978).

18. R. J. Jensen, J. G. Marinuzzi, C. P. Robinson, and S. D. Rockwood, Laser Focus, May 1976, pp.51-63.

19. R. N. Zare, Scientific American, February 1977, pp.86-98.

20. P. M. Kroger, S. J. Riley, and G. H. Kwei, J. Chem. Phys., 68, 4195 (1978).

21. K. C. Kim, R. Fleming, D. Seitz, and M. Reisfeld, Chem. Phys. Lett., 62, 61 (1979).

22. W. B. Lewis, F. B. Wampler, E. J. Huber, and G. C. Fitzgibbon, J. Photochemistry, 11, 393 (1979).

23. A. Andreoni, R. Cubeddu, S. De Silvestri, and F. Zaraga, Chem. Phys. Lett., 69, 161 (1980).

24. E. Borsella, F. Catoni, and G. Freddi, J. Chem. Phys., 73, 316 (1980).

25. K. C. Kim, M. Reisfeld, and D. Seitz, J. Chem. Phys., 73, 5605 (1980).

26. K. C. Kim and G. A. Laguna, Chem. Phys. Lett., 82, 292 (1981).

27. S. W. Allison, Ph.D. Dissertation, The University of Virginia, Charlottesville, Virginia, 1979.

28. S. De Silvestri, O. Svelto, and F. Zaraga, Appl. Phys., 21, 1 (1980).

29. M. B. Robin, Appl. Opt., 19, 3941 (1980).

30. A. Gedanken, M. B. Robin, and N. A. Kuebler, J. Phys. Chem., 86, 4096 (1982).

31. R. B. Bernstein, J. Phys. Chem., 86, 1178 (1982).

32. D. A. Gobeli, J. J. Yang, and M. A. El-Sayed, Chem. Rev., 85, 529 (1985).

33. V. S. Letokhov, "Nonlinear Laser Chemistry", Springer Series in Chemical Physics, Vol. 22, Springer-Verlag, Berlin, Germany, 1983.

34. S. L. Chin and P. Lambropoulos, Eds., "Multiphoton Ionization of Atoms", Academic Press, Orlando, Florida, 1984.

35. G. Mainfray and C. Manus, Rep. Prog. Phys., 54, 1333 (1991).

36. R. N. Compton and J. C. Miller in "Laser Applications in Physical Chemistry," D.K. Evans, Ed., Marcel Dekker, Inc., New York, N.Y., 1989, pp. 221-306.

37. K. Codling, L. J. Frasinski, P. Hatherly, and J. R. M. Barr, J. Phys. B, 20, L525 (1987).

38. L. J. Fasinski, K. Codling, and P. A. Hatherly, Phys. Lett. A, 142, 499 (1989).

39. P. A. Hatherly, L. J. Frasinski, K. Codling, A. J. Langley, and W. Shaikh, J. Phys. B, 23, L291 (1990).

40. K. Boyer, T. S. Luk, J. C. Solem, and C. K. Rhodes, Phys. Rev. A, 39, 1186 (1989).

41. C. Cornaggia, J. Lavancier, D. Normand, J. Morellec, and H. X. Liu, Phys. Rev. A, 42, 5464 (1990).

42. D. Normand, C. Cornaggia, J. Lavancier, J. Morellec, and H. X. Liu, Phys. Rev. A, 44, 475 (1991).

43. M. A. Duncan, T. G. Dietz, and R. E. Smalley, Chem. Phys., 44, 415 (1979).

44. Z. Karny, R. Naaman, and R. N. Zare, Chem. Phys. Lett., 59, 33 (1978).

45. P. C. Engelking, Chem. Phys. Lett., 74, 207 (1980).

46. F. B. Wampler, W. W. Rice, R. C. Oldenborg, M. A. Akerman, D. W. Magnuson, D. F. Smith, and G. K. Werner, Opt. Lett., 4, 143 (1979).

47. M. Stuke and C. Wittig, Chem. Phys. Lett., 81, 168 (1981).

48. M. Stuke, H. Reisler, and C. Wittig, Appl. Phys. Lett., 39, 201 (1981).

49. J. S. Chou, D. Sumida, M. Stuke, and C. Wittig, Laser Chem., 1, 1 (1982).

50. T. S. Luk, H. Pummer, K. Boyer, M. Shahidi, H. Egger, and C. K. Rhodes, Phys. Rev. Lett., 51, 110 (1983).

51. P. Lambropoulos and X. Tang, J. Opt. Soc. Am. B, 4, 821 (1987).

52. P. Dore, M. I. Schisano, M. Menghini, and P. Morales, Chem. Phys. Lett., 116, 521 (1985).

53. W. C. Wiley and I. H. McLaren, Rev. Sci. Instrum., 26, 1150 (1955).

54. "The Theory and Practice of Injection Seeding", Spectra-Physics Laser Technical Bulletin No. 10, B. Perry, Spectra-Physics Lasers, Inc., Mountain View, CA 1987.

55. D. Billings and K. Leggett, Spectra-Physics Lasers, Inc., Mountain View, CA, personal communication, 1991.

56. J. L. Wiza, Nuclear Instruments and Methods, 162, 587 (1979).

57. H. Haberland, U. Buck, and M. Tolle, Rev. Sci. Instrum., 56, 1712 (1985).

58. S. J. Bajic, Ph.D. Dissertation, The University of Tennessee, Knoxville, Tennessee, 1991.

59. S. J. Bajič, R. N. Compton, X. Tang, and P. Lambropoulos, Phys. Rev. A, 44, 2102 (1991).

60. P. R. Blazewicz, X. Tang, R. N. Compton, and J. A. D. Stockdale, J. Opt. Soc. Am. B, 4, 770 (1987).

61. H. D. V. Bohm, W. Michaelis, and C. Weitkamp, Opt. Commun., 26, 177 (1978).

62. D. L. Donohue, J. P. Young, and D. H. Smith, Appl. Spectrosc., 39, 93 (1985).

63. L. W. Green and F. C. Sopchyshyn, Int. J. Mass Spectrom. Ion Processes, 89, 81 (1989).

64. D. L. Hildenbrand and K. H. Lau, J. Chem. Phys., 94, 1420 (1991).

65. D. L. Hildenbrand, J. Chem. Phys., 66, 4788 (1977).

66. K. H. Lau and D. L. Hildenbrand, J. Chem. Phys., 76, 2646 (1982).

67. T. A. Carlson, C. W. Nestor, Jr., N. Wasserman, and J. D. McDowell, Atomic Data, 2, 63 (1970).

68. J. Blaise and L. J. Radziemski, Jr., J. Opt. Soc. Am., 66, 644 (1976).

69. R. W. Solarz, C. A. May, L. R. Carlson, E. F. Worden, S. A. Johnson, and J. A. Paisner, Phys. Rev. A, 14, 1129 (1976).

70. G. L. DePoorter and C. K. Rofer-DePoorter, Spectrosc. Lett., 8, 521 (1975).

71. S. K. Srivastava, D. C. Cartwright, S. Trajmar, A. Chutjian, and W. X. Williams, J. Chem. Phys., 65, 208 (1976).

72. J. P. Connerade, "Cooperative Effects In Atomic Physics", in Advances In Atomic, Molecular, and Optical Physics, Vol. 29, pp. 325-367, Academic Press, Orlando, Florida, 1992.

73. M. B. Robin, Chem. Phys. Lett., 119, 33 (1985).

74. R. McDiarmid, J. Chem. Phys., 65, 168 (1976).

75. D. D. Koelling, D. E. Ellis, and R. J. Bartlett, J. Chem. Phys., 65, 3331 (1976).

76. J. P. Connerade, M. W. D. Mansfield, M. Cukier, and M. Pantelouris, J. Phys. B: Atom. Molec. Phys., 13, L235 (1980).

77. C. J. Powell, Phys. Rev., 175, 972 (1968).

78. T. L. Ferrell, T. A. Callcott, and R. J. Warmack, Amer. Scientist, 73, 344 (1985).

79. J. P. Connerade and K. Dietz, J. Phys. B: At. Mol. Opt. Phys., 25, 1185 (1992).

80. H. S. Carmen, Jr. and R. N. Compton, J. Chem. Phys., 90, 1307 (1989).

81. K. C. Kim and W. B. Person, J. Chem. Phys., 74, 171 (1981).

82. B. J. Krohn and K. C. Kim, J. Chem. Phys., 77, 1645 (1982).

83. R. Bersohn, IEEE J. Quantum Electronics, QE-16, 1208 (1980).

84. Y. Nagano, Y. Achiba, K. Sato, and K. Kimura, Chem. Phys. Lett., 93, 510 (1982).

85. Y. Nagano, Y. Achiba, and K. Kimura, J. Phys. Chem., 90, 615 (1986).

86. Y. Nagano, Y. Achiba, and K. Kimura, J. Phys. Chem., 90, 1288 (1986).

87. Y. Nagano, Y. Achiba, and K. Kimura, J. Chem. Phys., 84, 1063 (1986).

88. S. R. Gandhi and R. B. Bernstein, Chem. Phys., 105, 423 (1986).

APPENDIX

APPENDIX

FOCUSED BEAM CALCULATIONS

Accurate (< 5%) absolute measurements of laser power are somewhat difficult, especially at the low power limit. More importantly, it is necessary to be able to reproducibly measure the power and then calculate the relative laser power densities which interact with the sample. As this study involved different lenses, wavelengths, and laser output powers a sample calculation of the power density is described here. The slope values described in Chapter III were acquired using λ=266 nm light; therefore, the example to be shown is the 7.5-cm lens data for this wavelength.

The focused beam diameter, d, for a diffraction-limited Gaussian light beam is given by the equation:

$$d = 4\lambda F/\pi D, \tag{3}$$

where F = lens focal length, D = laser beam diameter, and λ=266 nm. Substituting the measured beam parameters gives:

$$d = 4(266\text{ nm})(10^{-6}\text{ mm nm}^{-1})(75\text{ mm})/\pi\ (6.4\text{ mm}) = 3.969 \times (10^{-3})\text{ mm}. \tag{4}$$

The focused beam area, A, is given as:

$$A = \pi d^2/4, \tag{5}$$

where d = focused beam diameter (from Equation 3). Substituting for d, gives the area, $A = 1.237 \times (10^{-7})$ cm^2. The pulse energy, PE, is the average power (P_{avg}), which is measured, divided by the laser repetition rate, 10 Hz, such that:

$$PE = P_{avg}/10\ s^{-1}. \tag{6}$$

P_{avg} was measured as 0.50 mW (= 0.50 mJ s^{-1}); therefore, the pulse energy was $5.0 \times (10^{-2})$ mJ. Uncoated quartz optics were used to direct the laser beam, each causing a 4% reflective

loss per surface. The incident pulse energy was corrected for each optic which the beam encounters on its way to the center of the TOFMS. For this calculation, the beam passed through one prism, one window, and one lens after the power measurement point. The corrected pulse energy is 3.913 x (10^{-2}) mJ. The peak power, P_{peak}, is expressed as:

$$P_{peak} = \text{Pulse Energy/Pulse Duration}, \quad (7)$$

where PE is defined above and the pulse duration for this wavelength is given by the manufacturer as 5 ns. Solving Equation 6 yields P_{peak} = 7.827 x (10^{3}) W. The laser power density, $P_{density}$, is expressed as:

$$P_{density} = P_{peak}/A, \quad (8)$$

and substituting for P_{peak} and A give the initial power density for this set of data as $P_{density}$ = 6.327 x (10^{10}) W/cm^2. Each addition of a quartz plate into the beam path results in an attenuation of the power density by a factor of 0.9216, hence for each data set the power was measured initially and each successive attenuation was a calculated value. The number of photons (n) per laser pulse relates the pulse energy to the wavelength according to:

$$PE = nh\nu = nhc/\lambda, \quad (9)$$

where PE is the pulse energy, h is the Planck constant, c is the speed of light, and λ=266 nm. Solving for the number of photons per pulse gives the value, n = 6.697 x (10^{14}) photons/pulse. An alternate calculation for the beam diameter, which employs the beam divergence, is given as follows:

$$d = f\,\theta, \quad (10)$$

where f = lens focal length and θ = beam divergence. The manufacturer gives the value of 0.5 milliradadians for θ and the lens focal length is 7.5 cm. Solving for d gives a diameter of 3.75 (10^{-3}) cm, a value approximately 10 times larger than from Equation 4. Correspondingly, the value of A calculated using this value for d yields an area $\approx$ 100 times greater than that

calculated using the previously described method. The absolute power densities are expected to fall within the values calculated using the two different methods. The important point is that the slope values do not change with either method, only the relative power densities.

For a MPI process which follows an n-th order laser power law ($n \geq 2$), the ionization yield at any given value of the laser power depends upon the focal length, f, of the focusing lens. In a very elegant treatment, Gandhi and Bernstein have shown the interrelation of the number of ions formed per pulse (Q) with the confocal beam parameters.[88] Though the interested reader is referred to their publication for the actual mathematical derivations, the important result is that the ionization signal strength (Q') is proportional to the beam parameters of volume, V, and area, A. The parameters of volume and area are related directly to the lens focal length; therefore, the ionization signal is proportional to the lens focal length according to the following equation:

$$Q' \propto f^{4-2n}. \tag{11}$$

If this equation is solved using the lenses of this experiment (i.e., f = 7.5 cm, 35 cm, and 50 cm) and the value of 11 for n, then the resulting values (when normalized to the 35-cm lens value) show that $Q'_{50\text{ cm}} > Q'_{35\text{ cm}}$ by a factor of $\approx$ 600, but $Q'_{35\text{ cm}} > Q'_{7.5\text{ cm}}$ by a factor of $\approx 10^{14}$. The values of $Q'_{50\text{ cm}}$ and $Q'_{35\text{ cm}}$ are qualitatively indicative of the experimental results; however, the comparison to $Q'_{7.5\text{ cm}}$ is irrelavent since the power density cannot be directly compared to the other two. Using a shorter focal length lens decreases the focal volume, and yields a smaller signal at saturation. The practical implication of this description is that to increase MPI sensitivity, once "saturation" is achieved, one should use a longer focal length lens, thereby achieving a larger effective focal volume and thus a larger ion signal.

VITA

Donald Philip Armstrong was born in Paducah, Kentucky, on July 28, 1955. He graduated from Reidland High School in 1973. While employed at a local department store, he enrolled at Paducah Community College and attended there from fall semester 1973 to fall semester 1975. In October 1975, he moved to Knoxville, Tennessee, and began working for Union Carbide Corp.-Nuclear Division (now known as Martin Marietta Energy Systems, Inc.). He enrolled as a part-time student at the University of Tennessee, Knoxville, in spring quarter 1976, but shortly thereafter was forced to withdraw. He enrolled again as a part-time student in winter quarter 1977 and attended the next 19 of 21 quarters to receive a Bachelor of Science degree (with honors) in chemistry in March 1982. Upon completion of the undergraduate degree, he enrolled in the chemistry graduate program at the University of Tennessee, Knoxville, specializing in physical chemistry and working initially under the direction of Dr. George K. Schweitzer and finally under the direction of Dr. Robert N. Compton. His graduate research interests included lasers and mass spectroscopy, as well as Raman and Fourier-transform spectroscopies. To date he has published two articles in Applied Spectroscopy, one article in The Journal Of Raman Spectroscopy, and two articles in the Proceedings of the 28th Conference on Analytical Chemistry in Energy Technology. The author is a member of the American Chemical Society and the Optical Society of America. He was married to Diane Binford, of Paducah, Kentucky, from July 1976 until January 1990. He is the father of one son, Bret Tyler, who was born in September 1983. Following completion of the graduate program, the author hopes to continue in his present position as a development staff member in the Uranium Enrichment Organization of Martin Marietta Energy Systems, Inc., where he has been employed for 16½ years.